Developing a Smart Monitoring System for Leakage Currents from Insulators on Wooden Poles

A thesis submitted

in fulfilment of the requirements for the degree of

Doctor of Philosophy

Peter Sokolowski

BMath BEng(Elec)(Hons) CPEng NPER RPEQ

School of Electrical and Computer Engineering

College of Science Engineering and Health

RMIT University

June 2014

Declaration

I certify that except where due acknowledgement has been made, the work is that of the author alone; the work has not been submitted previously, in whole or in part, to qualify for any other academic award; the content of the thesis/project is the result of work which has been carried out since the official commencement date of the approved research program; any editorial work, paid or unpaid, carried out by a third party is acknowledged; and, ethics procedures and guidelines have been followed.

Peter Sokolowski

June 2014

I would like to dedicate this thesis to my father, Edward Sokolowski, who passed away unexpectedly in July 2007 and was unable to see me work through to the completion of this thesis, and owing to World War II, who missed gaining the education I have been privileged to receive.

Declaration

I certify that except where due acknowledgement has been made, the work is that of the author alone; the work has not been submitted previously, in whole or in part, to qualify for any other academic award; the content of the thesis is the result of work which has been carried out since the official commencement date of the approved research program; any editorial work, paid or unpaid, carried out by a third party is acknowledged; and, ethics procedures and guidelines have been followed.

Peter Sokolowski

June 2014

Acknowledgements

I would like to thank all those who have in some way helped me achieve the completion of my PhD research program culminating in the authoring of this dissertation and reaching an important career and life milestone.

First and foremost, I would like to express my deepest and sincere gratitude to my senior supervisor, Professor Xinghuo Yu, for his excellent guidance, indefinite patience, valuable advice and tremendous encouragement throughout my candidature. He has a unique skill of providing amazingly powerful words at those times when most needed, creating unbridled vigour and priceless motivation. This thesis would not have been possible without his help and crucial support during some most difficult times.

I would like to thank my associate supervisor, Professor Liuping Wang, for recommending the industry-based research program at RMIT University, as well as for her continuing support, discussion of ideas and invaluable feedback during my program.

I am also indebted to two Victorian power distribution network utilities Powercor Australia (and their associate distribution network Citipower) and Jemena (and their subsidiary companies Alinta Asset Management, Jemena Electricity Networks (Vic) and United Energy) and the Australian Research Council for their initiation and funding of the research project. I would especially like to thank Mr Peter Wong (Jemena) and Mr Fulvio Buratto (Citipower and Powercor Australia) for their constant support and feedback on my research ideas. Furthermore, their provision of wooden poles, high voltage insulators, access to smart power quality metering, and much other system data have made this dissertation possible. I

must also thank the numerous staff from Jemena and Powercor Australia who patiently answered many questions regarding pole top fires as well as helped me access many systems to retrieve all the data available and necessary for completing this research.

I must thank Dr Ajendra Dwivedi and Dr Sachin Pathak for assisting in conducting experiments in the High Voltage laboratory on wooden poles. I also thank Mr Ivan Kiss and Mr Sinisa Gavrilovic for helping set these experiments up safely. I would especially like to thank Dr Xiangjun Li, Professor Yong Feng and Associate Professor Alan Wong with their help in conducting experiments in the High Voltage laboratory on insulators while I was experiencing life challenges and very pressed for time.

I would like to thank my friends and colleagues in our research group, aspiring in their own endeavours while being an incredible motivational source of energy to me. Their knowledge sharing, know-how and feedback have been invaluable. I much appreciate the support by Dr Wei Peng, Dr William Becker, Dr Xiangjun Li, Dr Ajendra Dwivedi, Dr Sachin Pathak, Dr Quingmai Wang and Mr Miguel Combariza who have kindly shared many of their research experiences for guidance while I was experiencing difficult and stressful times, providing a much needed and necessary uplift. Additionally, Dr Ajendra Dwivedi and Dr Xiangjun Li have been prodigious in assistance and support when I was posed with challenging time constraints.

I owe my deepest gratitude to my engineering mentor and work supervisor, Mr Ken Youman, former Engineering Technology Manager and Chief Engineer of the Newcastle BHP Steelworks and a director of Escape Technologies, who encouraged and inspired me in completing my PhD research program. I especially would like to thank Associate Professor David Pask who encouraged me to take up the electrical engineering PhD research program and Professor Ian Hiskens who has inspired me to excel in understanding electrical systems and their nonlinear behaviour. I also would like to thank my work colleagues who have always been there for me when I needed to sound out non-trivial ideas.

I am blessed and indebted by the support of my family during my studies, providing me with unconditional love, support and encouragement during many trying and difficult periods. Lastly, but not least, I would like to thank all those whose names I may have missed but who have joined me in some way on my research journey.

Contents

List of Figures

List of Tables

Nomenclature

Symbols

d_b	Box (counting) fractal dimension
d_c	Correlation fractal dimension
d_i	Information fractal dimension
n_d	Nonlinearity measure
$r_{x,y}$	Cross-correlation between x and y
$\rho_{x,y}$	Correlation coefficient between x and y

Acronyms / Abbreviations

AAC	All Aluminium Conductor
AC	Alternating Current
ACSR	Aluminium Conductor with Steel Reinforcement
ANN	Artificial Neural Network
AS	Australian Standard
CB	Circuit Breaker

CCA	Copper Chromium Arsenate
DC	Direct Current
DFA	Distribution Fault Anticipation
DMS	Distribution Management System
DWT	Discrete Wavelet Transform
EF	Earth Fault
EHV	Extra High Voltage, voltages exceeding 345 kV AC
FDR	Feeder
FFT	Fast Fourier Transform
FS	Fuse Switch
GIS	Geographic Information System
GPS	Geosynchronous Position System
HD	High Density
HIF	High Impedance Fault
HV	High Voltage, voltages exceeding 1000 V AC, or 1500 V DC
IEC	International Electrotechnical Commission
IED	Intelligent Electronic Device
IR	Infrared
LCA	Level Crossing Activity

LCHI	Leakage Current Health Index
LC	Leakage Current / Load Current
MC	Mordialloc, Melbourne, Victoria
MRA	Multi Resolution Analysis
NSW	New South Wales, Australia
O/C	Overcurrent
PCP	Pentachlorophenol
PD	Partial Discharge
RMS	Root Mean Square
SAIDI	System Average Interruption Duration Index
SCADA	Supervisory Control And Data Acquisition
SLD	Single Line Diagram
TDS	Total Dissolved Solids
THD	Total Harmonic Distortion
UHV	Ultra High Voltage, voltages exceeding 800 kV AC

Publications

P. Sokolowski, X. Li, X. Yu, and Y. Feng, “Characterizing Leakage Current on Polluted Insulators by Measuring Nonlinearity,” *Proceedings of IEEE International Symposium on Industrial Electronics (ISIE 2014)*, Istanbul, Turkey, June 2014.

X. Li, Y. Feng, K. L. Wong, **P. Sokolowski**, and X. Yu, “Analysis of the leakage current on polluted insulators using correlation coefficient,” *Proceedings of IEEE International Conference on Industrial Electronics (IECON 2011)*, Melbourne, Australia, November 2011.

A. Dwivedi, **P. J. Sokolowski**, X. Yu , P. Wong, and F. Buratto, “Fault Location In Power Networks Using Graph Theory,” *Proceedings of IEEE International Conference on Industrial Electronics (IECON 2010)*, Glendale, Arizona, November 2010.

A. Dwivedi, X. Yu, and **P. J. Sokolowski**, “Analyzing power network vulnerability with maximum flow based centrality approach,” *Proceedings of IEEE International Conference on Industrial Informatics (INDIN 2010)*, Osaka, Japan, July 2010 (**Best Conference Paper Award**).

X. Yu, A. Dwivedi, and **P. J. Sokolowski**, “On complex networks approach for fault detection in power grids,” *Proceedings of IEEE International Conference on Control and Au-*

tomation (ICCA 2009), Christchurch, New Zealand, 9-11 December 2009.

A. Dwivedi, X. Yu, and **P. J. Sokolowski**, "Identifying vulnerable lines in a power network using complex network theory," *Proceedings of IEEE International Symposium on Industrial Electronics (ISIE 2009)*, Seoul, Korea, 5-8 July 2009.

P. J. Sokolowski, A. Dwivedi, S. Pathak, F. Buratto, and X. Yu, "Investigating the impedance on a Wooden Power Pole after a Pole Fire," *Proceedings of Australasian Universities Power Engineering Conference (AUPEC 2008)*, Sydney, Australia, 2008.

S. Pathak, **P. J. Sokolowski**, A. Dwivedi, F. Buratto, X. Yu, and K. L. Wong, "Investigation of pole fire on a 22 kV Wooden Power Pole Structure," *Proceedings of Inaugural Symposium on Electrical Energy Evolution in China and Australia*, Palm Cove, Australia, 2008.

Abstract

In Australia and many other countries of the world, power distribution lines are carried on wooden poles. These lines suspended on insulators, which are fixed to wooden poles, pass cities as well as bushlands. Under different weather conditions, insulators become contaminated, and in particular, with damp weather, these insulators lose their ability to provide a perfect insulation between the high voltage conductor and the ground (through high impedance objects such as wood). A leakage current, small in magnitude, starts flowing from the high voltage conductor to the ground across the polluted insulator and through the wooden pole. If this phenomenon continues over some time, the currents start heating the wood where there is an abundance of wood-to-metal contact. At a certain stage, it will start smoking and this may lead to a pole fire. The obvious consequences of this are the loss of power to customers, public safety hazards and potential disasters such as bushfires.

This project aims at determining which measure or combination of measures of leakage current are best suited for creating a 'Leakage Current Health Index' (LCHI) that can be later used to provide a power system operator with health status for a feeder or system, indicating how urgent a response is needed.

To achieve this goal, the impedance characteristics of wooden poles altering the leakage current from insulators are investigated to better understand the role of wood in leakage current signatures. The effective impedance of wood used for poles in Victoria, Australia is established for the first time. Examining the impedance properties of typical Copper Chromium Arsenate (CCA) impregnated wood for 66 kV distribution poles shows danger-

ous conductance properties of wood at this voltage, providing an explanation for these poles catching fire at triple the rate of 22 kV distribution poles. After a systematic investigation of wood used for poles, a typical impedance characteristic is established for a weathered CCA impregnated wooden pole operating at 22 kV under both dry and wet weather conditions.

Next, the leakage current from a single high voltage insulator is examined for various contamination levels and under different weather conditions. A new nonlinearity measure is established which utilises the Pearson correlation coefficient to measure the degree of leakage current nonlinearity and to build leakage current profiles of a single insulator under different conditions prior to flashover. Several fractal dimensions are also considered for the first time to measure characteristics of the leakage current profile of a single insulator. These measures are able to quantitatively differentiate between various levels of insulator contamination and different weather conditions, showing an enhanced level of nonlinear activity in the stage prior to insulator flashover.

After developing an understanding of a single insulator, systematic modelling is used to build measure profiles of leakage currents for a simple power line, a lossless power line and a lossy power line. Finally, power utility zone substation data for a pole top fire are examined to verify the validity of the profiles observed utilising the measuring techniques determined suitable for establishing a LCHI.

Chapter 1

Introduction

1.1 Overview

This chapter provides an overall background to the project and the purpose of the research work. Section 1.2 provides a preliminary discourse of the thesis. Section 1.3 introduces power systems and how they consist of several subsystems working together. This section explains power system security, and the systems which are needed to create this security. Next, Section 1.4 discusses the motivation for this research utilising a combination of these systems, and defines the scope for this research study. Further, in Section 1.5, the objectives and contributions of this research are outlined. Finally, the chapter is concluded with the structure of the thesis in Section 1.6.

1.2 Prologue

Power systems connect generation via transmission, sub-transmission and distribution networks to supply electricity to customers. New technologies are pushing power systems past their original design limits with connection of electric motor vehicles, solar distributed generation and the like. Engineers must continue to create smarter technologies to address this

ever-changing climate while promoting saving fossil fuel consumption, reducing operational costs and increasing reliability for a sustainable future. Government enforced roll-outs of smart meters are assisting distribution companies around the world by collecting data for engineers and scientists to optimise the power system creating a 'smart grid'. However, data being collected does not always capture the needs of engineers, and require post-event fine-tuning for better data capture into the future.

The increasing reliance of our daily lives on electricity warrants 24 hours a day, 7 days a week access unassumingly. However, the assets providing electricity are ageing and require higher levels of maintenance or replacement. One such asset in Australia are the wooden poles that carry power lines. These power lines are suspended on insulators, which are fixed to wooden poles, passing through cities as well as bushlands. Under different weather conditions, insulators become contaminated, and in particular, with damp weather, these insulators lose their ability to provide a perfect insulation between the high voltage wire (or conductor) and the ground. A leakage current, very small in magnitude, starts flowing from the high voltage conductor to the ground through the wooden pole. If this phenomenon continues over some time, given the right circumstances, the current starts heating the wood. At a certain stage, it will start smoking and this may lead to a 'pole top fire'. If that power line is passing bushland, under hot weather and windy conditions, the dry bush may touch the wooden pole close to the leaking insulator, and as a consequence initiate a serious bush-fire. A major disaster may ensue presenting danger to property and the safety of the public.

With the advances in available metering technology and the ageing of power networks, this re-invigorates an area of study which has lay dormant for many years, studied when there was no computer power that may assist in better understanding phenomena present. Oversimplification for ease of computation may have overlooked detail that alters the now accepted norm. Superior metering accuracy available today may also affect results of years ago. Current research in this area has attempted to add knowledge to existing techniques

that model or detect leakage current of a contaminated insulator, without accounting for their fixing to wooden poles nor that they are rarely used in isolation. This thesis is dedicated to studying leakage currents from high voltage insulators on wooden power poles.

1.3 Power Systems

A power system is usually defined as all the electrical components which create an electrical network for transmitting and distributing electrical power from the point of generation (that is, power plants or power stations) to the point of supply (that is, the end-user or customer).

1.3.1 Primary Systems

The primary systems which create a power system are the power stations which generate electrical power, the transmission substation where electricity is stepped up to a transmission voltage level thereby reducing energy losses, high voltage transmission lines used to transmit electrical power to distribution terminal stations and zone substations where it is stepped down to distribution voltage levels. Electrical power is then distributed to industries and major substations, where voltages are again stepped down to consumer mains voltage for use in residential homes and commercial premises. A basic representation of a simple power system is shown in Figure 1.1 [4].

Power System Design and Power System Security

Power systems are typically designed to be $N-1$, that is a power system with N buses will sufficiently operate with the loss of one (1) network connection supply or feeder to any given bus, where a bus is the busbar which commonly connects voltage supply feeders and load feeders. This type of design provides what is known as *power system security*. The purpose of designing a power system to an $N-1$ level is to give maintenance crews

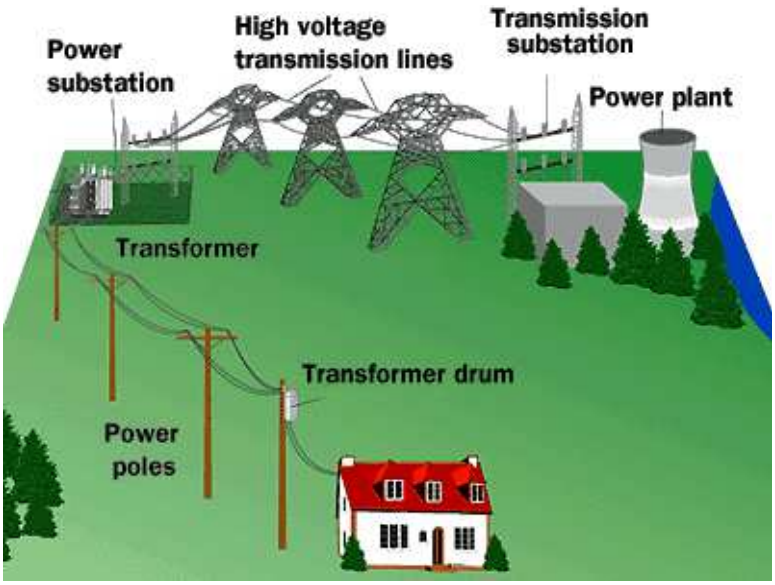

Fig. 1.1 Layout of a simple power system

sufficient time to respond to a single failure before customers experience loss of power. Of course, for an $N-1$ power system design if more than one feeder supply to a substation fails, then some customers fed by that substation will experience power loss.

1.3.2 Secondary Systems

Secondary systems are required to support the functionality of what is traditionally thought of as a power system, or the primary system. Without these secondary systems services, electrical engineering problems are sure to occur. Some of these problems include: (a) when the load demand changes there would be no control of system voltages, causing large currents to flow when the demand is high, and depending on how low the voltages drive down, possible instability issues; and, (b) when different types of faults occur there would be no tripping of circuit breakers which would cause large amounts of energy to flow, with an extreme subsequent fire where the power source is part of a large energy grid network. Following are the typical systems used to make a power system 'work'.

Protection Systems

Unfortunately, power system faults cannot be eliminated owing to the physics behind electrical systems. Therefore the objective of protection systems is to minimise the impact of a fault.

Faults (including short circuits and high impedance faults) can be owing to many different types of events including:

- overvoltages caused by lightning or switching
- mechanical failure, e.g. fallen conductors
- natural causes, e.g., trees growing into conductors, climbing animals, vermin
- insulation contamination, e.g. coastal salt pollution, industrial pollution

Faults typically cause currents that are several orders of magnitude larger than normal load currents. In the case of contamination on high voltage insulators, these fault currents are not significantly larger than load currents and as such are not cleared by the usual protection until the fault has dramatically accelerated to the point of a pole top fire.

Consequences of faults include:

- arcing or flashover, leading to high temperatures, and a possible fire or explosion
- sustained overheating due to high currents may reduce the useful life of equipment, for example, insulation damage and conductor annealing
- destructive mechanical forces on transformer windings and busbars owing to high currents
- overvoltages stressing insulation beyond its breakdown value.

Protection systems must:

- remove each fault from the system as quickly as possible

- remove no more parts of the system than is absolutely necessary.

Faults are removed from a power system by opening or 'tripping' circuit breakers, or by blowing fuses. The protection system should be designed to operate only those circuit breakers or fuses closest to the fault so to 'clear' the fault while keeping the remainder of the power system intact.

Fault conditions are detected by continuously monitoring voltages and currents throughout the power system. Fuses blow when subject to high currents for specified periods of time, protecting conductors, cables and transformers. Circuit breakers are coupled with relays which will operate tripping circuits when subject to abnormal voltage or current magnitudes.

Finally, faults can occur in the protection equipment itself. Thus there is always a need for forms of backup protection, whether by duplicated protection schemes, circuit breaker failure schemes, or if all else fails separation by different magnitudes of fault level.

Control Systems

Power system loads continue to change instant by instant. Therefore the objective of control systems is to balance the supply and demand, while maintaining power system voltage stability. In addition to these automatic control systems, utilising substation Supervisory Control And Data Acquisition (SCADA) systems, further control, indication and monitoring may be available to substation feeder components which can be used for status and diagnostic purposes. The SCADA systems available at each substation are dependent on criticality and regulatory requirements [5].

Metering Systems

Power systems come at considerable capital and operational expense. Further, with carbon emission costs also being accounted for in recent times, accurate metering of emissions is necessary. Therefore the objective of metering systems is to measure the consumption of energy for billing and the revenue used for the capital, operational and carbon expenses.

With the advent of new smart metering technologies, the roll-out of this technology in Australia and across the globe has enabled engineers and power distributors to store and monitor time of use electrical parameters for later analysis. These parameters include load voltages, voltage sags and swells, demand profiles, maximum demands, power factor, harmonic content and waveforms for triggered events.

Battery and DC Systems

Power systems may not always have access to mains power to operate. Therefore the objective of battery and DC systems is to provide an alternative power source in case of unavailable mains power to operate all parts of the secondary systems.

Cabling, Wiring and Pilot Cables

Power systems are constructed out of many components. These components are located over a large geographic area. Therefore the objective of cabling, wiring and pilot cables is to connect secondary system components together so that each component, however big or small, is wired to measure the appropriate electrical parameters for correct operation.

1.4 Motivation and Scope

1.4.1 Motivation

Despite the numerous systems in place to create power system security, these systems fail to provide protection from incipient pole top fires, remaining one of the most challenging problems faced by power distributors. In 1998 the Australian electricity supply industry commenced a reform agenda moving to market-based operation rather than the previous demand-based operation. During the early years following this reform, deregulation and privatisation of the Victorian power distributors and generators was also implemented. Following privatisation, the Victorian power distributors have been performance driven, rated on their System Average Interruption Duration Index (SAIDI) [6], that is, the average outage duration for each customer served, calculated as the sum of all customer interruption durations divided by the total number of customers served. The SAIDI of a Victorian power distributor for a typical warm weather month is shown in Figure 1.2. The figure shows the breakdown of the types of fault causing power outages, and specifically, that pole top fires account for over 7% of interruptions [1]. Pole fires are the second largest cause of outages just behind plant failure. When a distributor does not meet a SAIDI performance target, they incur penalties which have totalled millions of dollars over years gone by [7, 8]. An example of the physical consequence of a pole top fire outage is shown in Figure 1.3, along with another pole related incident where scorching is visible at the bolt fixing bracing to a steel crossarm.

Power distributors invest significant amounts of money on preventive maintenance strategies to mitigate the risk of pole top fires including insulator washing, silicon coating of insulators, installation of self-cleaning insulators and replacement of higher risk wooden crossarms with steel crossarms [3]. Examples of steel crossarm replacements are shown in Figure 1.4. Historically, maintenance operations are scheduled according subjective judge-

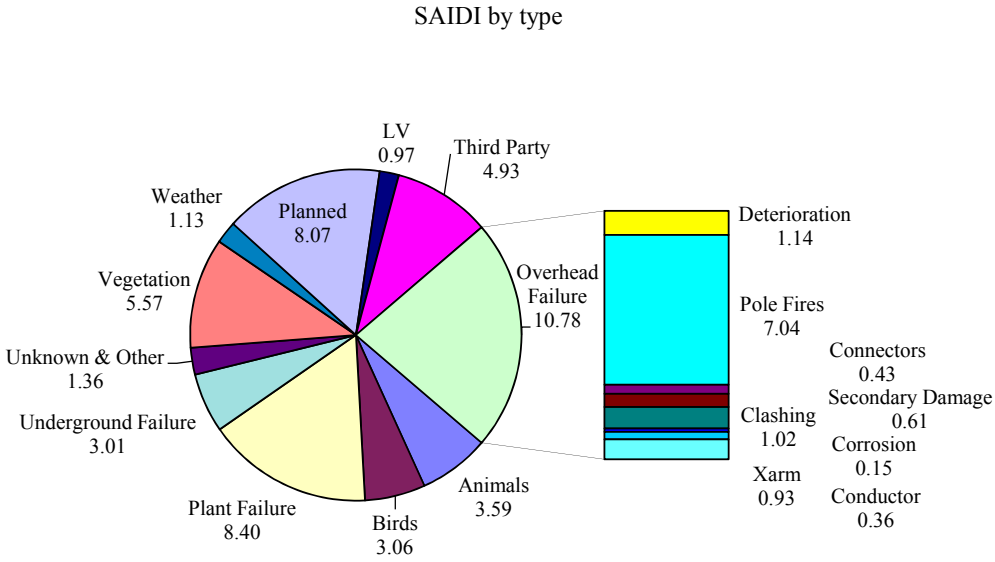

Fig. 1.2 System Average Interruption Duration Index (SAIDI) by Fault Type for a typical warm weather month in Victoria [1].

(a) (b)

Fig. 1.3 (a) a pole with a crossarm burnt into two sections after a pole top fire; (b) a sub-transmission pole with localised scorching at bracing bolt.

ment of power line inspectors. Since privatisation, lines have been inspected on a 5 year cycle. In 2009, Victoria experienced catastrophic bushfires resulting in 173 fatalities. Five of the major fires that occurred on 7 February 2009 were caused by failure of ageing electricity assets [9]. Following recommendations from the 2009 Victorian Bushfire Royal Commission, an inspection is now required at least every three years in areas of high bushfire risk [9]. However, without on-going monitoring, rapid power pole or insulator deterioration will continue to go unchecked, with only anecdotal evidence choosing a period of three years as a sufficient time between inspections to visually find ageing or deterioration defects. The 2009 Victorian Bushfire Royal Commission also noted one of the Victorian power distributors managed 11,374 kilometres of distribution line structures aged between 55 and 64 years, and 10,318 kilometres aged between 65 and 74 years, with upgrades of these ageing assets needing a capital investment of over $7.5 billion while resulting in consumers paying over 20% more on their electricity bills every year. Clearly, in addition to large capital investment, other technologies should also be pursued to mitigate the risk of pole top fires.

Section 1.2 described how the leakage current phenomenon over a period of time, given the right situational circumstances can lead to a pole top fire. Leakage current during this period of time appears intermittently as a High Impedance Fault (HIF). Past research [10–17] has investigated the leakage current performance of a high voltage insulator under different external environmental conditions, however there is no study to date which has investigated measuring or monitoring the progression of leakage current signatures from power lines suspended on insulators fixed on wooden poles. These leakage current signatures may characterise the specific electromagnetic phenomena suitable for identifying incipient pole top fires [18]. By integrating metering systems (to measure parameters), control systems (to alert power system operators) and protection systems (to trip and isolate power line feeders prior to a catastrophic pole top failure), an integrated smart monitoring system may be able to detect, alert, and prevent leakage currents from polluted insulators on wooden poles

(a) (b)

Fig. 1.4 Solutions employed by distribution companies utilising steel crossarms and self cleaning insulators: (a) fitted in place of traditional location of a wooden crossarm; (b) fitted at the pole top extremity, taking advantage of the electrical properties of the full length of the pole.

causing pole top fires and subsequent consequential losses. This thesis initiates the process of developing a smart monitoring system for leakage currents from insulators on wooden poles by building an understanding of the mechanisms causing leakage current and finding methodologies to detect them.

1.4.2 Research Scope

The first part of this thesis is devoted to investigating the role wood used for power poles plays on leakage current. Typical wooden poles used in Victoria, Australia are sourced from local distribution companies, and sectioned to manageable sizes that can be examined in close detail within a high voltage laboratory. Thorough testing is performed to verify research hypotheses. Further tests on effective impedance are carried out to gain a better understanding of the capacitive effects on wood resistance as well as how the electrical performance of wood is affected by the power line voltage.

The second part of the thesis is dedicated to demonstrating several measures as suitable for quantitatively measuring leakage current while differentiating between insulator condition.This is achieved by measuring leakage current nonlinearity for a high voltage insulator in isolation. There are several existing techniques for detecting abnormal leakage currents, although most are unsuitable for use in real-time condition monitoring. A new nonlinearity measure is proposed and studied as a quantitative measure of leakage current on a high voltage insulator. Experimental data of leakage current from a high voltage insulator are collected in a high voltage laboratory for application of the nonlinearity measure. Further measures established as suited to high impedance faults are also applied to the leakage current on a high voltage insulator and studied in detail.

The final part of the thesis extends the application of measuring an isolated high voltage insulator to a full overhead power line and a group of power lines. An understanding of the measures for an overhead power line is built up, and, utilising zone substation data for

a pole top fire, these measures are verified and validated as suitable for detecting pole top fires.

1.5 Thesis Objectives and Contributions

1.5.1 Objectives

The overall goal of this thesis is to determine which measure or combination of measures of leakage current are best suited for creating a 'Leakage Current Health Index' (LCHI), which can later be used to provide a power system operator with health status for a feeder or system, indicating how urgent a response is needed. To achieve this goal, the individual goals of the thesis can be grouped into three parts:

1. Build an understanding of the leakage currents from high voltage insulators on wooden poles by investigating the role of wood on leakage current;
2. Determine the appropriate methodologies that measure and quantify leakage current by:
   (a) measuring the nonlinearity of leakage current for a high voltage insulator under several contamination levels and different weather conditions; and,
   (b) tracking the changes in the measure of leakage current during the period prior to an insulator flashover;
3. Test the methodologies determined above by:
   (a) investigating and evaluating the effect of applying these measures to power lines rather than to single insulators typically studied in the literature; and,
   (b) applying these measures to zone substation data for a pole top fire for verification and validation as suitable measures of leakage current that cause pole top fires.

1.5.2 Contributions

The contributions of the research which forms this thesis can be summarised as below:

1. The effective impedance of a wooden pole is considered for the first time, where previous studies have ignored both capacitive components and how effective impedance varies for different voltages, while assuming a purely resistive pole. Utilising the effective impedance an understanding of the mechanisms causing leakage current signature is gained:

   (a) studying the effective impedance demonstrates a wooden pole's capacitive components increase during wet weather, while also reducing the resistive components of impedance and promoting increased leakage current;

   (b) it is demonstrated that leakage current density at wood-metal contact points contributes to significant heating. When heating of these contact points reach temperatures greater than 50 °C, smouldering may initiate;

   (c) the impedance studies reveal wet weather reduces effective resistance to approximately 60% of the resistance in a dry state;

   (d) the impedance studies uncover that when operating at 66 kV, pole lengths appear inadequate for limiting the leakage current at a similar level to 22 kV and perhaps explains these assets catching fire at triple the rate of 22 kV assets;

2. Methodologies that measure and quantify leakage current signature for identifying insulator condition and detecting incipient pole fires are found:

   (a) a new nonlinearity measure is proposed based on the Pearson correlation coefficient. The nonlinearity measure is deemed suitable as a high voltage insulator condition identifier;

(b) a new representative power measure is proposed, suitable for corroborating the presence of heat dissipation by leakage current;

(c) fractal dimensions are used for the first time to identify shapely leakage current activity on a single high voltage insulator as well as measure leakage current nonlinearities;

3. The methodologies found above are tested for identifying insulator condition and detecting incipient pole fires:

(a) application of measuring leakage current nonlinearity is extended to several overhead power line scenarios for the first time; and,

(b) the measures of leakage current deemed suitable above are tested on pole top fire data collected from a zone substation for the first time.

1.6 Structure of Thesis

This thesis is organised into six chapters. An outline of the chapters is summarised below:

Chapter 1 provides a background to the problem posing this research. It introduces power systems and their breakdown into the subsystems which make power systems 'work'. Next, the motivation and scope of the research is outlined. Finally, the thesis objectives and contributions of this research are highlighted.

Chapter 2 summarises past research performed in the areas of leakage current in wood, leakage current on contaminated insulators, modelling of contaminated insulators, leakage current signature hypotheses, leakage current analysis techniques, high impedance fault detection techniques, real-time leakage current monitoring systems and current industry practices for reducing the number of pole top fires. The chapter concludes by identifying where there are gaps in the current knowledge base and where there is scope for improvement.

Chapter 3 investigates systematically the effective impedance of wood used for power poles. One particular pole fire event is examined in detail, with experimental work undertaken in the controlled environment of a high voltage laboratory to determine the electrical performance properties of wooden poles used in Victoria. Environmental factors such as moisture and contamination on porcelain insulators and wetting of the wooden pole itself are all determined to be contributing factors for initiating the pole fire. Effective impedance studies consider a wooden pole as consisting of a resistive and capacitive component, accounting for the phase shifts observed between the measured supply voltages and leakage currents. These studies enable examination of effective wood resistances at several operating voltages under different weathering conditions. Theses studies show that simulated wet weather conditions dramatically reduce the magnitude of the leakage path resistance characteristic, raising the current density and hence creating localised heating in areas with wood-metal connections. They also reveal dangerous conductance properties of wooden poles operating at 66 kV when being of a similar length as 22 kV poles.

Chapter 4 introduces a new nonlinearity measure to study the leakage current nonlinearity for a single high voltage insulator. This measure is defined in terms of the Pearson correlation coefficient, and captures the overall leakage current signature including interharmonic behaviour, omitted by other leakage current detection techniques. Experimental data is collected in a high voltage laboratory for a single high voltage insulator under various contamination conditions. Phase portraits are employed to provide qualitative information regarding the leakage current signature, revealing shapely changes in trajectories for different insulator conditions. Fractal dimensions are used to help measure quantitatively the leakage current signature changes. The nonlinearity measure and fractal correlation dimension are shown to distinguish different insulator conditions by measuring nonlinearities in leakage current signatures prior to flashover, making them well suited to contributing to a LCHI.

Chapter 5 extends the application of the measures deemed suitable for identifying the condition of a single high voltage insulator to overhead power lines and a group of power lines. Three power line scenarios are considered utilising the data collected from the laboratory for a single insulator. These data are used to systematically create leakage current profiles for power lines. Next, data collected from a power distributor's zone substation for a pole fire event are used to verify and validate the measures that are suitable for establishing a LCHI.

Chapter 6 concludes the thesis with discussion of the contributions of this research. Finally, further extensions to the study are recommended as well as possible directions for future study.

Outside of the main text, the thesis includes a bibliography to cite other relevant work and sources of information, and a list of conference papers published during the course of undertaking this research.

1.7 Summary

This chapter has introduced power systems and their composition. The power poles and insulators that carry power lines are also described, and in particular, the leakage current phenomenon. Next, attention is brought to the motivation and scope of this research, and the main contributions listed. Finally, the thesis structure and main contents of each chapter are briefly outlined.

Chapter 2

Literature Review

2.1 Overview

This chapter presents a comprehensive review of the research in the area of leakage current from high voltage insulators on wooden poles. By the nature of the system being comprised of several components, the research on each component is reviewed in turn. Section 2.2 provides some background to the problem of incipient pole top fires. Next, Section 2.3 examines leakage current properties of wooden poles and how its corresponding resistance may be altered. Section 2.4 reviews the leakage current signature on high voltage and how it changes under various conditions. This section includes modelling of contaminated insulators, and the typical leakage current observed when arcing occurs in the period prior to flashover. Section 2.5 presents current leakage current analysis techniques, leakage current signature hypotheses relating to arcing and flashover, and high impedance fault detection techniques. Section 2.6 addresses methods which have been used to detect faults similar to leakage current problems on power lines. Section 2.7 discusses when real-time leakage current data has been captured during research, and the proposals for tracking parameters which may indicate an incipient pole top fire. Section 2.8 reviews the current industry practices which address pole top fires. Finally, based on the literature survey, Section 2.9 summarises

the key issues identified.

2.2 Incipient Pole Top Fires

The build-up of salt and dust contamination on the surface of overhead insulators installed near the coast contribute towards lowered insulation levels and higher leakage current flow. Under different weather conditions, insulators become contaminated, and in particular, with damp weather, these insulators lose their ability to provide a perfect insulation between the high voltage conductor and the ground. The higher leakage current flow activity leading to wooden pole fire remains a pervasive maintenance problem for power distribution companies in most of Australia. The subject has received very little attention in the recent past especially for insulator contamination leading to wooden pole/crossarm fires. For many years, analyses of leakage current leading to wooden pole fires have indicated that a great number of them have been caused by insulator pollution. It should be noted main conclusions on this subject in the past were drawn from statistics of outages on operating distribution lines rather than from experimental research [19].

Examining the location of where pole fires occur in the state of Victoria in Australia, it was found that almost all pole fires occurred in particular geographic locations [1, 20, 21]. This could be for a number of reasons including the time of construction of distribution lines and hence the choice of insulator and wooden pole, the geography of the area creating ideal conditions for flashover and the weather in the area also impacting on flashover conditions [22]. Given the numerous influencing factors which may lead to causing a pole fire, a few assumptions have been made to analyse past wooden pole top fires.

Recently, in Victoria, Australia a long period of drought has created very dry conditions. These dry conditions in combination with high winds causes a build up of dry contaminant on insulators. The dry contaminant is not conductive, but with light drizzle-type rain, which is also typical for the area, the contaminant becomes wet and in turn initiates leakage current.

Victoria also has a vast coastline where seasalt spray and mist causes wetting and pollution simultaneously. This again can initiate leakage current. As such, identifying leakage current is critical to detecting incipient and imminent pole fires. Leakage current signature has been the most useful way to identify problem poles to date.

2.3 Leakage Current Signature for Wooden Poles

There are approximately 8 million wooden poles throughout Australia that are in service in the power and communication networks. Out of these wooden poles, 5 million are in use for power distribution and transmission [23]. Various power distribution companies have experienced pole top fires owing to fog, drizzle or heavy dew after spells without heavy rain.

The influence of leakage current flow in wooden structures from a pole fire perspective has had extensive research [24–39]. The majority of the research on wooden poles was conducted from 1940 to 1980 with significantly less research after 1980. However, in recent years environmental conditions have changed owing to many factors including global warming [15, 40, 41], as well as the use of new insulating technologies [17, 42]. Electrical equipment has also changed, with customers and governments mindful of energy efficiency, introducing new harmonic components and changing power quality.

Ross [24] was motivated by the resulting damage and service interruption of pole fires to study the burning of wood structures by leakage currents for gaining an understanding of how pole fires may be prevented. He observed that fires often occur when three conditions occur simultaneously, that is, (a) a preceding prolonged dry period; (b) accumulated insulator surface contamination; and, (c) the dry period being followed by a fog, misty rain, or even snow. He extensively tested wooden crossarm and pole samples by simulating dry and wet weather conditions. The study surmised coincident occurrence of dry wood and selective wetting of the pole and crossarm surfaces leaves dry wood areas in series with the

leakage current path and can result in a fire. The dry area, with high resistance in comparison with wetted wood surfaces result in voltage concentration across the dry zone, and if that surface is sufficiently short can cause electrical breakdown. As a solution [25], Ross suggested that electrical assets be terminated snugly against wooden pole and crossarms, and further suggested the use of wood treatment to eliminate voltage concentration, thereby increasing dry wood conductivity.

Wickham et al. [26] studied factors which may cause pole top fires. These factors included contamination, power line design, the high voltage insulators and pins, and the wooden structures. He concluded after insulator insulation breakdown, burning was more likely to occur in wood freshly impregnated with creosote than untreated wood, and the fire is most likely to initiate where the crossarm and pole connect together. He also showed caulking this connection with a suitable compound could prevent fires occurring under the conditions which initiated fires without that caulking. However, this does not necessarily prevent fires from occurring under other conditions.

Clayton et al. [27] considered the impulse strength of wood and concluded that wood insulation is governed by the length of the wood, the number of insulators in series, and whether the conditions are wet or dry, with standard rain reducing the impulse strength of the insulators. Darveniza et al. [28] studied using the insulating properties of wooden poles for electrical impulse strength and electrical arc quenching, showing that these electrical properties influence performance. The authors corroborated Ross's [24] pole top fire condition characterisation, while adding the phenomenon of spark discharge at loose metal to wood interfaces where there is an adequate supply of air.

Darveniza [29] conducted a leakage current study to evaluate the factors which may increase the risk of a pole top fire. Precipitation produced non-uniform wetting on the wood and when combined with wind found to cause ignition. Wood decay and natural shrinkage causing loose wood-metal connection may allow spark discharge inside the drilled

hole housing the bolt where sufficient leakage current and adequate air causes sparking. Prevention solutions proposed by Darveniza et al. include the painting of the wood in the vicinity of wood-metal connection with conducting paints, and the use of a guard electrode on the kingbolt (metal) of each wooden crossarm [28, 29]. However, these pole top fire solutions have been unable to prevent pole top fires occurring around the world.

Robertson [30, 31] investigated the treatment of wooden poles concluding, that particularly when new, treatment may allow sufficient leakage current to flow under earth fault conditions on the pole to present a hazard to persons in the vicinity of the pole, however no matter the treatment, similar conditions exist. He also noted from his studies that natural wet weather conditions seldom exceed moisture levels of 20%. This detail shall be useful in simulating wet weather conditions for a wooden pole which are realistic. Clarke et al. [32] showed that wood treatment with a salt formulated preservative (such as creosote) increased the electrical conductivity of sapwood samples compared to that of water treated samples (such as Copper Chromium Arsenate (CCA) preservative) at the same moisture content. Thus, utilising CCA treated wooden pole decreases the leakage current that would flow for an equivalent creosote treated wooden pole, adding another factor which may alter the characteristics of when a pole top fire may start.

Filter [33] investigated the electrical performance of CCA treatment compared to pentachlorophenol (PCP). He concluded that pole fire starts are two to three times more likely in CCA treated poles compared to PCP treated poles. PCP was widely used as a wood preservative from the mid-1930s, however in later years was found to be extremely toxic to humans from ingestion and inhalation exposure [43]. The ceasing of PCP treatment has had the unfortunate consequence of increasing the likelihood of pole fire starts owing to different treatment.

Lusk et al. [34] investigated causes and cures of Extra High Voltage (EHV) wood pole fires. Several wood tower fires had occurred that could not be explained by known causes.

The cause was found to be owing to high electric field impinging on the pole surfaces, so that when the surface layers of the pole were moist, the wood became sufficiently conductive to act as an electrode for the conductor-tower capacitive coupling currents. This conclusion added the conductor capacitive coupling as another cause of pole top fire, rather than the leakage current. However, this finding does not add capacitive effects of the pole itself on phase shifting of leakage currents at voltages lower than EHV, nor does it investigate the effect of variation in applied voltages.

Filter et al. [35] proposed a wooden pole resistive network model for understanding leakage current for the purposes of calculating body current of personnel working on a wooden pole. His results showed that older models forecast pessimistic (that is, high) body currents, however the authors' modelling did not account for capacitive effects of the pole nor variation in applied voltages altering the resistance, and hence leakage current.

Al-Dabbagh et al. [36] proposed an improved mathematical model for leakage current with various wood parameters using dimensional analysis, concluding their model takes into account various environmental factors including temperature, humidity, atmospheric pressure and resistance. However, the authors' model did not account for capacitive effects of the pole nor variation in applied voltages altering the resistance and leakage current.

Rasara et al. [37] and Wong et al. [38] investigated extensions to the wooden pole model considered by Filter [35], concluding that under normal dry conditions that the majority of leakage current travels through the heartwood. However, their modelling did not account for capacitive effects, variation in applied voltages, weathering (environmental exposure) conditions of the pole, nor wet weather conditions.

Following this review of leakage current signature for wooden pole, it is now clear that previous research has not considered the phase shift between the supply voltage and leakage current, only considering purely resistive wooden poles.

2.4 Leakage Current Signature on High Voltage Insulators

Contamination of the surface of the insulator reduces the breakdown strength and increases the tendency to flashover, which is damaging to insulators. It is the most common cause of flashover in industrial and coastal areas which often leads to power blackouts [44]. Leakage current on a contaminated insulator heats up the pollutant on the leakage path leading to pole top fires and consequential power outages. On the east coast of Australia, where most of the power distribution poles are made of wood, the heat generated by leakage current can burn the pole and cause catastrophic events such as bushfires [45]. Therefore, regular maintenance is of much importance. Usually, insulators are washed and inspected on a routine basis to remove heavy contamination from the surface of each insulator. However, this is very costly and time consuming. In the past decade the period between inspection of insulators in Victoria had been increased from 3 to 5 years owing to the benefits on new condition monitoring methods which reduced the likelihood of fire starts. However, this only offset the reduction in the number of fire starts by an increase in the number of fire starts missed by the reduced maintenance [9], that is keeping the number of fire starts constant. This identifies if the insulator condition can be continuously monitored, maintenance programs [46, 47] such as washing for certain parts of the power system may be carried out when critically necessary, particularly during bushfire season.

2.4.1 Leakage Current Signature on Polluted Insulators

There is extensive work on studying the leakage current from high voltage insulators [36, 48–76]. The widely recognized methods to study leakage current are the model-based technique and the spectrum analysis methods. Almost all these works are based on the initial relationship between the critical stress (or voltage) E_c and the maximum leakage current I_{max} derived by Obenaus in 1958 [48].

The physical processes involved leading to surface discharges and partial arcing which

precede flashover are complex. Hampton [49] reported on the voltage distribution along a wet polluted surface of a flat-strip insulator. He concluded that an arc rooted on a cylinder having constant resistivity will propagate along the surface if the voltage gradient in the arc column is less than that along the cylinder. He also showed that when a steamy atmosphere was present, that the arc gradient was considerably higher than a similar arc burning in an atmosphere of air. For an arc formed on a wet polluted surface, the behaviour was more complex, and inconclusive, but this was the first of many models for the progress of the flashover mechanism. Wilkins [50] introduced a model for the case of a discharge burning on a rectangular strip following Hampton's study.

Kawai [52] studied Ultra High Voltage (UHV) line installation arrangements, and observed pronounced nonlinearity on standard insulator strings, while also noting that some parts of an insulator did not 'flash' during a flashover, hence introducing the concept of 'effective leakage distance'. Rizk [53] examined in detail models based on the initial work of Obenaus [48]. Many models have been proposed for both static and dynamic arc modelling of both alternating current (AC) and direct current (DC) voltages. His model describes a dynamic arc equation, arc ignition and re-ignition, arc propagation speed, the insulator with a leakage path length, surface resistivity owing to its pollution and form factor describing its shape, and circuit equations for modelling the leakage current signature. This model contains an arc and surface resistances shown diagrammatically in Figure 2.1 which can be modelled as an electrical circuit as shown in Figure 2.2, where I_L is the line current, I_{leak} is the leakage current on the polluted insulator, R_{pol} is the pollution resistance per unit length of the insulator, I_{arc} is the arcing current between a skirt and shed of the insulator, I_{pol} is the current which continues to flow along the polluted insulator while arcing, L is the leakage path along the entire insulator, L_{arc} is the length of the arc between the skirt and shed, and R_{arc} is the arc resistance per unit length.

The AC model combines Rizk's direct current DC model with an arc reignition model,

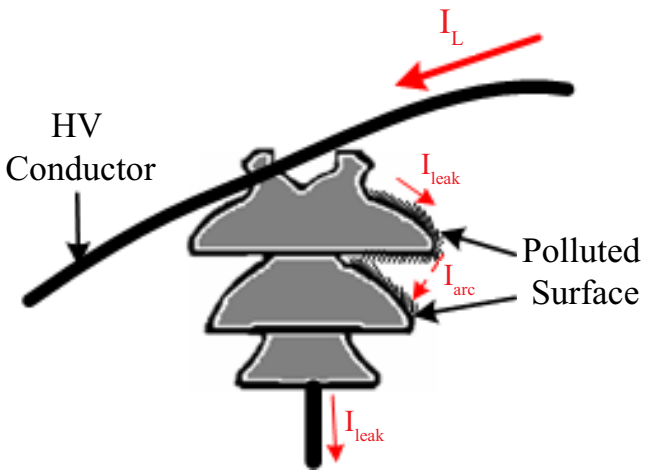

Fig. 2.1 Polluted insulator

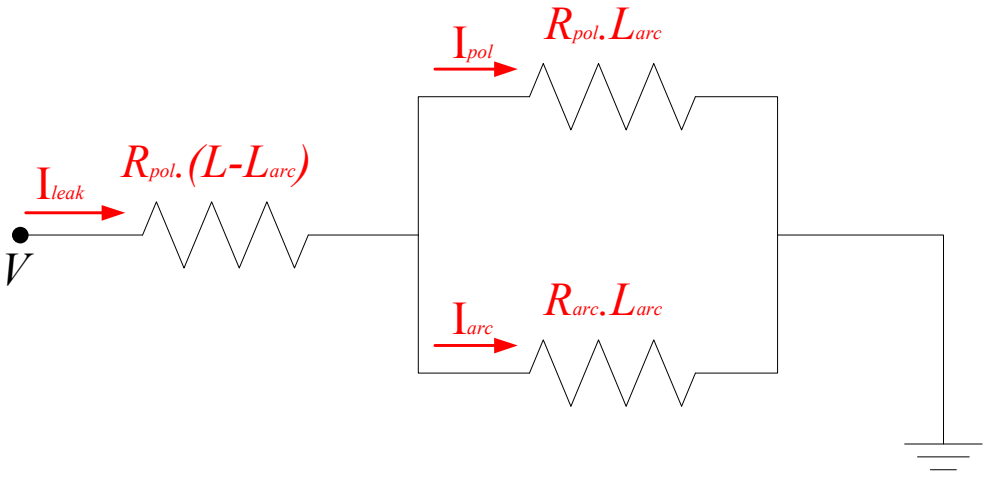

Fig. 2.2 Insulator leakage current circuit

owing to the AC arc being extinguished as the current passes through zero each half cycle. This model forms a switched set of simultaneous differential equations containing the paramaters listed above, which Rizk et al. [54, 55] later studied in greater detail, investigating the effects of the voltage source parameters on the flashover voltages, finding leakage current pulse is influenced by the source parameters. These studies conclusively found that leakage current observations are necessary to understand insulator arcing and the flashover process.

Verma [65, 77] measured the peak leakage current I_{max} and correlated the current with the flashover voltage, determining a criterion for pollution flashover. He hypothesises that insulator flashover is imminent (that is, inevitable) if the leakage current peak exceeds 100 mA, with flashover occurring within about 10 ms. However, this hypothesis has no practical application, as protection mechanisms take in excess of 25 ms to operate, and have no useful application to condition monitoring to pre-empt a pole top fire.

Ely et al. [65, 78] proposed a 'booster shed', which is an additional moulding fitted to an insulator skirt to prevent the bypassing of leakage path by cascading water while suppressing the discharge running between the booster shed and the insulator skirt. The booster shed was shown to increase the flashover voltage during light wetting, however performed less effectively during salt fog. Furthermore, with a booster shed fitted, this hinders the effectiveness of washing during heavy rain or at periods of routine maintenance. This technology has not been pursued owing to the increased costs of fitting and maintenance but rather, changes to the insulator design, by way of material and form factor (that is profile) have served as better solutions [79–83].

Holtzhausen et al. [56–58] investigated the application of prior theoretical models to predict the flashover of practical post type insulators, finding that arcing parameters vary with pollution severity, attributable to the arc across dry bands not following the insulator surface, but rather taking shorter routes as illustrated in Figure 2.1.

Dhahbi-Megriche et al. [59–61] refined previous models [48–50, 53] that simplified the

representation of a propagating arc in series with the resistance of the polluted layer. They proposed a new arc propagation criterion based on an equivalent impedance of a whole electrical circuit simulating the polluted insulator on which an arc propagates. This new criterion altered the leakage current output of the model, and aligned with measured leakage currents in the laboratory. The authors later [62] extended their model from uniformly polluted insulators to discontinuously polluted insulators which was validated experimentally.

Piah et al. [64] applied a dimensional analysis technique to develop a model which describes the behaviour of leakage current and electric field under environmental stresses. Dimensional analysis techniques were employed by Rizk [53] and Al-Dabbagh et al.[36] which can prove useful when examining changes in atmospheric pressure or altitude, ambient temperature, relative humidity and other environmental parameters.

An equivalent RC circuit was employed to describe the behaviour of the non-uniformly contaminated insulator at the fundamental frequency by Douar et al. [63], similar to the behaviour proposed by Dhahbi-Megriche et al. [62]. This model-based technique looks into the leakage current generation mechanism underlying the phenomenon where some general principles were used for the prediction of flashover. However, in terms of giving quantitative indications, the above model-based methods have limited effectiveness owing to the difficulties in building accurate models for a large variety of insulators.

2.4.2 Leakage Current Signature in the Stage prior to Flashover

Past research has found that the surface discharge of the contaminated insulators has several distinctive stages prior to the development of flashover [46, 84–87] suggesting it may be possible to predict the flashover by observing the status of the discharges. Leakage current, which carries important information reflecting the working condition, or health state of an insulator, can be monitored and analysed for flashover prediction and contamination level estimation purposes [44–47, 49, 63, 84–93]. Li et al. [84] classified leakage current into

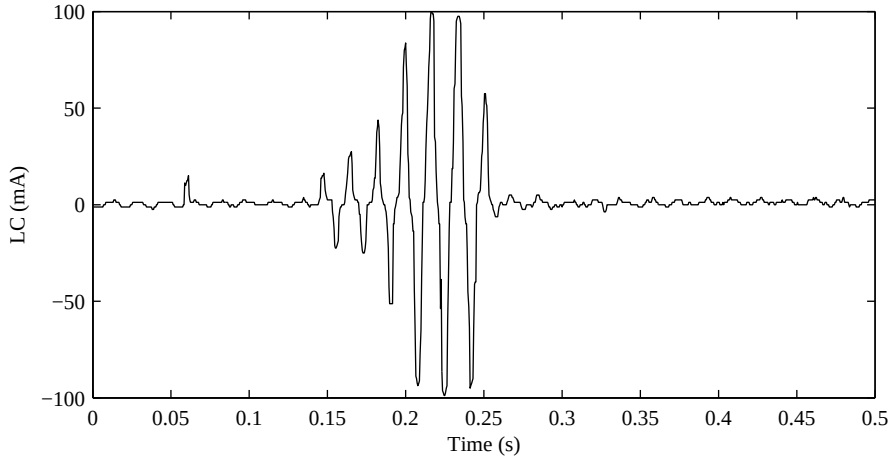

Fig. 2.3 A typical leakage current waveform in the transition stage prior to a flashover.

three stages: (a) the security stage (where there is minimal elevation in leakage current); (b) the forecast stage (where there is considerable arcing, usually in a 25 minute window prior to flashover); and, (c) the danger stage (where flashover is only minutes away from occurring). Suda [85–87] also classified leakage current into stages prior to flashover: (1) no discharge; (2) faint discharges with no visible signal; (3) some visible point discharges; (4) linear weak local arcs; (5) intermittent strong local arcs; (6) intermittent stronger local arcs (just before flashover); and, (7) flashover.

Following these established concepts, there is a stage prior to flashover where the leakage current appears as isolated peaks that occur with increasing frequency [84–87] owing to the increasing intensity of arcing activity [46]. The waveform is aperiodic which is a typical phenomenon during the period prior to flashover, caused by arcing between the skirt and shed of the insulator. This stage is the *transition period* prior to flashover. An accepted typical leakage current waveform during the transition period stage is depicted in Figure 2.3 [46], where the supply voltage has a frequency of 60 Hz.

2.5 Signature Analysis Methodologies

2.5.1 Leakage Current Signature Analysis Techniques and Hypotheses

To form hypotheses of how the leakage current signature may be utilised for characterising insulator conditions approaching flashover, researchers have proposed and tested many analysis techniques. Leakage current spectral analysis examining harmonic content [44, 84–87, 94–99], leakage current envelope analysis using linear stochastic methods [46, 100–102], and leakage current multi resolution analysis using discrete wavelet transforms (DWTs) [63, 103] have all previously been tested.

Spectral analysis is very useful providing quantitative measures for the severity of surface discharge of insulator. It is widely adopted in the analysis of leakage current. In 1996, Shah [94] conducted the first study of harmonic components of an insulator's surface leakage current, showing a correlation with arcing activity of wetted insulators. Karady et al. [44, 95] investigated leakage current waveforms using high resolution digital spectrum analysis methods, finding the relative magnitudes of the odd harmonics in the leakage current increase with increasing arcing intensity. Furthermore, significant growth of the third harmonic component was observed, reaching 20% of the fundamental component prior to flashover.

Suwarno [97] examined the spectrum of leakage current on a 20 kV post-pin ceramic insulator under various contamination conditions. He found a significant correlation between the total harmonic distortion (THD) and the surface condition of the insulator. El-Hag [96] tested the surfaces of non-ceramic insulators, characterising the third harmonic component of leakage current as an indicator of dry-band arcing. Furthermore, the degree of insulator surface degradation could be identified using the fundamental and third harmonic components of the leakage current.

Ahmad et al. [98] tested these hypotheses of Karady et al. while studying the ageing of

insulators. Ahmad found that the third harmonic component appears only in aged toughened glass insulators, concluding that the third harmonic component may be used as an indicator for ageing of toughened glass. Bashir et al. [99] also tested these hypotheses on ageing insulators. He found numerous results from their study including: (a) THD corresponding with the degree of ageing; (b) a strong correlation between the ratio of the third to fifth harmonic amplitudes and the degree of ageing; and, (c) distinct odd harmonic features corresponding to insulator ageing. Kordkheili et al. [47] also proposed using harmonic ratios for attempting the forecast of a flashover, in particular the ratio of the fifth to third harmonic component. These studies show apart from contamination and wetting, ageing also influences the harmonic content of leakage current on insulators.

Profiles for leakage current from a high voltage insulator in the frequency domain were built by Suda [85–87] and continued by Li et al. [84]. Harmonic phenomena of the leakage current were observed prior to flashover occurring. Frequency spectrum analysis was also adopted by Richards et al. [88] to investigate the leakage current on an insulator exposed to various humidity levels.

Karady et al. [100] applied a new technique using extreme value theory for analysing the leakage current signature, where the risk of flashover was hypothesised as increasing with increases in the levels and frequency of large excursions from the leakage current envelope. His findings were inconclusive, however dependent on measuring leakage current, which is impractical for power distribution lines.

Amarh et al. [46, 102] presented the notion of level crossing activity (LCA) applied to leakage current, relating the mean distance between successive crossings of the envelope at the prescribed level. Fast Fourier Transforms (FFTs) were adopted to calculate the leakage current envelope. By tracking this measure, he hypothesised that the risk of flashover correlated with the LCA measure. Again, this measure is dependent on measuring insulator leakage current, which is impractical for application to power lines.

Another technique applicable to analysing leakage current is a wavelet-based method for multi resolution analysis (MRA) [104, 105]. This method has previously been used for detecting high impedance faults (HIFs) [106–110]. Chandrasekar et al. [103] utilised this method to investigate the leakage current and the phase angles between the applied voltage and leakage current. The discrete wavelet transform (DWT) was employed to understand the time-frequency characteristics of the leakage current, while FFTs were used to calculate the magnitude of the phase angle between the applied voltage and the leakage current. The authors concluded the phase angle analysis to be useful in predicting surface wetness, while the MRA was inconclusive. Douar et al. [63] also investigated the flashover process and leakage current on an insulator using the same methods as Chandrasekar et al., albeit under non-uniform contamination conditions. Their results identified pollution severity with the MRA representation of leakage current.

One further technique used for the detection of HIFs not yet trialled on leakage current is fractal analysis. The next section shall review fractals in more detail.

The above review of leakage current signature on high voltage insulators identifies that there is no analysis for measuring the nonlinearity of the full leakage current signature, nor is there any analysis of leakage current interharmonics. Furthermore, each method studied is limited to a particular model or insulator, with no generic measure for detecting abnormal leakage current signature from any type of high voltage insulator.

2.5.2 Fractal Dimension and its Application to High Impedance Fault Detection

Section 2.5.1 described how leakage current signature may be analysed to forecast the circumstances which lead to a pole top fire. Leakage current during this period of time appears intermittently as a High Impedance Fault (HIF). There has been some research in recent years [111–113] on using fractal dimension as a HIF detection technique, owing to the ef-

fective impedance constantly and randomly changing as the fault's arcing activity increases. This leakage current activity or signature in turn causes the fault current magnitude to be very chaotic. This section is devoted to fractal dimension and its application to HIF detection.

The study of fractals and fractal geometry are best suited for describing or simulating natural objects and processes than the shapes and ideas and constructions from Euclidean geometry. Fractals' complexity and infinite detail are suited to analysis where the usual quantities of traditional geometry such as length, area, volume and so on do not give enough information. The work of Mandelbrot [114] has shown the concept of *fractal dimension* as a powerful tool for this purpose. For example, snowflakes, crystals, lightning, ferns, signals, or even systems of blood vessels can all be described by fractals easily, whereas Euclidean geometry has difficulty in achieving this. However, the concept of fractal dimension is a varied one and so there are many different definitions of fractal dimension, both theoretical and practical.

The method most appropriate for analysing the leakage current signature's fractal dimension, is debatable as there are several fractal dimensions proposed as measures of a chaotic system's behaviour. The general case of fractal dimension is the *generalised dimension* [115] with square coverings of size r being defined as

$$d_q = \lim_{r \to 0} \frac{1}{q-1} \frac{log \sum_i P_i^q}{log r} \tag{2.1}$$

where P_i is the probability that a point is in a square i. The fractal dimensions that shall be used for measuring leakage current signature are three specific cases of the generalised dimension. The case $q = 0$ produces the *box-counting dimension* or *capacity dimension* or simply *box dimension* ($d_b = d_0$), the case $q = 1$ produces the *information dimension* ($d_i = d_1$), and the case $q = 2$ produces the *correlation dimension* ($d_c = d_2$).

The relationship between these three fractal dimensions is given by the following in-

equality [115]:

$$d_c \leq d_i \leq d_b. \tag{2.2}$$

This is a theoretical equation, which may not necessarily always hold, depending on the quality of the estimation of each fractal dimension.

Ko et al. [111] successfully applied fractal dimension to a HIF to extract arcing fault current properties. Mamishev et al. [112] were able to detect a signature of a HIF by applying fractal analysis to time series data post-fault, although they found direct calculation of fractal dimension somewhat ineffective when examining small data sets. Zhao et al. [113] used the box dimension to detect a single phase HIF by analysing the zero-sequence current.

Following this review, and to the author's knowledge, there has been no attempt of researchers to apply fractal dimension to leakage current signature as a technique for forecasting incipient pole top fires. Fractal dimension has successfully been applied to other high impedance faults, making leakage current signature an ideal candidate.

2.6 Leakage Current Signature on Power Lines

Very little research has been performed in leakage current signature on power lines [116, 117]. There has however been some research into High Impedance Fault (HIF) detection in power distribution systems using artificial neural networks (ANN) based algorithms and wavelet transform based algorithms [106, 108–110, 118]. One study also examined the impulse response of a power line for HIF detection [117]. An incipient pole top fire is a type of HIF.

Kanashiro et al. [116] studied distribution and transmission lines exposed to coastal and industrial pollution. Insulators were installed at corresponding sites for testing, then, by measuring leakage current and calculating contamination based on that leakage current, suitable insulators for distribution lines were selected. This study corroborated laboratory

tests with field tests to choose suitable insulators for coastal and industrial regions. So, by design, the insulators selected were chosen to prevent flashover. The authors did not address whether these insulators may be mounted on wooden poles, which could serve as a source of fuel for starting a fire if there is any associated leakage current power dissipation.

Silva et al. [117] studied the impulse response of one power line for the purposes of HIF detection. Once the impulse response was first measured, this could be used to monitor operating response of the power line. This concept was tested on a radial feeder with approximately 120 km of conductor. The technique was capable of identifying HIFs with no current, or with current in the order of milliamps; and arcing was also detected. This technique requires keeping a record of the impulse response for each feeder, which can change whenever a power system operator changes the configuration of the network. Owing to the technique not being adaptable to configuration changes, this makes it an unattractive technique to power distribution companies.

Sharaf et al. [119] proposed using relay protection that would detect and discriminate harmonic ripple on a radial power line. As tuning of this relay is necessary, any new loads or changes to the power network configuration may require re-tuning of this relay to prevent unnecessary trips. Owing to the high serviceability necessary to ensure this relay functions as expected, this is not a solution power distributors would employ.

Several authors [106, 108–110, 118] have investigated using artificial neural networks and wavelet transforms for HIF detection. Each study requires a feature for fault discrimination, for example the third and fifth harmonic components of voltages and currents [118]. In this case the algorithms learn how to discriminate that fault. In the case of leakage current signature, there is not necessarily a specific harmonic to detect, rather, the nonlinearity and the changes in nonlinearity are of interest. The studies performed do not address these features of leakage current signature.

Following the review of leakage current signature on power lines, at the time of writing

and to the author's knowledge there was no study into the nonlinearity of leakage current signature for High Voltage insulators mounted on wooden poles forming power lines.

2.7 Real-time Leakage Current Monitoring Systems

Since 1988, there have been many proposals for a monitoring system that tracks leakage current on polluted insulators [120–126]. Khalifa et al. [120] proposed an apparatus that mounts at the base of an insulator chain or a busbar support which monitors insulator pollution by sensing and analysing leakage current bursts. If these bursts are judged to correspond to dangerous pollution levels, then the apparatus transmits an alarm signal to service crew. The bursts were simply judged on the number of times the leakage current magnitudes exceeding 45, 60, 75 and 90 mA. The previous sections have indicated that the magnitude of the leakage current signature which may cause power pole fires may never reach 45 mA, and is dependent on the leakage current signature rather than its magnitude alone. This method also requires the mounting of apparatus on each and every insulator, which is an expensive exercise for condition monitoring after equipment installation. However, this was the first attempt at tracking insulator pollution levels by monitoring leakage current.

Isaka et al. [121] developed a real-time system that simultaneously recorded visual partial discharge and leakage currents on direct current insulator surfaces. The authors determined a sampling frequency of 1.0 kHz was sufficient for recording leakage current that monitors partial discharge. However, this system is only suited to a laboratory for testing, rather than a full implementation across a distribution network.

Vlastos et al. [122] monitored leakage current on silicone composite insulators during severe salt-storms on the Swedish coast. This study again fitted apparatus to the high voltage assets which was then connected to data collection equipment via coaxial cable to a sheltered location. The collected data was transferred to a computer at a later stage for analysis. This system monitored and recorded current in real-time, however had no logic control

mechanisms. Unfortunately, the system requires adding apparatus to the existing equipment for monitoring but was a useful tool for observing in-service leakage current behaviour.

Kamwa et al. [123] proposed real-time tracking of harmonics in a stressed power system using Fast Fourier Transforms with time-domain windowing and frequency-domain interpolation. The authors also proposed another method utilising a combination of the fundamental frequency with a Kalman filer based harmonic analyser. They demonstrated that these advanced spectral analysis tools are necessary for correct assessment of total harmonic distortion when harmonics are changing, even slowly. Saiz et al. [124] developed hardware which enables continuous real-time tracking of harmonics of a power system. The hardware uses a Kalman filter to monitor specific harmonics as well as harmonic distortion. Further hardware development could turn this hardware into an Intelligent Electronic Device (IED) to interface with a SCADA for supervising harmonic distortion at each location the hardware is installed. However, this hardware does not directly monitor leakage current.

Lee et al. [125] proposed a device that monitors and discriminates the resistive and capacitive leakage currents of surge arresters in real time. The authors showed that their proposed algorithm for discrimination provided a better response than existing devices that use the detection method of the third harmonic magnitude component of leakage current. This study again required the installation of additional equipment for tracking leakage current but did prove successful.

Hengzhen et al. [126] hypothesised a leakage current online monitoring system for tracking insulator surface contamination, however their proposal is vague and would require monitoring of each and every insulator to calculate contamination levels which is impractical. After reviewing real-time monitoring systems related to leakage current and harmonic content, it is clear there is currently no real-time monitoring system for tracking leakage current signature on power lines and forecast incipient pole top fires.

2.8 Industry Practice and Asset Management Techniques

At the time of this literature review, there is no technology that specifically targets the detection of incipient pole fires within a distribution network. The nearest equivalent is research being carried out by the Electric Power Research Institute (EPRI) in North America. EPRI propose a Distribution Fault Anticipation (DFA) technology [127, 128], where IEDs on 60 power line feeders are collecting large volumes of data for developing fault and incipient fault detection methods. The DFA technology is only at a research stage, without any peer-reviewed research articles.

The corona camera is an off-line condition monitoring technology which can measure the partial discharge (PD) phenomenon of an electrical asset [129]. This technology has been used in the United States for pole fire detection during routine inspections, and proven useful. However, manual scanning of power lines is a time-consuming and costly process, so for practical reasons, can only be used under a targeted condition monitoring approach. Following the catastrophic 2009 Victoria bushfires and the Victorian Bushfires Royal Commission [9], one recommendation was for the biannual thermal scanning by corona camera on two distribution feeders which run through the Otway Range, highly prone to bushfire. Clearly, if a real-time leakage current monitoring system was available, then that technology would be highly suited to these two distribution feeders.

Other products which measure leakage current like those investigated in Section 2.7 have been trialled in Victoria, however require the installation of measuring devices attached to, or in the vicinity of each insulator being monitored. In addition to the device itself, this requires outages for installation, as well as installation and commissioning labour, becoming a very costly exercise for just a handful of insulators. The only other alternatives for reducing the likelihood of pole top fires are state-of-the-art asset replacements during maintenance cycles and other technologies which utilise existing secondary systems already in place.

One of the distribution utilities in Victoria has implemented a risk-based model for pole

Table 2.1 Asset attributes used by industry to risk rank a possible pole top fire event [3]

impact on supply reliability/quality	crossarm material
impact on public safety - wildfire ignition	crossarm age
impact on public safety - electrical contact	number of crossarms
pole age	pole species
insulator type	insulator number
structure voltage	structure type/complexity
location - geography/environment	period since last inspection
outstanding defects	restoration time & cost

top fire mitigation [3]. This model places a score on each pole determined by the 16 asset attributes in Table 2.1, and ranks the poles to prioritise mitigation solutions. These solutions include replacing existing timber crossarms with steel crossarms (for example the arrangements in Figure 1.4); replacing fog pin insulators with post insulators; applying silicone coating to in-service insulators [130]; electrically bonding all insulator pins together; tightening loose hardware; and washing. However, none of these solutions account for any drying of boron grease placed in drilled holes housing bolts which mount assets to CCA impregnated poles [131].

Ward [3] reported an analysis based on 298 poles over a 12 month period finding poles with pole top fires for 66 kV poles being approximately three times the rate of 22 kV poles. The risk-based model was weighted to reflect this finding. There was no apparent reason for this increased rate of pole top fires for 66 kV assets.

Australian Standards and guidelines only require overhead line design to minimise the risk of flashover, not for prevention [132, 133]. Hence, by design, insulator arcing is expected to occur at some stage. Furthermore, polluted conditions only incorporate insulator creepage (or leakage) distance and clearance in the design [134], with no requirement placed on the leakage distance of the pole.

Reviewing the current industry practice, and the standards and guidelines which they are governed by, there is clearly a need for technology which can monitor leakage current activity for power lines. Furthermore, identifying assets that require attention prior to any

failure provides some time to plan and coordinate asset maintenance and/or replacement, in turn reducing the cost when compared to an otherwise unplanned outage caused by a pole top fire.

2.9 Key Issues Identified

Following the comprehensive literature review performed in this chapter, the subsequent key issues were identified:

1. Previous research on wooden poles has only considered resistive models, and hence never observed a phase shift between the leakage current and the applied voltage;
2. There is no measure which quantifies the nonlinearity of a high voltage insulator;
3. Research studies have all focused on harmonic components for identifying features of high voltage insulators ignoring any leakage current interharmonics;
4. Mathematical modelling in past research has been insulator specific and so leakage current signature cannot be measured generically;
5. There are no studies of leakage current signature of power line feeders; and,
6. There is no understanding of why 66 kV pole top fires occur at a rate three times greater than the rate of 22 kV pole top fires.

2.10 Summary

This chapter has presented a comprehensive review of leakage current from insulators mounted on wooden poles. After explaining incipient pole top fires, leakage current signature for wooden poles is discussed in detail. The factors which affect leakage current signature on high voltage insulators are then addressed, including analysis techniques which have been

useful in gaining understanding of the leakage current signature. Combining insulators and wooden poles to form power lines with a leakage current signature was then discussed, in particular, how to implement a real-time system for monitoring power lines for incipient pole top fires. Current industry practices for addressing pole top fires were reviewed. Finally, key issues pertaining to leakage current and incipient pole top fires arising from the literature review were highlighted.

Chapter 3

Systematic Investigation into the Effective Impedance of Wood Used for Poles

3.1 Overview

This chapter starts by investigating an unconventional type of pole fire occurring at the bolt mounting a transformer to a wooden pole. This important investigation will lead to establishing a typical impedance characteristic of wooden poles used for mounting crossarms and high voltage insulators, which may be used in later smart monitoring analyses. Section 3.2 provides a background to wood used for power poles. Section 3.3 presents the configuration of the wooden pole, transformer, crossarm and high voltage insulators, the pole fire event, the climate and the environmental conditions. Section 3.4 describes the configuration of the laboratory experiment to study the factors which contribute to initiating the pole fire. Section 3.5 presents the methodology used and describes the results for (a) validating the simulated wet weather conditions, (b) thermographic imaging tests of the electrodes wood-metal connection points, (c) testing the pole surface conductivity, and (d) measuring and

calculating the leakage currents of the wooden samples. Section 3.6 follows on with studies that thoroughly investigate the effective impedance of the wooden pole samples, including the circuit configuration required to provide the observations, and circuit analysis deriving the system of equations necessary to make these observations. The operating voltage levels, the type of metallic electrode, the spacing of those electrodes, and the effect of Copper Chromium Arsenate (CCA) impregnated wood and its weathering are then considered. Section 3.7 discusses why the observations of these studies occurred. Section 3.8 summarises the findings and deduces environmental factors and the pole configuration creating the right circumstances for the resulting pole fire. Furthermore, a typical impedance characteristic is deduced for CCA impregnated wooden poles used in the Victorian distribution network.

3.2 Preliminaries

The literature review established leakage current signature as the most useful way to identify and detect incipient and imminent wooden pole fires in Section 2.2. A number of alternative solutions for preventing pole fires were examined in Section 2.3. However, none of these pole top fire solutions have been able to prevent pole top fires occurring around the world. Figure 3.1 shows the pole in-situ after the fire, and part of that pole in the laboratory which is investigated throughout this chapter. The fire occurred at the transformer mount kingbolt junction and as a result the transformer fell to the ground.

Work by Darveniza [28] considered the combination of the impulse strength of wood and porcelain insulation for line design purposes. In other work by Darveniza [29], a comparison between the effect of Copper Chromium Arsenate (CCA) treatment and Creosote impregnation of wooden poles on leakage current flow was studied in detail. Prentice [135] carried out an investigation of pole and crossarm fires occurring in the State Electricity Commission of Victoria in 1950 and found ageing, cracking and shrinkage of wood as the main causes. This investigation focuses on understanding the major factors influencing the

(a)

(b)

Fig. 3.1 (a) Pole damaged by fire at the transformer mounting bolt; (b) part of damaged pole relocated to the laboratory.

electrical performance of wood in an unconventional type of wooden pole fire, that is at the position of a pole-mounted transformer, as well as gaining a better understanding of the electrical performance of a wooden pole in general.

3.3 Pole Fire Event Investigation

The pole fire occurred on a 12.5 metre long wooden pole made of spotted gum species as shown in Figure 3.1. A fuse unit consisting of 24 kV (nominal) insulators was mounted on steel crossarm. A 100 kVA transformer was mounted on a bracket bolted to the wooden pole at a distance of 3 metres from the top end of the pole. A 19/2.0 High Density (HD) copper earth wire was connected to earth via a hole on the side of the bottom bracket. The pole was CCA treated with H5 level in June 2005 as per Australian Standard AS1604.1-2005 *Specification for preservative treatment - Sawn and round timber* [136] and clause 5.2.2 of Australian Standard AS2209-1994 *Timber - Poles for overhead lines* [137]. The pole was

(a) (b)

Fig. 3.2 Pole samples used during testing in the HV laboratory; (a) Sample A, (b) Sample B.

located at a distance of approximately 500 metres from the coast. This pole was in service for approximately 2 years before catching fire and thus being taken out of service.

As depicted in Figure 3.2, both the pole damaged by fire (Sample A) and an undamaged wooden pole (Sample B) were brought into the High Voltage (HV) laboratory. The damaged pole was cut to a length of approximately 2 metres consisting of the top section of the original pole. The top cap of the pole was removed and its cross-section was vertically cut to avoid the effect of paint on the leakage current performance of the wood. The undamaged wooden pole sample was cut to a length of 2.73 metres, the maximum size which was safe to handle within the HV laboratory. This sample was kept in an indoor facility for two years prior to being brought into the HV laboratory and had also been treated with CCA preservative of H5 class. Holes were drilled in the samples to a diameter of 16 mm to ensure a tight fitting of the galvanised bolts and the maximum wood-metallic contact, similar to a typical configuration of a wooden power pole in service. The galvanised bolts were used as high voltage electrode connection points. Nails were also used as high voltage electrode connection points, but with a smaller wood-metallic contact surface area compared to the galvanised bolts.

The high impedance of any wooden pole can be affected by weather conditions, being

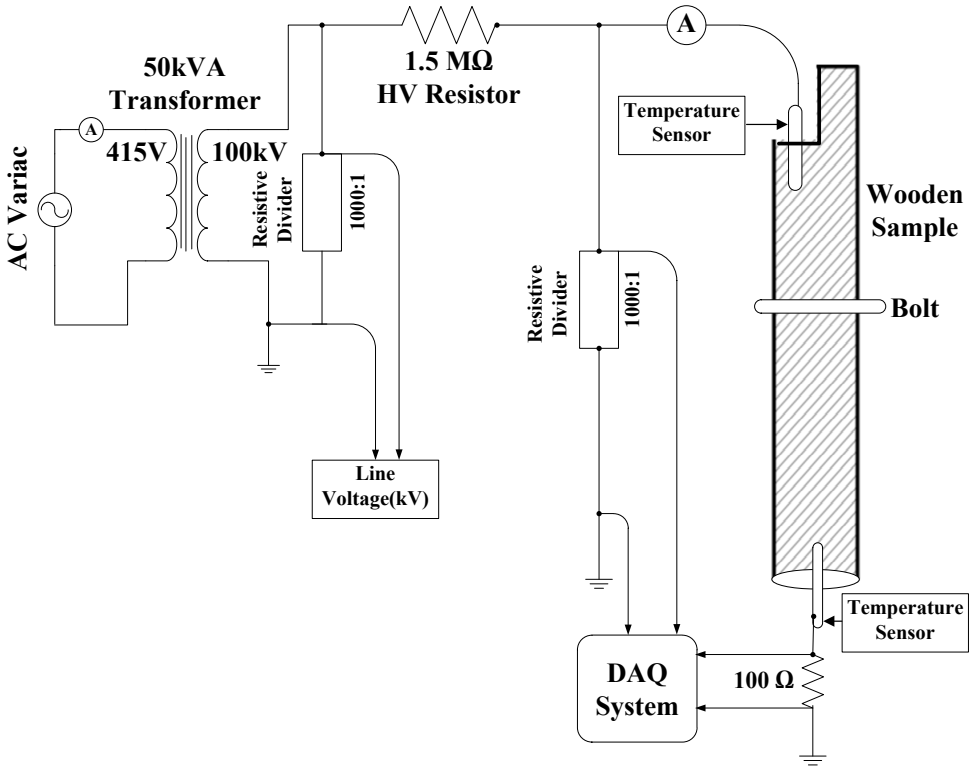

Fig. 3.3 Schematic of testing equipment configuration in the HV laboratory.

reduced to the extent that, in the right circumstances could promote a wooden pole fire occurring. As a wooden pole exhibits a non-linear impedance characteristic, and there is no available literature on this type of impedance, an extensive study was carried out on the damaged pole sample, and a similarly aged undamaged wooden pole sample to understand why certain measured leakage currents flow for varying applied voltage levels.

3.4 Experimental Configuration

The HV laboratory experimental configuration shown in Figure 3.3 consisted of a 50 kVA, 415 V/100 kV, single phase power transformer connected to a single phase Variac, two 1000:1 resistive voltage dividers, a wooden sample, galvanised bolts and nails, a 100 Ω resistor, a Tektronix®, 350 MHz, TDS5034B series digital phosphorous oscilloscope, two temperature sensors and a current clamp transformer ammeter. The Variac was used to con-

trol the voltage applied for a range of experiments conducted as part of the investigation. A 1000:1 resistive voltage divider was connected across the secondary of the transformer to monitor the energised line voltage supplied to the wooden sample via the 1.5 MΩ resistor representing a leaking ceramic insulator. A 1.5 MΩ High Voltage (HV) resistor was connected in series with the transformer secondary and the wooden sample under test. This HV resistor was used to represent a heavily polluted insulator during the tests [138]. The temperature sensors were used for measuring the temperature of the bolts inserted into the wooden samples and the temperature of the HV resistor.

A current clamp transformer ammeter was employed to measure the leakage current flow in the wood. The leakage current through the wooden sample was also calculated by measuring the voltage across a 100 Ω resistor connected to ground in series with each test sample. Another 1000:1 resistive voltage divider was connected across the wooden sample to ground to enable measuring the voltage difference across the wooden sample. The Tektronix®, 350 MHz, TDS5034B series digital phosphorous oscilloscope was used to store experimental data and capture leakage current waveforms.

A ThermoVision® A320 Infrared (IR) camera was used for hot spot tracking of the wooden surface while the samples were being tested. Immediately after testing and isolation of the HV equipment, the spot temperatures of the metallic electrode connection points were removed from the wooden samples under test for measuring. The IR camera used specifies it can measure temperatures between −20 °C and 1200 °C and detects temperature variations within 0.08 °C [139].

3.5 Investigation Methodology and Experimental Results

Fundamental to understanding how to reduce the risk of pole fires are controlling the four fire elements of *fuel*, a *heat source*, *oxygen* [3] and *time*. A typical pole fire is thought to start at the junction of the kingbolt, wooden pole and wooden crossarm, where the crossarm

acts as the fuel source. In this case, there is no wooden crossarm, nor is there any other wooden apparatus connected to the wooden pole, thus the wooden pole itself is the source of fuel.

The heating mechanism in a typical pole fire is at the kingbolt where localised heating is thought to be sufficient with access to oxygen in air-gaps between the kingbolt and wooden crossarm connection, especially after many years of ageing where this connection becomes loose. In this case, with the absence of a wooden crossarm, this heating mechanism must be at the kingbolt and wooden pole connection. Past research has supported the idea of utilising conductive grease [29] to firstly remove the air gap between the kingbolt and wooden pole, and thus removing the access to oxygen at this gap. Secondly the grease provides a conductive path to ground by-passing any air gaps, thus eliminating the likelihood of a pole fire event caused by sparking. Owing to the occurrence of this pole fire event, the theory of eliminating pole fire likelihood utilising mechanisms to remove spark gaps come under question.

The time required for leakage current to cause sustained smouldering may be longer than that of a typical pole top fire, where the fuel source is a wooden crossarm. In this case, the fuel source is the wooden pole itself, thus any interruption of the leakage current prior to the extended time necessary for that smouldering to lead to ignition of the wood could have prevented this fire.

Several key research questions are now posed to understand the sequence of events and the contributing factors leading up to the catastrophic failure and subsequent fire of this particular wooden pole:

- what were the actual causes of this pole fire: was it caused by leakage current, or a short-circuit current, or the failure of the transformer;
- why has this wooden pole fire occurred at the transformer mounted junction bolt rather than the crossarm kingbolt location?

The hypotheses formed based on these key research questions are:

1. a certain amount of *leakage current* triggers smouldering;
2. when a high enough *temperature* of the wood-metallic contact is reached, the wood starts to smoulder;
3. the *surface conductivity* of the wooden pole leads to an increase in leakage current;
4. the leakage current sharply increases under *wet weather* conditions owing to a dramatic reduction in the wooden pole's *resistance* at the operating voltage; and,
5. sustained smouldering for *sufficient time* will lead to ignition and fire.

To verify these hypotheses, the following tests were conducted on both the damaged and undamaged wooden pole samples:

1. Moisture content verification;
2. Thermographic imaging tests;
3. Pole surface conductivity tests;
4. Leakage current tests under dry and wet weather conditions; and,
5. Wooden pole impedance studies

3.5.1 Moisture Content Verification

Saline water of 1.5 mS/cm conductivity was sprayed onto the surface of the wooden pole to simulate a typical 30 minute Victorian coastal rainfall. The middle section was kept dry [33] to simulate that portion of the pole shielded by a pole-mounted transformer, while the top and bottom portions of the samples were sprayed as shown in Figure 3.4. The average moisture of each portion was measured using a Timbermaster® Protimeter moisture meter

Fig. 3.4 An example of a wooden pole sample being tested under wet weather conditions

and is shown in Table 3.1. The wet surfaces of the wooden pole sample were 32% and 30% for the top and bottom surfaces respectively. The average moisture for the dry surface at the middle of the sample was 8%. The Electricity Authority of NSW demonstrated in 1967 [31, 140] that seldom does a wooden power line pole exposed to natural weather conditions reach a moisture level exceeding much more than 20%, so this type of drenching is verified to be a good simulation of rain falling on these partial surfaces of the pole, leaving the middle of the pole dry. This procedure was confirmed as sufficient for simulating rainfall and subsequently used for the leakage current test under wet weather conditions in Section 3.5.4.

Table 3.1 Average moisture content of wood samples.

Sample Position	Weather Condition	Moisture Content
Top	Wet	32%
Middle	Dry	8%
Bottom	Wet	30%
Typical [140]	Wet	18 – 20%

3.5.2 Thermographic Imaging Tests

Infrared thermographic imaging was performed on Samples A and B in the HV laboratory using the ThermoVision® A320 Infrared (IR) camera described in Section 3.4 to study the temperatures reached at the wood-metal connection points. The IR camera captured the heat distribution caused by the leakage current flow through each wooden sample not visible

to the naked eye. The voltage applied to the bolt while inserted into a hole in the pole was increased to cause an increasing leakage current flow through the wooden sample. A sustained flow of leakage current through the wood caused the metallic contacts to heat up and eventually start the smouldering of the wood. At this time point the supply was turned off and the bolt was removed from the wood.

Infrared images of the bolt and the hole where the bolt was inserted into the sample were captured. Figure 3.5 shows the maximum temperature of the metal bolt was 66.7 °C while the maximum temperature of wood in contact with the bolt was 93.3 °C. The magnitude of the RMS leakage current that caused smouldering was measured as 3.2 mA in Sample A and 4.1 mA in Sample B. Further infrared images were taken of the grounding electrode which also exhibited heating. The maximum temperature in this case was 53.1 °C.

The observations verify the heating mechanism of a pole fire occurring at the junction between metallic accessories and wood, with the largest amount of heating occurring at the wood-metal connection point with the greatest surface area contact. This is intriguing as anecdotal evidence suggested that the ignition of pole top fires usually occur at the wooden crossarm junction where the kingbolt connects the crossarm to the wooden pole, with the wooden crossarm serving as fuel to the fire. In the case of crossarm fires, the larger amount of heating may initiate at the pole-kingbolt junction, however as the crossarm wood is of a smaller cross-sectional area compared to the pole then it is more likely to be the first source of fuel from the heating at the pole-kingbolt junction.

3.5.3 Pole Surface Conductivity Tests

A 2 cm × 2 cm area was softly scrubbed using a chisel to obtain an approximately 1 gram amount of wood dust from 8 uniformly spaced locations at either end of the pole. The samples were dissolved in approximately 20 mL of distilled water and the ExStik® EC400 Conductivity/TDS/Salinity Meter was used to measure the conductivity of the solution and

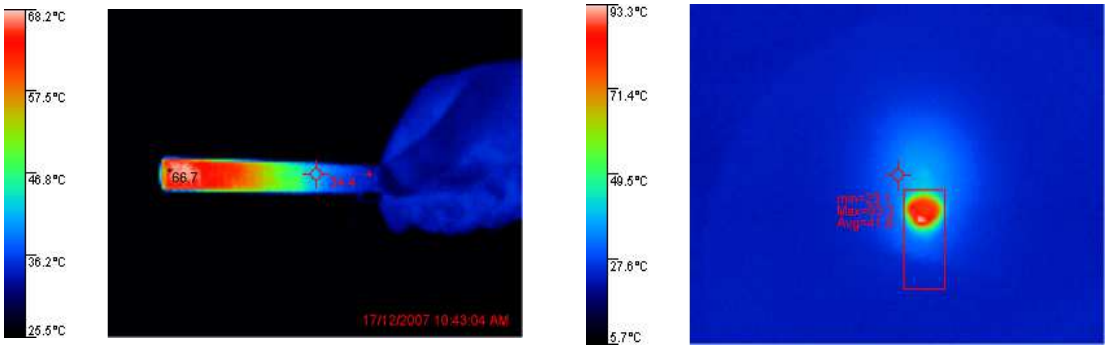

(a) (b)

Fig. 3.5 (a) Infrared image of a bolt removed from bolt-hole immediately after a high voltage causing smouldering was applied; (b) Infrared image of the bolt-hole where the bolt was removed, immediately after a high voltage causing smouldering was applied.

is shown in Table 3.2. The mean conductivity was 13.9 µS with a standard deviation of 1.8 µS.

Table 3.2 Conductivity of eight locations on pole Sample A

Sample Position	Conductivity (μS)
Top-East	14.9
Top-South	13.2
Top-West	16.2
Top-North	14.0
Bottom-East	14.7
Bottom-South	10.4
Bottom-West	14.6
Bottom-North	12.6

While conducting the leakage current tests in the next section, the metallic contact with the wood samples was observed to start heating when a leakage current of a magnitude 4 to 5 mA was flowing. At this sustained leakage current, smouldering of the wood was initiated. With the surface conductivity of the wooden pole Sample A being a mean of 13.9 µS and having a small standard deviation, the conclusion drawn is the deposition of salt on the surface of the wood in this case had no effect on the leakage current activity in the wood.

3.5.4 Leakage Current Tests under Dry and Wet Weather Conditions

The experimental configuration is shown in Figure 3.3. A galvanised bolt/pin was inserted at various locations of the wooden pole sample and was subjected to high voltage through a 1.5 MΩ resistor bank. The base end of the wooden pole sample was earthed through a metal nail. The wooden pole samples were subjected to a leakage current by varying the high voltage applied to the series HV resistor from 0 kV to 50 kV. The measured leakage currents for when the pin was inserted in the top cross-section of a pole sample are shown in Figure 3.6 (a).

The leakage current tests above were repeated under simulated wet conditions as described in Section 3.5.1 with similar voltage levels. The calculated leakage currents for when the pin was inserted in the top cross-section of Samples A and B are shown in Figure 3.6 (b).

Figure 3.6 (a) shows that a higher RMS leakage current was observed for Sample A than Sample B. This could be attributed to Sample A being exposed to a coastal environment and harsh climatic conditions for 2 years while Sample B had been stored in a controlled environment. Laboratory study results by Wickham et al. [26] showed that the treatment, or impregnation, of the wooden pole and crossarm is an important factor in the occurrence of fires. The exposure to weather caused the outer surface impregnation to be leached, thus resulting in a higher contribution to leakage current by the surface leakage current. Thus the results above are validated by the earlier results of Wickham et al. in 1948.

Figure 3.6 (b) shows that while under wet weather conditions the RMS leakage current observed for Sample A is higher than Sample B albeit marginally higher. This can again be attributed to the pre-weathering of Sample A. Now when comparing these results to that of dry weather conditions in Figure 3.6 (a), the RMS leakage current observed is double the magnitude of that in dry weather conditions. This must be attributed to the surface moisture reducing the electrical resistance of both samples, thereby increasing the RMS

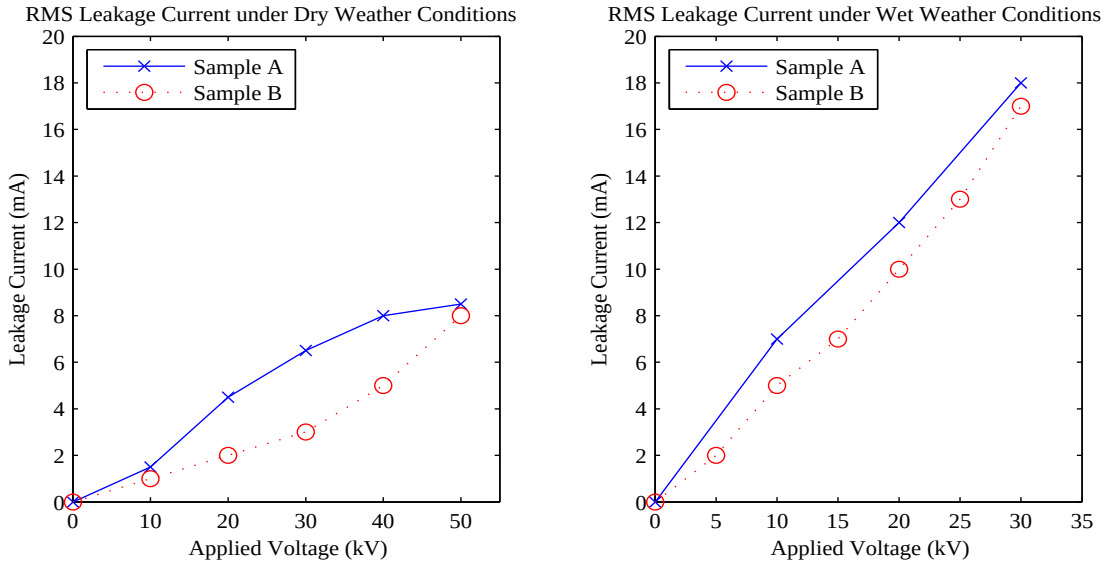

(a) (b)

Fig. 3.6 Leakage current for Samples A and B via a simulated HV insulator under (a) dry weather conditions; and, (b) wet weather conditions.

leakage currents.

3.6 Wooden Pole Impedance Studies

To gain a better understanding of the effect of the wooden pole's impedance has on the pole top insulator leakage current circuit, a series of studies were conducted to evaluate the electrical performance of: (a) the metallic electrodes connecting the wooden samples to the electrical circuit; (b) the resistance of the wooden samples when connected directly to the source voltage; (c) the impedance of the wooden samples when connected to a simulated ceramic insulator; (d) the effect of the electrode spacing across the wooden samples; (e) the effect of the wooden sample being 'un-weathered' and partially dried during storage in a controlled laboratory environment; and, (f) the effect of CCA treatment on the conductivity of wood when compared to an untreated wooden sample. These results can then be compared with the limited published research in this area [29].

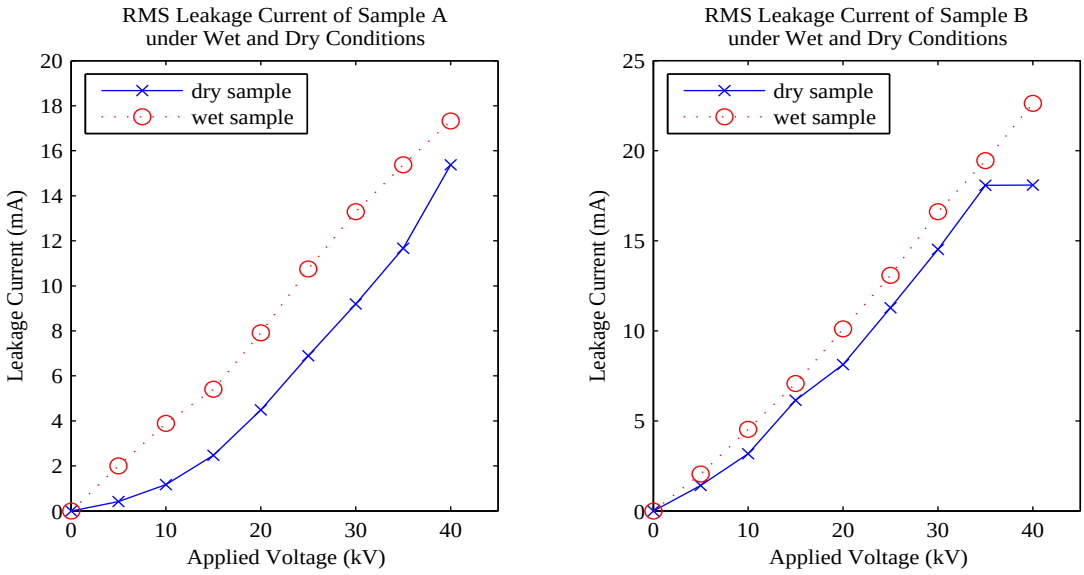

(a) (b)

Fig. 3.7 Comparison of the leakage current for Samples A and B under dry and wet weather conditions, with a direct HV connection to the sample

3.6.1 Resistance Performance Test of a Wooden Pole under Direct HV Connection

The configuration for the resistance performance test is the same as depicted in Figure 3.3 except with the 1.5 MΩ resistor replaced by a short circuit, that is, the resistor was disconnected from the circuit and the high voltage supply was connected directly to the bolt inserted into the wooden pole sample. Thus, simply using Ohm's law, the voltage applied across the wooden pole and the short circuit current through the pole will give the pole's resistance. The short circuit RMS leakage currents for Samples A and B with various applied voltages are shown in Figures 3.7 (a) and (b) respectively. The slope of the line gives the conductivity of each wooden sample under both dry and wet weather conditions, that is the inverse of the resistance.

Now, knowing that these voltages would only ever be applied in an operational pole of a feeder when the conductor becomes detached from an insulator and comes into contact with the pole, the voltage to examine is $V_{ln} = V_s/\sqrt{3}$ where $V_s = 22$ kV is the applied source

voltage, and V_{ln} is the line to neutral voltage, being 12.7 kV in this operational situation. Therefore the resistances of Sample A under dry weather and wet weather conditions were 3850 kΩ and 3290 kΩ respectively. Similarly, the effective resistances of Sample B under dry weather and wet weather conditions were 1680 kΩ and 1970 kΩ respectively. Thus the average resistances and ranges of the samples for dry weather and wet weather conditions were 2760 kΩ ±1090 kΩ and 2630 kΩ ±660 kΩ respectively.

Noting a significant difference between the resistances of Sample A and Sample B, this cannot be attributed to the pre-weathering of Sample A owing to Sample A's resistance being 67% greater than Sample B's resistance in the wet weather condition. The difference in effective resistance is difficult to explain under this extreme voltage condition without increasing the number of samples tested. Examining the average resistances of the samples does show that the resistance under a wet weather condition is slightly less than the dry weather condition. However, under any of these conditions, whether it being a wet or dry pole, the capacitive effect of the wooden pole samples has been ignored, thus producing only a general result. Furthermore, variation in the applied voltage appearing across the pole has also been ignored. To gain a better understanding of the effective impedance of a wooden pole under normal operating conditions, further study is required.

Also worthy of mention is the gradient of the lines in these graphs. When each wooden sample is in a dry weather condition, the gradient is much flatter for lower voltages, and much steeper for higher voltages. This means in a dry weather condition the wooden samples are more resistive for lower voltages, and become more conductive at higher voltages. However, in a wet weather condition, for both samples, the gradient is steep at lower voltages and continues to be steep at higher voltages. This means in a wet weather condition the wooden samples are more conductive than the dry condition, no matter the applied voltage level.

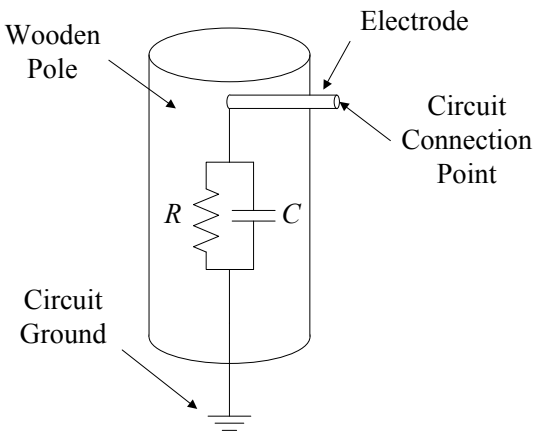

Fig. 3.8 Diagram of the circuit model representing a wooden pole

3.6.2 Effective Impedance Study of a Wooden Pole under Normal Operation

The observations from the testing performed in Section 3.6.1 revealed marked variation in resistances of samples when stressed with high voltages (25% in the wet weather condition, and 40% in the dry weather condition), which may be attributed to ignoring the capacitive components of each sample's impedance. Otherwise, it may be caused by the variation in the applied voltage across each sample. This section will undertake a comprehensive study into the effective impedance of the wooden pole samples under normal operating conditions. In this context, normal operating conditions means the high voltage conductor is tied to an insulator mounted on a crossarm, rather than a conductor directly in contact with the wooden pole. The wooden pole is modelled as two circuit elements, R being the resistive component of the wood, and C being the capacitive component of the wood. This model is shown in Figure 3.8. The literature review found there is no established research on the capacitive component of wooden poles at distribution or sub-transmission voltages [34]. The literature review also found there is no established research on the effect of the variation on the applied voltage across wooden poles.

Table 3.3 Circuit parameters and values

Element	Value	Description
R_{ins}	1.5 MΩ	simulated polluted insulator resistance
R_{xarm}	0 MΩ	metal crossarm resistance
R_2	100 Ω	resistor used to measure leakage current
R	*unknown*	wooden pole sample resistance being calculated
C	*unknown*	wooden pole sample capacitance being calculated
i_2	*unknown*	leakage current through wooden pole sample
V_s	*varied*	applied supply voltage
$V_2\angle\theta_2$	*measured*	voltage measured across R_2
$V_1\angle\theta_1$	*measured*	voltage measured across the pole sample in series with R_2

Circuit Configuration, Circuit Analysis and Study Observations

The circuit diagram for the laboratory configuration of the wooden pole impedance study now using the model established in Figure 3.8 is shown in Figure 3.9 and the circuit parameters are as described in Table 3.3. In this test, the 1.5 MΩ resistor (R_{ins}) is once again used to simulate a polluted ceramic insulator, and owing to the crossarm in operation being of a metal type, no further resistor needs to be added to the circuit (and R_{xarm} is set to zero). The high impedance fault current (i_2) flows through this 1.5 MΩ resistor and through the wooden pole sample via the 100 Ω resistor to ground.

Analysing this circuit to solve for R and C, according to Ohm's Law the voltage across resistor R_2 is:

$$V_2 = i_2 R_2 \tag{3.1}$$

and according to Kirchhoff's Voltage Law and Ohm's Law the voltage across the wooden sample in series with R_2 is:

$$V_1 = i_2 \times \left(R_2 + \frac{R \times \frac{1}{j\omega C}}{R + \frac{1}{j\omega C}} \right) \tag{3.2}$$

where $\omega = 2\pi f$ is the power supply frequency with $f = 50$ Hz. Substituting i_2 from (3.1)

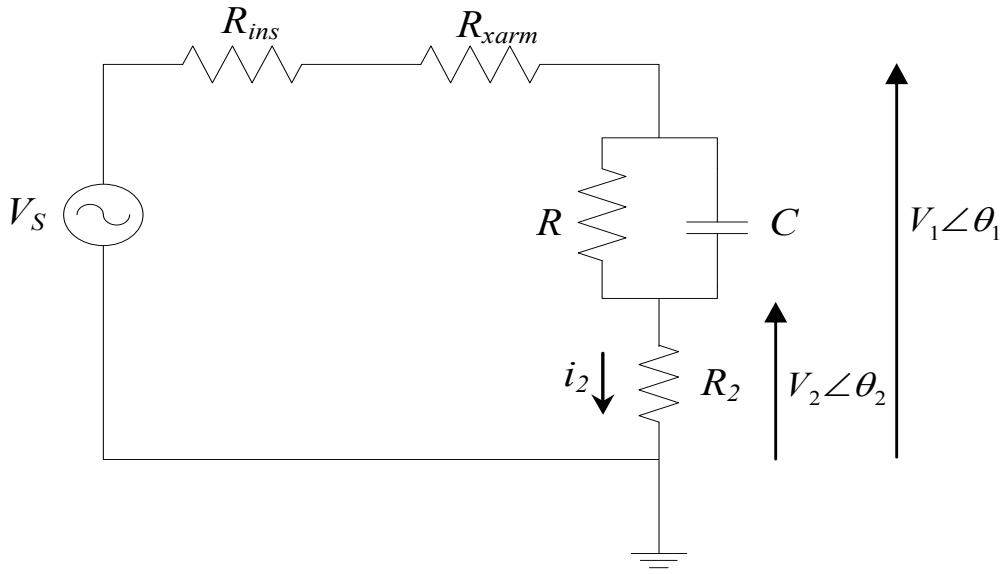

Fig. 3.9 Circuit diagram for pole impedance studies

into (3.2) yields the following equation:

$$\frac{V_2\angle\theta_2}{V_1\angle\theta_1} = \frac{R_2^2 + RR_2 + (\omega R_2 RC)^2 + j\omega R^2 R_2 C}{(R + R_2^2)^2 + (\omega R_2 RC)^2} \tag{3.3}$$

where θ_2 and θ_1 are the phase angles of V_2 and V_1 respectively. Let $\Delta\theta = \theta_2 - \theta_1$, then the left hand side of equation (3.3) can be rewritten into its real and complex components as follows:

$$\begin{aligned}\frac{V_2\angle\theta_2}{V_1\angle\theta_1} &= \frac{V_2}{V_1}\angle\Delta\theta \\ &= \frac{V_2}{V_1}(cos\Delta\theta + jsin\Delta\theta)\end{aligned} \tag{3.4}$$

Now substituting the expression at (3.4) into equation (3.3) and solving for the real and complex components, and noting $R_2 = 100$, the following system of equations hold:

$$\frac{100\omega R^2 C}{10000\omega^2 R^2 C^2 + R^2 + 200R + 10000} = \frac{V_2}{V_1} sin\Delta\theta \tag{3.5}$$

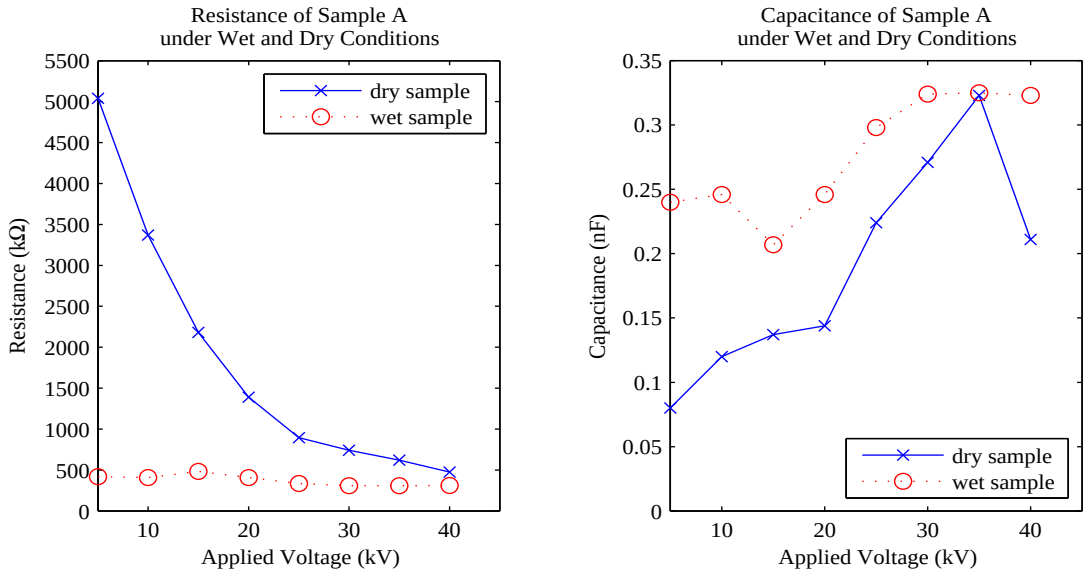

(a) (b)

Fig. 3.10 Impedance Components of Sample A for various applied voltages

$$\frac{10000\omega^2R^2C^2+100R+10000}{10000\omega^2R^2C^2+R^2+200R+10000}=\frac{V_2}{V_1}cos\Delta\theta \tag{3.6}$$

Thus, the impedance of the pole in Figure 3.9 can now be found by solving the system of equations (3.5) and (3.6) for R and C, using the measurements and circuit parameters described in Table 3.3.

By applying various source voltages, and measuring $V_1\angle\theta_1$ and $V_2\angle\theta_2$, the impedance of the wooden pole Sample A under dry and wet weather conditions, as well as the impedance of the similarly aged wooden pole Sample B under dry and wet weather conditions were calculated as described above and are shown as their resistive and capacitive components in Figure 3.10 (a) and (b), Figure 3.11 (a) and (b) respectively.

In general, these results show a dramatic *reduction* in the resistance of both samples under wet weather conditions. Also, as the capacitance of each sample increases under wet weather conditions, this reduces the resistive component of the impedance, which may account for the marked variation in resistance between the samples observed in Section 3.6.1.

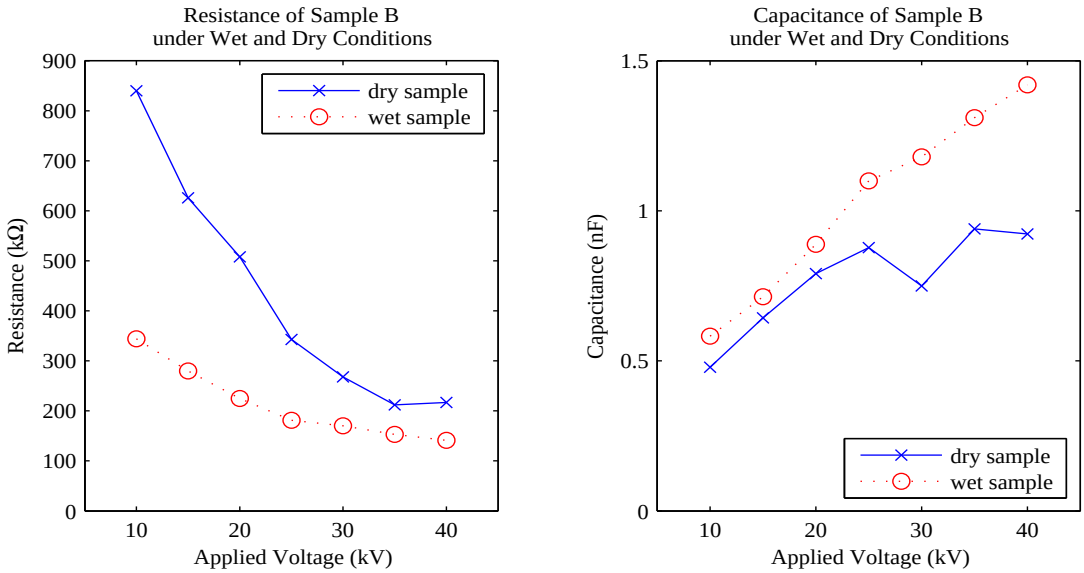

(a) (b)

Fig. 3.11 Impedance Components of Sample B for various applied voltages

This decrease in resistance leads to a higher flow of leakage current, in turn creating higher I^2R power dissipation, ultimately contributing significantly to the heating of wood-metal connection points.

Operating at 22 kV

More specifically, at the nominal operating line voltage of 22 kV (that is a phase-to-ground voltage of 12.7 kV), the effective resistance and capacitance of Sample A under dry weather and wet weather conditions were 2725 kΩ and 0.13 nF, and, 450 kΩ and 0.23 nF respectively. When this sample was directly connected to a high voltage source in Section 3.6.1 the corresponding resistances at this operating voltage in dry and wet weather conditions were 3850 kΩ and 3290 kΩ respectively. These values were calculated by using the inverse gradient as an estimate for the effective resistance. However, this method is sensitive to changes in the leakage current measurements for the selected applied voltage levels and neglects the nonlinear nature of the resistance observed in Figures 3.10 and 3.10 where the linear estimation has a nonzero intercept. By using circuit analysis with appropriate mea-

surement of voltages and phase shifts, the leakage current measurement sensitivity has been eliminated while revealing the nonlinear impedance components of the samples as the applied voltage varies. Now the observed effective resistance under wet weather conditions is approximately one fifth of the effective resistance under dry weather conditions, that is, the effective resistance is significantly reduced. Furthermore, when taking into account the capacitive component contribution to the impedance, the impedance is approximately equal to the effective resistance, that is, the capacitive component has little effect on the value of the impedance.

Similarly, the effective resistance and capacitance of Sample B under dry weather and wet weather conditions were 724 kΩ and 0.57 nF, and, 309 kΩ and 0.65 nF respectively. When this sample was directly connected to a high voltage source in Section 3.6.1 the corresponding resistances at this operating voltage in dry and wet weather conditions were 1680 kΩ and 1970 kΩ respectively. In this case, the wet weather resistance is unusual, that is, it has increased from the dry weather condition. This reflects the sensitive nature of using the inverse gradient for resistance estimation of pole samples. Now, the effective resistance of Sample B was observed to reduce from 724 kΩ in dry weather conditions to 309 kΩ in wet weather conditions. This corresponds to anecdotal evidence that leakage current increases during wet weather, where it may be audible. Furthermore, the capacitance of Sample B was 3-5 times larger than Sample A. This may provide insight into explaining the much lower effective resistance of Sample B compared to Sample A in both dry and wet weather conditions, that is, owing to a lower effective leakage path length, accordingly altering the capacitive component of the impedance.

This impedance study highlights the importance of removing sensitive measurements when observing nonlinear impedances of different wooden poles dependent upon applied voltages, and hence reveals the large errors which may occur in measuring pole resistance when sensitive measurements are used in any analysis.

Table 3.4 Effective resistance reduction when operating at 66 kV phase-to-phase

Sample	Weather Condition	R @ 22 kV	R @ 66 kV	Resistance Reduction
A	dry	2725 kΩ	530 kΩ	80%
A	wet	450 kΩ	310 kΩ	30%
B	dry	724 kΩ	215 kΩ	70%
B	wet	309 kΩ	145 kΩ	50%

Operating at 66 kV

Analysis by Ward et al. [3] of pole top fires on a distribution network within Victoria [141] concluded that 66 kV pole top fires occurred at three times the rate of 22 kV pole top fires. The nominal line to ground voltage for 66 kV is 38.1 kV. Examining the resistance observed at 38.1 kV in Figures 3.10 (a) and Figure 3.11 (a), the effective resistances for Sample A under dry and wet weather conditions are 530 kΩ and 310 kΩ respectively. Similarly, the effective resistances for Sample B are 215 kΩ and 145 kΩ respectively. A comparison of these resistances with those observed at a nominal phase-to-ground voltage of 12.7 kV is shown in Table 3.4. These observations show the massive reduction in effective resistance of the wooden samples with this length at 66 kV phase-to-phase operating voltage in dry weather conditions. This justifies utilising wooden poles with a length in the order of 3-5 times the length of 22 kV poles if the pole is to provide similar resistive properties under dry weather conditions. Under wet weather conditions, the 66 kV wooden pole length required to provide similar resistive properties to 22 kV poles would about 1.5-2 times in length. These additional length requirements for 66 kV poles may explain why pole top fires occur at triple the rate of 66 kV poles that are similar in length to 22 kV poles [3].

The 2010 Australian Standard detailing the procedures for overhead line design [133] places no requirements on the effective resistances required of wooden poles. This standard only seeks to utilise the arc quenching properties of wood [29] to provide lightning performance of the overhead lines when mounted via insulators on wooden poles. Thus, this standard currently places no design requirements on poles which may experience high

impedance faults owing to leakage current that cause pole top fires. In the absence of such a design standard, there is currently no regulatory requirement for transmission or distribution network service providers to design overhead lines which consider the effective resistances of wooden structures so as to maximise the resistance and hence minimise the leakage current path to ground, reducing the likelihood of the electrical design contributing to initiating a pole top fire.

3.6.3 Metallic Electrode Performance Test

After performing the tests examining pole impedance under normal operating conditions in Section 3.6.2 the effect of the type of electrode used that provided the leakage current path through the wooden pole sample came into question. That study utilised a tight-fitting bolt as the electrode connection to the wooden pole sample. Limited research has been carried out on the effect of electrodes used to study impedance, with Darveniza [29] reporting in 1980 when wooden samples similar to those used in this study were stressed to a voltage of 240 V with a bolt electrode, that leakage currents of approximately 20-30 mA flowed in both dry and wet weather conditions. Other types of electrodes such as surface pads have also been studied in the past [29], however studying these other types would be inappropriate as they are not used on wooden poles in practice. Thus, this metallic electrode performance test aims to compare the observed leakage currents with dated studies and research [24, 25, 28–31, 140] and to compare the effect of using a nail electrode in place of a bolt electrode.

The RMS leakage currents measured for both tight-fitting bolt and nail electrodes are shown in Table 3.5. The variation between these electrodes have no significant difference. Comparing to the Australian results reported by Darveniza [29], the leakage current is of similar magnitude when assuming the voltage drop across the HV insulator reduces the voltage at the electrode to 240 V. The similarity of the bolt and nail electrode leakage currents with each other also suggests that the leakage current ‘flows’ on the surface of the

Table 3.5 RMS leakage current for different electrodes

Applied Voltage (kV)	Bolt Electrode (mA)	Nail Electrode (mA)
10	6.788	6.788
20	11.88	12.45
30	18.10	18.10

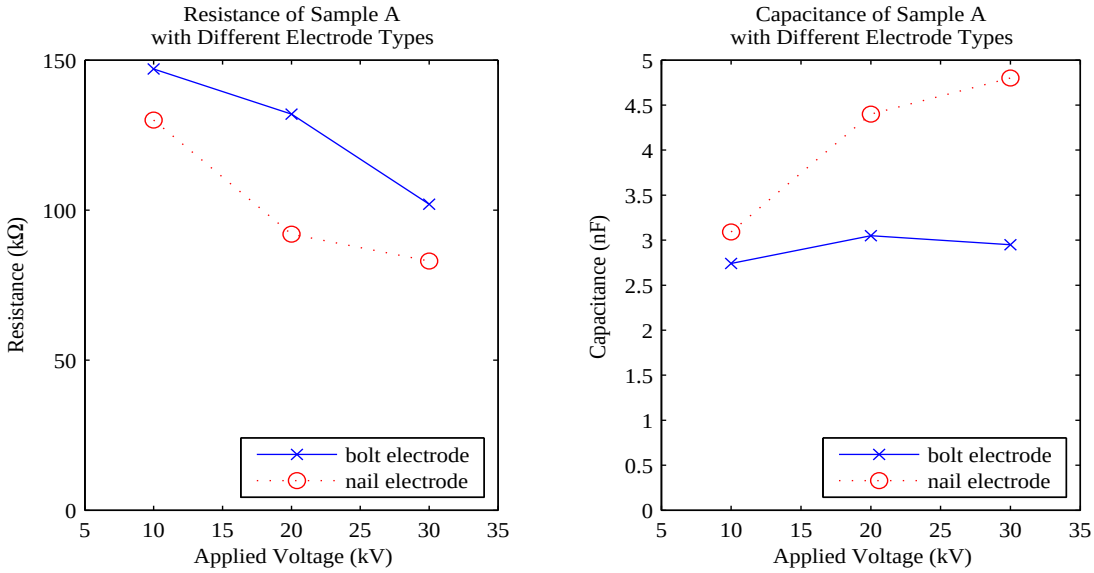

(a) (b)

Fig. 3.12 Impedance Components of Sample A for different types of electrode

pole as the longer dimension of the bolt has not changed the observed leakage current.

Further examination of the two different electrode scenarios was performed on the wooden pole Sample A. Specifically, the effective impedance was observed for each electrode at various applied voltages and are shown in Figure 3.12 to better understand the leakage current results observed, and to validate the use of a bolt as an electrode when performing impedance tests.

When examining the sample's effective resistance for different electrode types in Figure 3.12 (a) rather than the observed leakage current above, there is a significant difference in the resistance owing to nonlinear variation for the applied voltage across each sample. Furthermore, the resistances observed show that the bolt electrode always provides a more resistive path. This provides credence to the hypothesis of the leakage current taking the

pole surface as the leakage path of least resistance. This result firstly validates using a kingbolt as the electrode in impedance studies, reproducing the effective resistance which would be typically observed in the field. Secondly, this highlights the danger of using short nails to attach apparatus to wooden poles which carry high voltage assets, as personnel or the public may be exposed to a more conductive path should they touch such apparatus, especially for line voltages above 34 kV (that is line-to-ground voltages above 20 kV).

3.6.4 Electrode Spacing Effect on Measuring the Impedance of a Wooden Pole

The results from Section 3.6.2 in dry and wet conditions operating at 22 kV and 66 kV system voltages brought into question safe effective pole resistance, and hence the distance at which these high voltage assets are mounted from the ground. Studies by Robertson [30] and Darveniza [29] have measured resistances of pole sections for a number of electrode spacings, however, these studies did not take into account variation in applied voltage affecting the effective resistance and effective capacitance. Thus, studying the effect of the electrode spacing of wooden samples should be investigated.

In this section the RMS leakage current of Sample B under dry weather conditions was measured for a range of applied source voltages at various electrode spacings and are shown in Figure 3.13. The length of Sample B is 2.73 metres show these results should be treated with caution as typical electrode spacings on high voltage power poles are much larger, usually over 6 metres. Darveniza has reported on similar wooden poles with electrode spacings of 1.22 metres and 6.1 metres. The RMS leakage current observations in Figure 3.13 show little variation in magnitude for the same applied voltage source at various electrode spacings. Hence, study of the effective impedance may reveal more information.

The effective impedance of Sample B was now measured for the same range of applied voltages under similar dry weather conditions at various electrode spacings and are shown

in Figure 3.14. Note, the observed resistances of wooden poles with electrode spacings of 1.22 metres and 6.1 metres reported by Darveniza mentioned above were 7-13 kΩ and 12-30 kΩ respectively. Examining Figure 3.14 shows effective resistances of 200-800 kΩ for a range of electrode spacings under dry weather conditions. These results are an order of magnitude higher than that observed by Darveniza which may be explained by a different applied voltage appearing across the pole in his study resulting in a different effective resistance, given the nonlinear voltage-resistance relationship of wooden poles established in Section 3.6.2. Furthermore, the high resistive component observed for the quarter length electrode spacing may be explained by the very small capacitive component of the wooden sample when the electrodes are spaced at the short distance of 0.68 metres.

The most significant observation of the various electrode spacings is the large capacitive component of the full length wooden sample when the line voltage is above 34 kV (that is above an applied voltage of 20 kV in the figure). This corresponds to a much lower resistive component for any leakage current path to take, and hence higher I^2R power dissipation that contributes to the heating of the wooden pole electrode with the increased likelihood of initiating a fire of the wooden structure. Unfortunately, the results were not able to provide further information about effective resistances between electrodes separated by a distance greater than 2.73 metres. The logistics of handling a wooden sample greater than this length, and the size of the HV laboratory made examining larger electrode separation distances of samples impractical, and so the question of what distance high voltage assets should be mounted above the ground for a safe effective pole resistance must go unanswered.

3.6.5 Drying Effect on a Copper Chromium Arsenate Impregnated Wooden Pole

The results from Section 3.6.2 highlighted the dramatic effect of wet weather changing the resistivity of CCA impregnated wooden poles. This begs the question what occurs in the

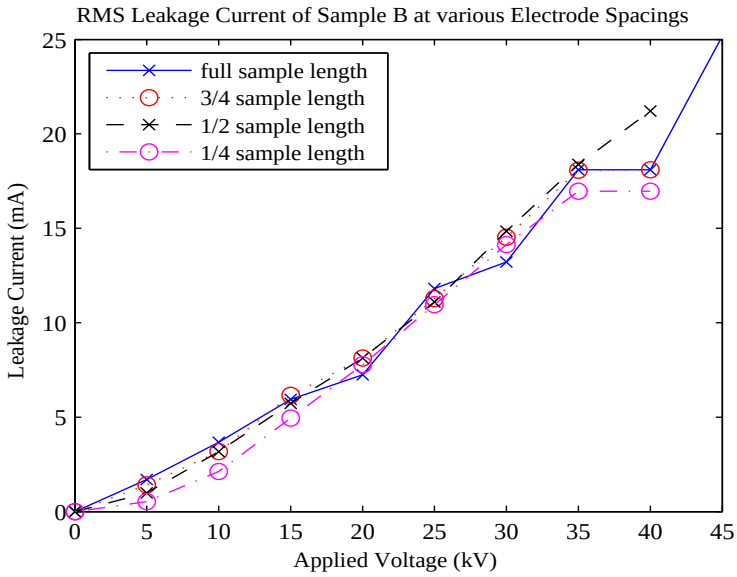

Fig. 3.13 RMS leakage current at various electrode spacings for different voltage levels

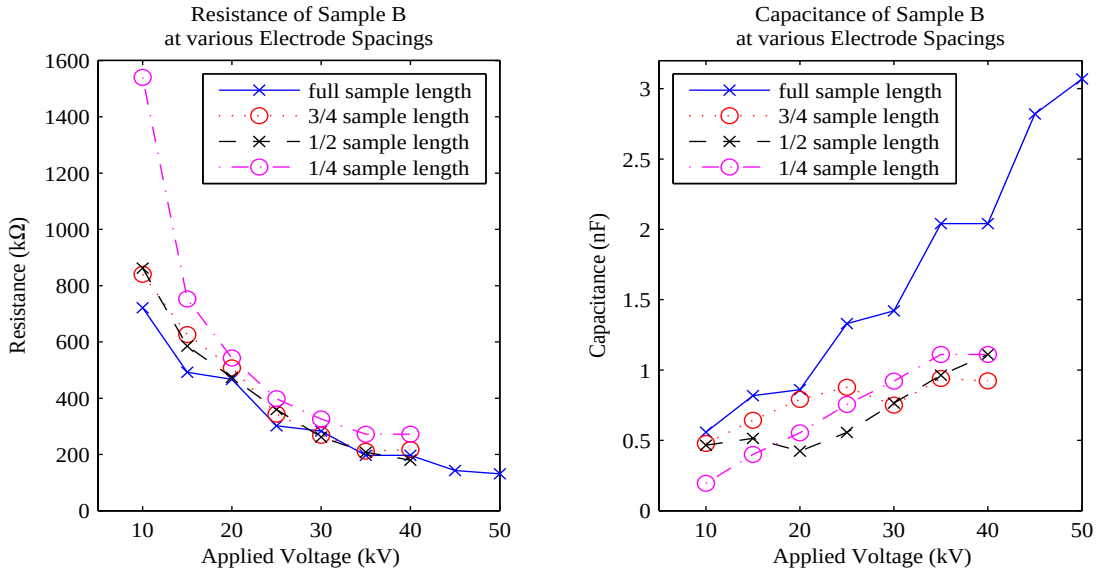

(a) (b)

Fig. 3.14 Impedance Components of Sample B at various electrode spacings

converse situation, that is, what changes will occur to the resistivity of a wooden pole when it is subject to extended periods of dry weather. To answer this question, the wooden pole Sample A which had been exposed to coastal weather for approximately 2 years was kept in an indoor laboratory for 6 months of controlled drying. The sample was then moved into the HV laboratory for further impedance tests under both dry and wet weather conditions, and these results were plotted together with results from 6 months prior in Figure 3.15.

Examining the resistance components of this figure, for the dry weather conditions there is a more pronounced hyperbolic resistance relationship after 6 months of controlled drying for the various voltages applied, with particularly strong resistive properties for distribution voltage levels. There are less dramatic changes in the resistance relationship for the case of varied voltages prior to drying (that is when weathered), although still seemingly hyperbolic. In either case, the wooden pole at 66 kV line voltages are 2-3 times more conductive than 22 kV line voltages, which may again explain the analysis by Ward et al. [3] where pole top fires with 66 kV line voltages occur at 3 times the rate of pole top fires with 22 kV line voltages.

Now examining the capacitive components of this figure, there is a ten-fold increase in the capacitance magnitude for the case of being a 2 year weathered pole when compared to 6 months of drying under wet weather conditions. Similarly, there is a five-fold increase in the capacitance magnitude for the case of being a 2 year weathered pole when compared to 6 months of drying under dry weather conditions. In either case, the wooden pole is much more capacitive when weathered, hence slightly more conductive and more prone to fire starts.

Furthermore, when comparing the wet weather and dry weather effects observed above, the wet weather effects are 2-3 times more resistive after 6 months of drying. Past research by Darveniza [29] had only drawn conclusion of the great influence of rain on pole resistance. This research shows the most significant difference occurs in both the resistance and

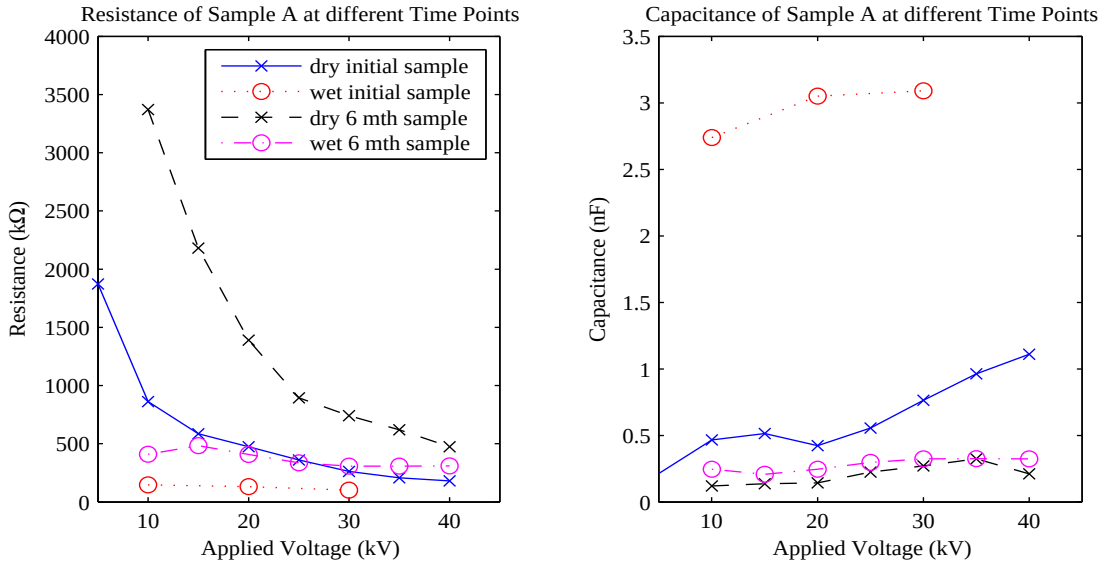

(a) (b)

Fig. 3.15 Impedance Components of Sample A under dry and wet conditions at initial laboratory investigation time and 6 months after the initial investigation time

capacitance components after 6 months of drying following exposure to 2 years of weathering and under wet weather conditions. Moreover, when the wooden pole was exposed to 2 or more years of weathering and under wet weather conditions it was at its most vulnerable for leakage currents causing pole fires at any distribution line voltage. This highlights the increased vulnerability of CCA poles to fire after coastal weather exposure.

3.6.6 Copper Chromium Arsenate Impregnation Effect on Conductivity of a Wooden Pole

The findings of Section 3.6.5 showed the variation of resistance and hence conductivity after 6 months of controlled drying. This section follows on to study the effect of CCA impregnated wood on the leakage current performance in wood. Leakage current testing was performed on both a CCA treated wooden sample and an untreated wooden sample. Both samples were tested under similar conditions. The impregnated wooden sample was a 2 year old spotted gum species with CCA treated H5 level. It was 2 metres in length and a

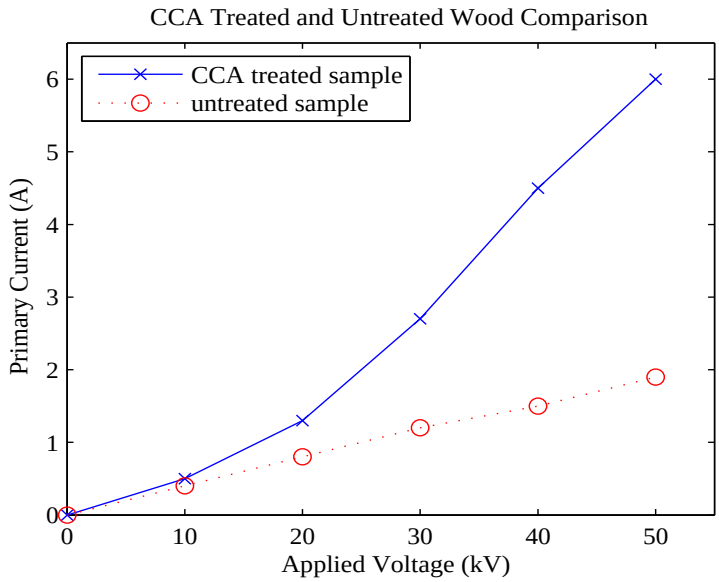

Fig. 3.16 Comparison of the electrical performance of CCA impregnated wood and untreated wood

pole sample. The untreated wooden sample was a 30 year old ironbark species, 1 metre in length, and a crossarm sample. As a similar untreated wood species of the same dimensions was unavailable, a crossarm sample of different species was used to study the effect of CCA impregnation on the wooden pole sample leakage current performance.

Comparing the primary current flow in the two samples, shown in Figure 3.16, the CCA treated sample drew more current than the untreated sample at various applied voltage levels. The leakage current was too difficult to quantify due to the high noise content. Based on the age and dimensions of the wood samples, one would expect higher current activity in the 30 year old sample than the 2 year old sample but the results were contradictory. The higher leakage current activity appearing in the 2 year old CCA impregnated sample can be attributed to a combination of the age and CCA treatment of the wood.

3.7 Discussion

The leakage current flow through the samples examined in Section 3.5.4 has shown that the sample exposed to a coastal environment and harsh climatic conditions for over 2 years (Sample A) has slightly higher flow than the control sample (Sample B, stored in an indoor facility and not subject to outdoor field conditions) under both dry and wet conditions. Owing to Sample A being exposed to harsh coastal environmental conditions causing changes in the properties of the pole, a higher leakage current activity was expected in comparison with Sample B. Under wet conditions, higher leakage current activity was also observed compared with the results obtained under dry conditions. The high moisture content in the wood decreases the resistance of wood and hence increases the conductivity [138].

While conducting the experiments, the metallic contact with the wood samples was observed to start heating when a leakage current of a magnitude 4 to 5 mA was flowing. At this sustained leakage current, smouldering of the wood was initiated which eventually leads to ignition. With the surface conductivity of Sample A being a mean of 13.9 μS and having a small standard deviation, the conclusion drawn is the deposition of salt on the surface of the wood in this case had negligible effect on the leakage current activity in the wood. On the contrary, the salt deposition on the insulator surface promoted leakage current to flow on its surface.

When examining the impedance characteristics of the pole samples in detail, a dramatic reduction in resistance of both Samples A and B under wet conditions was noticed when compared to the dry conditions, no matter the operating voltage level. This reduction in resistance would lead to higher leakage current flows, and create higher I^2R power dissipation that could contribute significantly to heating the wood-metal connections on the pole. A doubling in the leakage current flow like that in Section 3.5.4 would quadruple the power dissipation via heat, rapidly increasing the chances of igniting the pole at wood-metal connections where the leakage current flows.

A need to examine both the capacitive and resistive components was needed, as well as understanding how effective impedance varied for different voltages, owing to the unattributable significant difference of sample resistances in Section 3.6.1. Studying the effective impedance of wooden poles was considered a very important step prior to analysing the leakage current signatures of the insulators on wooden poles as there is no established research on the capacitive component of wooden pole impedances nor impedance variation for an applied voltage, at either distribution or sub-transmission voltages.

As the capacitance of the pole increases, this corresponds to a reduction in the resistive component of the impedance. An overall increase in the capacitive components is seen for both Samples A and B, shown in Figures 3.10 (b) and 3.11 (b) respectively. The capacitance would also have some effect on the voltage at the insulator, creating a localised phase shift. This would be unlikely to affect the power factor at the end of the line, but could have some limited effect on voltages fed from the transformer mounted on the pole. Furthermore, taking into account for the samples' capacitive components showed little effect on the impedance value, and hence resistance value. However, using circuit analysis to remove sensitive leakage current measurements from the linear estimation for effective resistance showed the true nonlinear nature of impedance for various applied voltages. This also revealed the linear estimation has a nonzero intercept, thus explaining the unattributable difference of sample resistances.

At the operating voltage of 22 kV, when the pole is affected by wet weather conditions, the resistance more than halves hence increasing the leakage current flow. This is the case for both samples examined. If the distribution supply voltage strays higher, this would further decrease the effective resistance between the insulator and ground, in turn increasing the leakage current and the heating of wood-metal connections. It would also increase the effective capacitance affecting the voltage phase angle, but as loads are usually always inductive, this would have a limited effect on customers connected to any locally mounted

transformer. Too much heating at the wood-metal connections will lead to ignition.

At the operating voltage of 66 kV, for a similar length line operating height on the pole, the effective resistance has a massive reduction of 3-5 times the resistance of a 22 kV line when operating in dry weather conditions. Thus, to provide similar resistive properties to that of a 22 kV line would require lengthening 66 kV poles by 3-5 times of the length of a 22 kV pole. Luckily such resistive properties are not required in dry weather conditions as leakage current magnitudes are usually much smaller than that of wet weather. For wet weather conditions, the experiments showed a length of 1.5-2 times the length of a 22 kV pole is needed for a 66 kV pole to provide similar resistive properties to that of a 22 kV pole. However, 66 kV poles used in practice are not of such lengths, and this result may explain why fires initiated on 66 kV pole tops occur at triple the rate of 22 kV pole tops.

For all high voltage operating voltages, Australian standards and regulations currently provide no requirement to design overhead lines in a way which consider the effective resistances of wooden structures so as to maximise the resistance, thus minimising the leakage current, ultimately reducing the likelihood of the electrical design contributing to pole fire starts. The author recommends that criteria for minimising wooden pole leakage current should be added to Australian standard electrical design requirements of overhead lines.

Leakage currents for different types of electrodes used in the experiments showed no significant difference in magnitude. Owing to the types of electrodes used suggests the majority of the leakage current ‘flows’ at the surface of a pole. Further impedance test results showed the bolt electrode (with a much longer length) always provides a more resistive path compared to a nail electrode (with a much shorter length) likely being caused by greater surface area of the wood-metal contact. This highlights the danger of using short nails in attaching apparatus to wooden poles that carry high voltage assets as personnel or the public may be exposed to a much more conductive path if they touch such apparatus. Furthermore, the electrode impedance test results validated the use of a bolt as an electrode for the

experiments.

The effective impedance of electrode spacing under dry weather conditions revealed effective resistances an order of magnitude higher than that in the literature. This large discrepancy was attributed to variation in the applied voltage across the wooden poles, affecting the observed effective resistance and effective capacitance. Most significantly, a large capacitive component was observed for the full length wooden sample when the line voltage was above 34 kV, corresponding to a much lower resistive component at these line voltages for any leakage current, creating much higher I^2R power dissipation and the increased likelihood of initiating a fire.

Examining the weathering and coastal climatic effects by drying Sample A in the laboratory revealed the wooden pole sample had become much less resistive and much more capacitive after weathering, hence more prone to initiating a fire. Furthermore, comparing wet and dry weather effects on the sample showed a significant difference in the change of resistance under wet weather conditions after 6 months of drying. This highlights that this particular specimen (that is a CCA impregnated pole sample exposed to a coastal environment and harsh climatic conditions for over 2 years) was at its most vulnerable to leakage current ignition when under wet weather conditions at any distribution line voltage. Furthermore, these findings emphasise the importance of immediately testing samples from the field for accurate condition reporting, particularly CCA impregnated wood.

Although the presence of CCA salts in a spotted gum wooden pole in comparison with an untreated ironbark crossarm showed significantly lower resistance, the presence of CCA salts in a spotted gum wooden pole has been shown to be insignificant compared with that owing to naturally occurring moisture in the heartwood of a spotted gum wooden pole by Robertson [30] and therefore would have little bearing in the matter of public/personnel safety concerns in contacting poles so treated. It is interesting to note that the 30 year old ironbark crossarm wooden sample offers a much higher resistance of approximately 2.5 MΩ

which would have enhanced the effective impedance between the insulators and the earth connected to the transformer mounting if a wooden crossarm had been used in place of the metal crossarm.

This unconventional type of pole fire occurring at the bolt mounting a transformer to a wooden pole at a distance of 3 metres from the top end of the pole was investigated. The results have shown that the leakage current travelled from the insulator surface into the steel crossarm and pole. The fuse unit consisting of the insulators was from a batch of units identified by the manufacturer as faulty, which would also encourage a rise in leakage current. Given that the crossarm was made from steel, rather than a wooden crossarm, and the crossarm was connected to the pole with a kingbolt and two braces, the leakage current bypassed the kingbolt through the metallic braces. Since the leakage current had three paths to flow, there was limited activity of heat concentration in the vicinity around the kingbolt. This may have avoided the occurrence of a pole fire at the crossarm-pole junction.

The majority of past pole fires in Victoria have occurred at the metallic kingbolt location connecting the crossarm to the pole. The unconventional type of pole fire investigated in this chapter has posed a unique type of pole fire for industry to accommodate. For smouldering to start in the wooden pole, a combination of both wet and dry wood surfaces is required to produce the right conditions for the four fire elements of fuel, a heat source, oxygen and sufficient time to initiate the smouldering. In this particular case, the area of pole above and below the earthed transformer mounting was wet by rain but the area in and around the transformer bolt was shielded from rain by the transformer body. The wet surface above the transformer mounting ensured higher leakage current flow in the wood to the earthed mount and the dry surface encouraged the heating up of the wood and hence the metallic bolt. Also the heat dissipated by the transformer also kept the nearby surface of wood dry with a higher surface temperature. It can also be concluded that the salt deposition on the wood surface did not adversely affect the leakage current flow in wood. Thus, a combination of environmental

factors such as moisture contamination on porcelain insulators and wet wooden power poles, and the pole configuration with pole-mounted assets creating dry sections of a wet wooden pole and earthed assets by-passing part of the pole as a leakage path can bring about the right circumstances for a pole fire starting at a position on a pole not usually considered.

The observations in Figure 3.15 discussed above of a wooden pole's effective impedance has produced a range of typical resistance and capacitance that may be used when analysing the leakage current signatures of insulators on wooden poles in Victoria, Australia. Previous research has not only omitted pole resistance from study but also pole capacitance. Thus, 2700 kΩ and 143 kΩ shall be used as the resistances of a typical weathered wooden pole operating at 22 kV in a dry and wet weather condition respectively for leakage current signature analysis in subsequent chapters. Similarly, 0.49 nF and 2.82 nF shall be used as the capacitances of a typical weathered wooden pole operating at 22 kV in a dry and wet weather condition respectively.

3.8 Summary

This chapter has presented a systematic investigation into the effective impedance of wood used for poles in Victoria, Australia. After establishing the contribution that pollution may play in providing suitable surface leakage currents on insulators, one particular pole fire event has been investigated in detail. For this fire event, a combination of environmental factors such as moisture contamination on porcelain insulators and wet wooden power poles, and the pole assets creating dry sections of a wet wooden pole and earthed assets by-passing part of the pole as a leakage path provided the right circumstances for a pole fire to start. The thermographic studies showed that heating of wood-metal connection points can initiate smoulder at temperatures just above 50 °C. A leakage current with a magnitude as small as 3 mA RMS can lead to smouldering, thus making leakage current magnitude difficult to use for establishing when a fire is incipient.

Further study into the impedance of a typical CCA impregnated wooden species revealed additional characteristics which were missed by studying leakage current alone. Comparing these impedance studies with past research showed the capacitive component of a pole's impedance had previously been ignored, however has little effect on using an impedance value for effective resistance. Moreover, the importance of observing the applied voltage level has been established, owing to the nonlinear nature of a pole's resistance. The impedance study established the dangerous conductance properties when using 66 kV poles with similar length to that of 22 kV, thus providing an explanation for 66 kV poles catching fire at triple the rate of 22 kV poles. Furthermore, a pole with 2 or more years of weathering and in wet weather was the most vulnerable situation for leakage currents to cause pole fires, no matter the line voltage. Finally, a typical impedance characteristic was established for a weathered wooden pole operating at 22 kV in both dry and wet weather conditions.

Chapter 4

Measuring Leakage Current Nonlinearity for a High Voltage Insulator

4.1 Overview

The previous chapter established that wet weather conditions dramatically alter the effective leakage path resistance characteristic, raising the current density and hence heating in areas with wood-metal contact. Following on from that idea, this chapter proposes a method for measuring the nonlinearity of high voltage insulator leakage current, utilising the correlation coefficient [92] to provide a quantitative measure of the leakage current signature, complementing existing leakage current analysis techniques, with particular attention to wet weather conditions. Further measures utilising fractal dimensions are also proposed. The purpose of these measures is to provide an overall 'health index' which may be used to smartly monitor leakage currents. Section 4.2 provides a brief background to high voltage insulators used on power poles. Section 4.3 establishes the nonlinearity measure and the correlation coefficient. Justification of the use of the correlation coefficient is presented. The high voltage insulator is introduced as a system and the nonlinearity measure is shown to be a condition identifier. Section 4.4 details the experimental configuration and results

obtained for both variation in the voltage supply and variation in contamination levels at a fixed voltage. Analysis is performed using the nonlinearity measure, representative power, and three fractal dimensions as a measure of the leakage current signature, building a general profile for a high voltage insulator. Section 4.6 discusses how each measure performs and their suitability for contributing to a 'Leakage Current Health Index' (LCHI). Section 4.7 summarises the measures and their usefulness in leakage current analysis and deduces a lightly contaminated insulator under wet weather conditions reduces in nonlinearity from that under dry weather conditions. Furthermore, when an insulator is in the stage prior to flashover, the measures identify that the nonlinearity of the leakage current can increase significantly, thus establishing the nonlinearity measure and the correlation fractal dimension as very useful tools for identifying incipient pole top fires.

4.2 Preliminaries

Insulators are designed to provide electrical insulation. Insulators can be made from many different types of material. Furthermore, insulators can be many different shapes and configurations. In practice, imperfect materials and the environment cause surface discharge and flashover. Leakage current exists especially on contaminated insulators. Contamination type and contamination levels are the main factors that will affect the leakage current. Therefore, the modelling of leakage current dynamics for each insulator or a string of insulators is a challenging task. When the leakage current increases to a critical point, electrical breakdown occurs and the magnitude of the leakage current surges which may initiate a sequence of events leading to a blackout or other failures. In most parts of Australia power poles are made of wood, which will be heated up by leakage current. This significantly jeopardises the operational security and safe operation of the power grid infrastructure as well as the safety of any nearby public and personnel.

The development of flashover on wet insulators is explained in [50] and Section 2.4.2 of

the literature review. The physical condition of the insulator varies during the development of flashover. This can be reflected by utilising a nonlinear model. Inspired by this idea, if the nonlinearity of the insulator (reflecting its physical condition) can be continuously monitored, then the health state of the insulator may be identified. Furthermore, knowing the health state of the insulator can identify incipient flashover.

4.3 Measuring Nonlinearity

This section presents a new way to measure a nonlinear system. Once this measure is established, the high voltage insulator is considered as a nonlinear system with the supply voltage as an input, and the leakage current as an output. The nonlinearity measure is proposed as a condition identifier, where the measure may be used as a health state or indicator of the insulator.

4.3.1 The Nonlinearity Measure

There are various measures which quantitatively describe the nonlinearity of a system. Here, we introduce the nonlinearity measure which is defined in [142]. Given a system with m inputs and n outputs, if the system is denoted by an operator $\mathcal{G}$, then its nonlinearity n_d can be described by

$$n_d = \min_{\mathcal{L}} \|\mathcal{G} - \mathcal{L}\| \tag{4.1}$$

where $\mathcal{L}$ is a linear system with m inputs and n outputs, and $\|\cdot\|$ is an induced norm of a system, defined by the norm of the input and output such that

$$\|\mathcal{G}\| = \max_{\|x\|=1} \frac{\|\mathcal{G}x\|}{\|x\|}. \tag{4.2}$$

Therefore, in light of equation (4.1), and using the Euclidean norm as the norm defined in equation (4.2), the nonlinearity of the system $\mathcal{G}$ is defined as

$$n_d = \min_{\mathcal{L}} \max_{\|x\|_2=1} \frac{\|(\mathcal{G}-\mathcal{L})\,x\|_2}{\|x\|_2}. \tag{4.3}$$

The idea behind this definition is to find a linear system which can best approximate the nonlinear system so that the 'distance' between these two systems is minimised.

Correlation refers to the relationship or dependence between two given waveforms. In the continuous time domain, for the two waveforms $x(t)$ and $y(t)$, the cross-correlation $r_{x,y}(\tau)$ is a measure of their similarity as a function of a time lag applied between them, and is defined as:

$$r_{x,y}(\tau) = \int_{-\infty}^{\infty} x^*(t)y(t+\tau)dt \tag{4.4}$$

where τ is the time lag applied to y. By plotting $r_{x,y}(\tau)$ against τ, the cross-correlation may be examined graphically for similarity. In discrete form, the cross-correlation between two waveform datasets x_i and y_i of length N, is defined as:

$$r_{x,y}(j) = \frac{1}{N}\sum_{i=0}^{N-1} x_i y_{i+j} \tag{4.5}$$

where j represents the number of sampling points in lag of τ by which y has been shifted. The discrete cross-correlation provides a simple quantitative measure of the linear correlation between data points. Normalising (4.5) by the factor

$$\frac{1}{N}\left(\sum_{i=0}^{N-1} x_i^2 \sum_{i=0}^{N-1} y_i^2\right)^{1/2}$$

produces the cross-correlation coefficient $\rho_{x,y}(j)$. The correlation coefficient is a normalised measurement of the degree of correlation between two waveforms. This is identical to the Pearson correlation coefficient with zero mean. When there is a perfect linear relationship

between given waveforms, the correlation coefficient is −1 or 1. Otherwise, the value will be between −1 and 1. Therefore, the Pearson correlation coefficient can reflect a certain degree of nonlinearity between two nonlinearly interdependent waveforms. Specifically, given a nonlinear system, if the input signal (as a waveform) is x and the output signal is y, then the correlation coefficient $\rho_{x,y}$ between x and y is defined as:

$$\rho_{x,y} = \frac{E\left[(x-\bar{x})\,(y-\bar{y})\right]}{\sigma_x \sigma_y} \tag{4.6}$$

where E is the expected value operator, σ_x and σ_y are standard deviations of x and y respectively, $\bar{x}$ and $\bar{y}$ are mean values of x and y. The value of $\rho_{x,y}$ reflects the nonlinear interdependency between the input signal and the output signal, and therefore it measures the nonlinearity of the system. As signals are sampled, then $\rho_{x,y}$ in discrete form is given by:

$$\rho_{x,y} = \frac{1}{\sigma_x \sigma_y} \sum_{i=0}^{N-1} (x_i - \bar{x})(y_i - \bar{y}) \tag{4.7}$$

where x_i and y_i are the samples of the input and output signals respectively at sample instance i, $\bar{x}$ and $\bar{y}$ are the corresponding mean values, and $\sigma_x = (\sum_{i=0}^{N-1}(x_i - \bar{x})^2)^{1/2}$ and $\sigma_y = (\sum_{i=0}^{N-1}(y_i - \bar{y})^2)^{1/2}$.

To examine the usefulness of this as a nonlinearity measure for the case of leakage current signature, two questions are posed:

1. How big does the sample window need to be to guarantee sufficient data is used for the calculation of the cross-correlation?

2. Understanding the supply voltage and leakage current are periodic-like waveforms with a superposition of noise, how does cross-correlation of these waveforms perform?

To answer the question on window size and implicitly the number of points captured in

that window, let's examine the cross-correlation given in (4.5), denoting it by

$$S_N = \frac{1}{N}\sum_{i=1}^{N} x_i y_{i+j}$$

where N is the length of the dataset. By adding one additional data point, then,

$$\begin{aligned} S_{N+1} &= \frac{1}{N+1}\sum_{i=1}^{N+1} x_i y_{i+j} \\ &= \frac{N}{N+1}\left(\frac{x_{N+1}y_{N+1+j}}{N+1} + \frac{1}{N}\sum_{i=1}^{N} x_i y_{i+j}\right) \\ &= \frac{N}{N+1}\left(\frac{x_{N+1}y_{N+1+j}}{N+1} + S_N\right) \\ &= S_N + \frac{1}{N+1}\left(x_{N+1}y_{N+1+j} - S_N\right) \end{aligned} \tag{4.8}$$

Thus as N increases, S_{N+1} approaches S_N, that is, the larger the window or dataset, the less effect it has in changing S_{N+1}, and hence the cross-correlation and correlation coefficient. Therefore the window size and dataset do not have to be too large to capture changes in the waveforms.

The second question requires construction of two noisy waveforms. Let the two waveforms be $x_i = v_i + \epsilon_i$ and $y_i = i_i + \varepsilon_i$, representing a voltage and current waveform respectively, where v_i and ϵ_i are assumed to be uncorrelated. Similarly, i_i and ε_i are assumed uncorrelated. The discrete cross-correlation $r_{x,y}(j)$ of the waveforms is then,

$$\begin{aligned} r_{x,y}(j) &= \frac{1}{N}\sum_{i=0}^{N-1}[v_i + \epsilon_i][i_{i+j} + \varepsilon_{i+j}] \\ &= \frac{1}{N}\sum_{i=0}^{N-1}[v_i i_{i+j} + v_i\varepsilon_{i+j} + \epsilon_i i_{i+j} + \epsilon_i\varepsilon_{i+j}] \\ &= r_{v,i}(j) + r_{v,\varepsilon}(j) + r_{\epsilon,i}(j) + r_{\epsilon,\varepsilon}(j) \end{aligned} \tag{4.9}$$

The final three terms in equation (4.9) tend towards zero with increasing window size (time

lag j) owing to the assumption that the chosen noises are uncorrelated with the voltage and current waveforms. For large N, (4.9) becomes

$$r_{x,y}(j) = r_{v,i}(j) + \overline{v}\,\overline{\varepsilon} + \overline{\epsilon}\,\overline{i} + \overline{\epsilon\varepsilon} \tag{4.10}$$

where $\overline{v}$, $\overline{\varepsilon}$ and $\overline{\epsilon}$ are the means of v, ε and ϵ respectively. As N increases, $\overline{\epsilon} \to 0$ and $\overline{\varepsilon} \to 0$ thus $r_{x,y}(j) \to r_{v,i}(j)$, the cross-correlation of the two waveforms. This analysis demonstrates that cross-correlation emphasises the signal properties by reducing the noise content. Thus the correlation coefficient is quite suitable as a measure for comparing these waveforms.

4.3.2 The Nonlinearity Measure as an Insulator Condition Identifier

The high voltage insulator can be viewed as a nonlinear system with the supply voltage as the input and the leakage current as the output. In the ideal case, the output is zero no matter how high the supply voltage. However, due to the imperfection of the material of the insulator and the influence of the surrounding environment, an insulator with a polluted surface is partially conductive, therefore a leakage current exists. The behaviour of the leakage current is a function of various factors, such as the configuration of the insulators, the types of insulators, and the pollution distribution, etc. Various models describing the leakage current and the occurrence of flashover have been proposed either based on experiments or theoretical analysis. These models differ from each other in health states and the configuration of insulators. If the modelling error is taken into account, it is almost impossible to build such a model that describes the leakage dynamics for all cases. However, among these models, common features exist which are:

1. The relationship between the supply voltage and the leakage current is nonlinear. In the frequency domain, this is represented by disproportionate changes in each spec-

trum component of the leakage current waveform [47, 86, 87].

2. As the leakage current increases in magnitude, the nonlinearity of the insulator model is reflected more in the output with distortion and impulses [44, 47].

3. The nonlinearity of the output signal changes according to the health state of the insulator [64, 84, 86–88].

Noting these features, if the nonlinearity of the insulator is measurable by monitoring the relationship between the supply voltage and the leakage current, then the health state of the insulator, such as the level of pollution can be detected. Furthermore, some catastrophic events in the power grid can be predicted by analysing the nonlinearity measure.

To explain and justify the use of the nonlinearity measure, let's look at the insulator as a system. Cross-correlation [143] can be used to compute the response of a linear system to an input signal. In this case, the input signal is the supply voltage waveform and the leakage current waveform is the output signal in response to the insulator system during each period at which the insulator is behaving in a linear fashion. The phase shift between the input and output signals must first be removed before examining the similarity of the input signal with the output signal. Now correlating two signals with each other will identify how alike they are, as well as whether they exhibit periodic or stochastic behaviour. Furthermore, the power spectrum reveals periodic components of a signal and is also very helpful in time series analysis. Let's again consider a waveform dataset x_i of length N sampled at intervals of δt such that,

$$x_i = x(i\delta t), \text{ where } i = 0, 1, ..., N-1 \tag{4.11}$$

The discrete Fourier transform [144] is defined by,

$$Z_k = \frac{1}{N}\sum_{i=0}^{N-1} x_i e^{-j2\pi ik/N} \tag{4.12}$$

and the power spectrum is defined as

$$P_k = \|Z_k\|^2 = Re\{Z_k\}^2 + Im\{Z_k\}^2 \tag{4.13}$$

Each value of k for which there is a peak in the power spectrum corresponds to a frequency component, that is a harmonic,

$$f_k = \frac{k}{N\delta t} \tag{4.14}$$

in the original time series waveform.

Now consider the following examples:

Example 1: In order to show the changing likeness of two waveforms, comparison of the Fourier transforms of the time series waveform data will reveal their evolving behaviour. As an example, Fast Fourier Transforms (FFTs) [145] of the data collected in Section 4.4 are shown for the supply voltage and leakage current in Figures 4.1 and 4.2 respectively. The axes labels have been removed from these figures for simplicity. The horizontal axes show the harmonic number, with a fundamental frequency $f_1 = 50$ Hz. The vertical axes are a scaled voltage of the supply voltage (V) and the leakage current (LC) in milliamps.

Examining Figure 4.2 clearly shows the power spectrum peaks of the leakage current increasing for an increasing level of insulator contamination under wet weather conditions. The power spectrum of the supply voltage in Figure 4.1 shows a sympathetic response to the leakage current which increases in magnitude for an increase in contamination levels. Also worthy of mentioning is the increase in the 9th, 11th and 13th harmonics in these

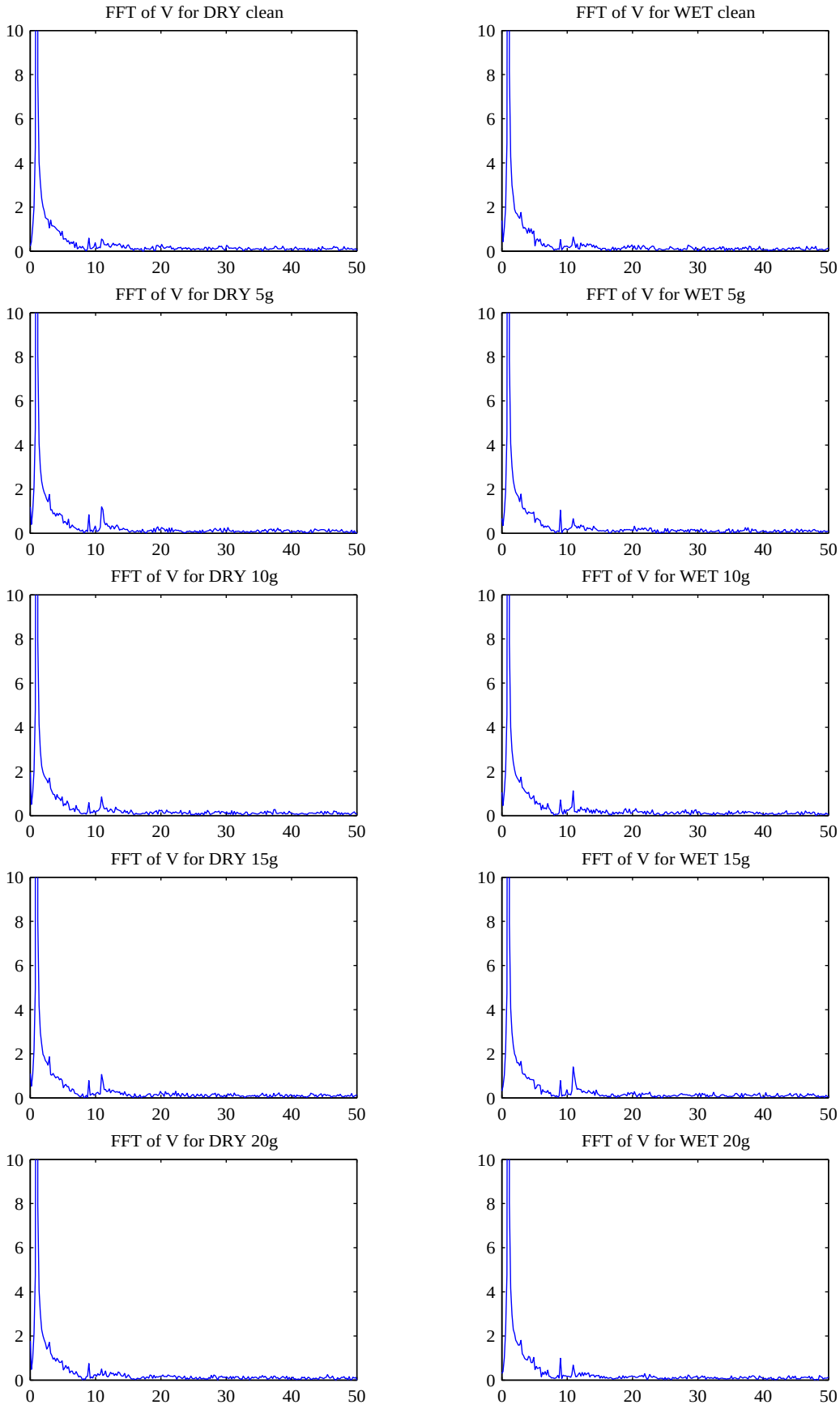

Fig. 4.1 FFTs of supply voltages (V) for various levels of contamination under dry and wet weather conditions (peaking to 51.73 at the fundamental frequency (not shown)).

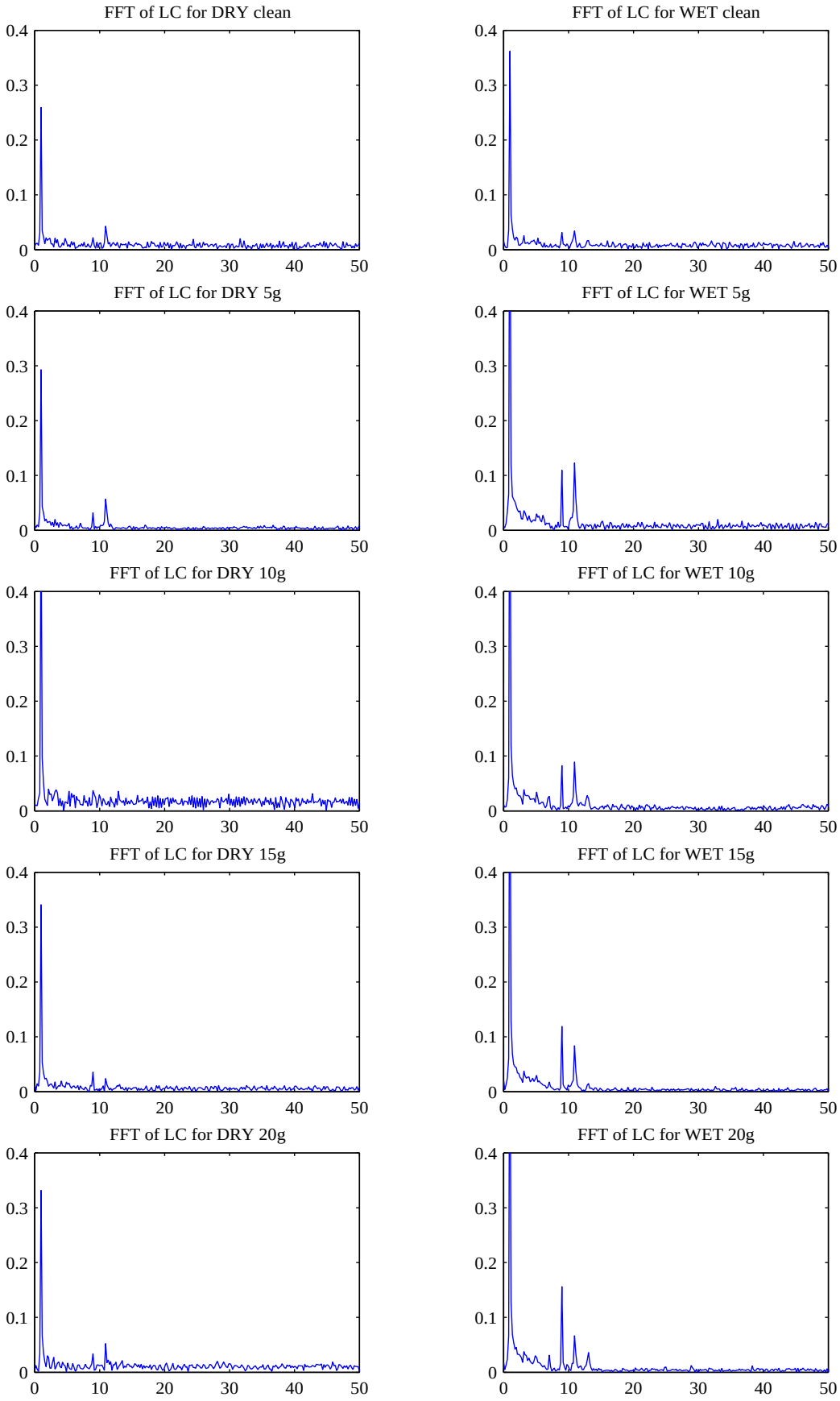

Fig. 4.2 FFTs of leakage currents (LC) for various levels of contamination under dry and wet weather conditions.

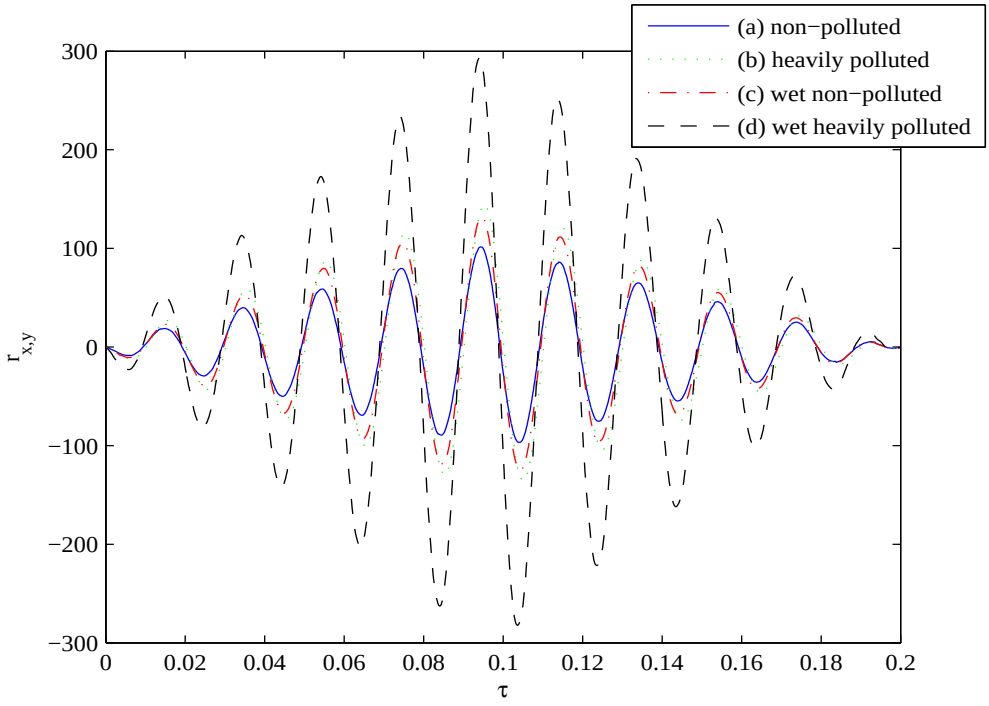

Fig. 4.3 Cross-correlations of phase compensated supply voltage with leakage current for various levels of pollution.

figures, however there is also a notable increase in the interharmonics as the contamination increases, further justifying the use of the cross-correlation technique which 'picks up' correlations across all frequencies.

Example 2: In order to demonstrate the likeness of two waveforms, or in fact the change in likeness of two waveforms, comparison of the cross-correlation of the waveforms with each other graphically displays the evolution. Consider the cross-correlation of the phase compensated waveforms for a supply voltage with the leakage current of (a) a non-polluted insulator; (b) a heavily polluted insulator; (c) a wet non-polluted insulator; and, (d) a wet heavily polluted insulator. The cross-correlations are displayed in Figure 4.3.

It is clear from Figure 4.3 that different leakage current signatures produce a range of cross-correlations, and hence correlation coefficients although being the resultant leakage current for the same insulator system. This identifies the nonlinear nature of a polluted high

voltage insulator. To quantify and identify the changing response of the insulator system, the nonlinearity measure is established as a quantitative measure reflecting the extent to which a waveform deviates from the ideal linear counterpart.

4.3.3 Defining the Nonlinearity Measure

Inspired by the ideology above, a nonlinearity measure of the insulator system can be defined by maximising the correlation coefficient between the supply voltage waveform and the leakage current waveform within a set time window with regard to the phase difference. To do this, the basic profile of these two waveforms needs to be clarified. From experiment, we know that the leakage current waveform is almost periodic prior to the development of flashover, denoted in [46] as the initial stage, and in [84] as the security stage. Varying phase shifts between the supply voltage waveform and the leakage current waveform exist. Then, more and more intermittent impulses appear in the waveform until flashover occurs. By adjusting the phase shift to align the zero crossings, the maximum value of the correlation coefficient, which will be a positive number, can be derived. If the period of the supply voltage is T, the time window is chosen to be $[t_0, t_0 + mT]$, and the two waveforms are denoted by $v(t)$ and $i(t)$ respectively, then the nonlinearity measure of the insulator can be defined as:

$$n_d = 1 - \max_o \rho_{\lfloor v(t+o) \rfloor, i(t)} \tag{4.15}$$

where $o \in [0, mT]$ is the phase offset, $t \in [t_0, t_0 + mT]$ and

$$\lfloor v(t+o) \rfloor = \begin{cases} v(t+o-mT) & \text{if } t+o > t_0 + mT \\ v(t+o) & \text{otherwise} \end{cases} \tag{4.16}$$

The value of n_d is monotonic with respect to the degree of nonlinearity. When the two waveforms are linearly correlated, in which case $\max_o \rho_{\lfloor v(t+o) \rfloor, i(t)} = 1$, the nonlinearity measure

$n_d = 0$.

The Pearson correlation coefficient is chosen as the measure of nonlinearity for four reasons even though it is not a norm:

1. The norm is a function to measure the 'size' of a signal or 'distance' between two signals. In this case, the correlation coefficient reflects the distance between two waveforms in the sense of the 'shape' of the signals. It is not sensitive to the scaling operation. Therefore, it captures the key feature of the insulator, namely the nonlinearity.

2. The correlation coefficient can be positive or negative. By carrying out the maximisation operation in the definition of n_d, the value of the correlation coefficient will be always positive since the supply voltage is practically in sinusoidal form. Let us suppose $\rho_{\lfloor v(t+o_0)\rfloor,i(t)} < 0$, then it is true that $\rho_{\lfloor v(t+o_0+0.5T)\rfloor,i(t)} > 0$.

3. The correlation coefficient is not sensitive to white noise. Calculating the correlation coefficient using the data acquired in the experiment suggests that the correlation coefficient is not sensitive to typical insulator noises consisting of random number of minor peaks in low amplitudes [93]. Therefore, it avoids preprocessing of the data by filtering the noise which induces information loss.

4. In practice, since the waveforms can only be sampled using digital equipment, the computation of the correlation coefficient will use discrete samples.

4.4 Experimental Configuration and Results for a Single Insulator System

The experimental system consists of a high voltage power supply, the insulator and data collection equipment. The configuration is shown in Figure 4.4. The supply voltage and the

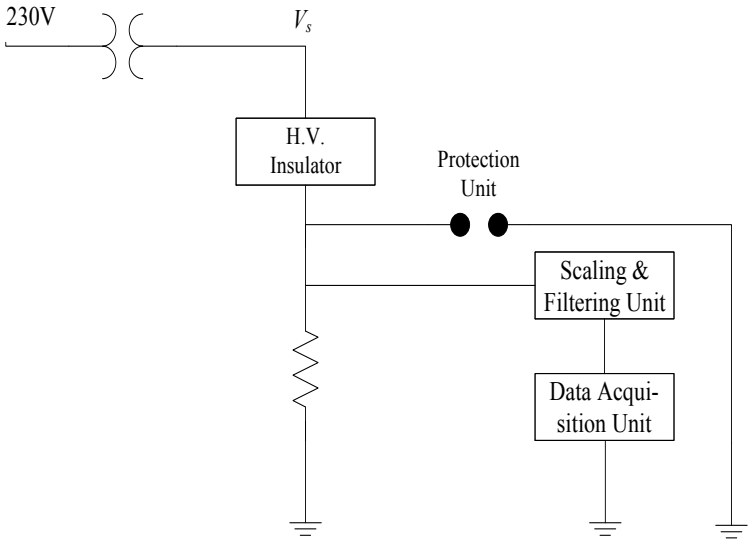

Fig. 4.4 The configuration of the leakage current measurement system

leakage current which is converted to a voltage waveform by a specifically designed circuit with an appropriate amplification factor are collected by a digital oscilloscope. The RMS value of the supply voltage V_s, was set at various voltages as described below. A time window with 5 periods is set to record the waveforms. The cap-and-pin type insulator was used as this is the typical insulator found where pole top fires occur in Victoria, Australia. The artificial contamination material was introduced according to the IEC insulator contamination standard [146]. One litre of water, 40 g of Kaolin and a certain amount of salt were mixed to form the contamination material to achieve various pollution layer conductivity levels. In this experiment, the mixture of water, Kaolin and a different amount of salt were sprayed onto the surface of an insulator to form the contamination layer. Dry and wet conditions for the insulator were carefully produced.

4.4.1 Varied Applied Supply Voltages

For the case of a dry heavily polluted insulator, the voltages were set to 12.7 kV, 8 kV, and 6 kV respectively. The voltage and current waveforms were recorded by the oscilloscope

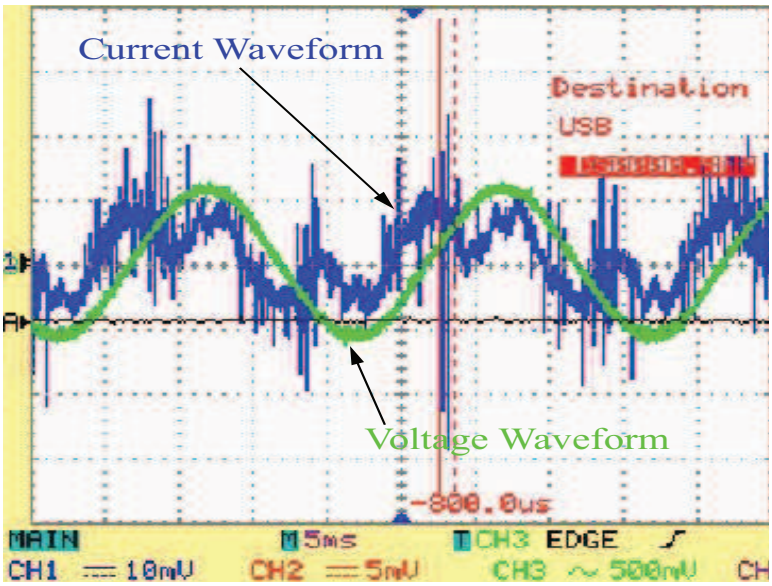

Fig. 4.5 Image captured from the oscilloscope (dry contaminated insulator with supply voltage 12.7 kV).

and one of the images captured is shown in Figure 4.5. In this image the insulator was in a dry weather condition and the supply voltage is 12.7 kV represented by the green waveform. The blue waveform is the voltage signal representing the leakage current. The leakage current shown in the image is distorted to such a degree with noise and harmonics that it is no longer sinusoidal. The two waveforms are both periodic in nature, with the same period. The image captured also depicts a phase shift or phase difference between the two waveforms. The results for when the supply voltages were set at 8 kV and 6 kV under dry weather conditions are shown in Figure 4.6.

Following examination of the dry insulator, water was sprayed onto the insulator to simulate the wet weather condition caused by a foggy atmosphere, that is heavy moisture in the air. The supply voltage was again set to 12.7 kV and the data acquired is shown in Figure 4.7. By examining all data captured, two pattern variations were found:

1. As the supply voltage is increased, the amplitude of the leakage current becomes larger, with stronger correlation to the supply voltage.

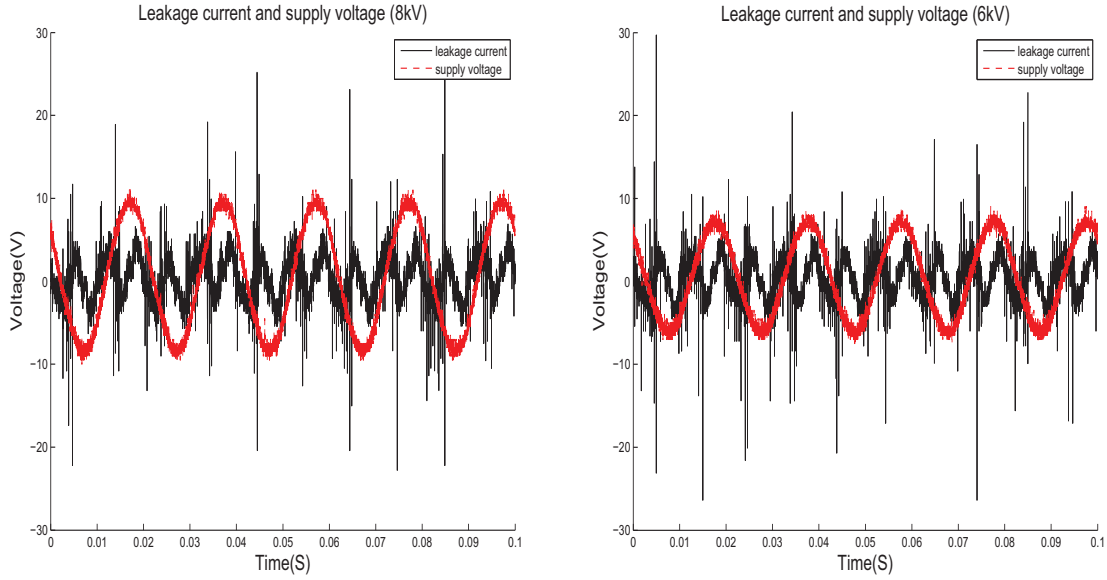

(a) (b)

Fig. 4.6 Measured supply voltages and leakage currents for: (a) a dry insulator at 8 kV; (b) a dry insulator at 6 kV.

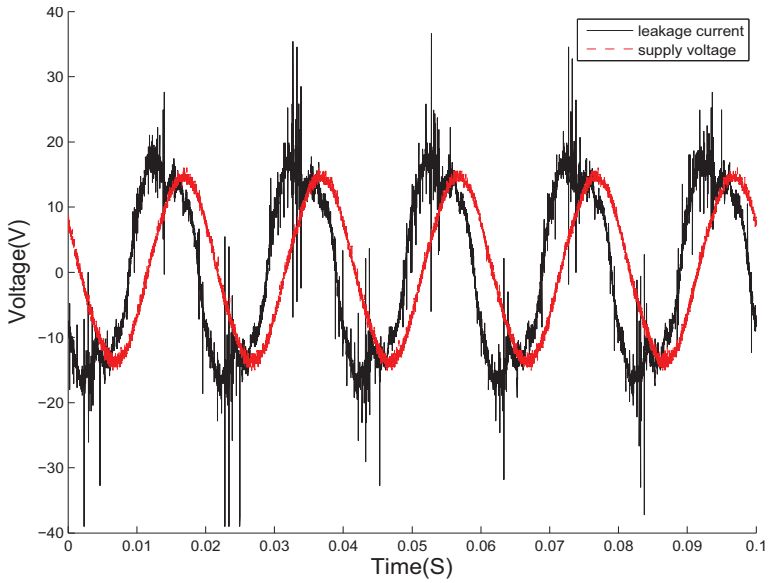

Fig. 4.7 Supply voltage and leakage current (wet contaminated insulator with supply voltage 12.7 kV).

2. After the insulator becomes wet, the amplitude of the leakage current increases significantly. There is a strong correlation between the supply voltage and the leakage current waveforms.

By virtue of equation (4.15), the derived results for the nonlinearity measure of the insulator are shown in Table 4.1. The table also shows the amount of energy dissipated by the leakage current (in scaled units). From these results, the following conclusions may be drawn:

1. Creating wet weather fog conditions by wetting the polluted layer on the high voltage insulator significantly decreases the nonlinearity measure while significantly increasing the energy of the leakage current.

2. As the supply voltage increases, the nonlinearity measure decreases while the leakage current energy increases.

When the supply voltage is so high that the pollution layer cannot tolerate, flashover and arcing occur. The leakage current then changes its shape and magnitude. The corresponding nonlinearity measure then increases. However, given a fixed supply voltage, based on the variation of the nonlinearity measure, it is not sufficient to identify an abnormal event of an insulator. For instance, when fog 'encumbers' insulators in an area, the nonlinearity measure monitored will decrease considerably. The leakage current is high if the insulator is heavily polluted. When the fog suddenly dissipates, the leakage current will heat up the polluted layer on the insulator and dry it very quickly while the nonlinearity measure rises sharply. When relying on this phenomenon only, it is difficult to distinguish this type of event from arcing where the nonlinearity measure may also rise. However, if the energy dissipated of the leakage current is also observed, these two events can be discriminated from each other, since one event occurs with the increase of energy while the other occurs with a decrease of energy.

Table 4.1 Nonlinearity measure for different supply voltages under dry and wet weather conditions for a heavily polluted insulator.

Supply Voltage	n_d (dry)	n_d (wet)	Energy (dry)	Energy (wet)
12.7 kV	0.2773	0.0327	13.9707	46.1519
8 kV	0.6728	0.0566	9.7615	32.1288
6 kV	0.8165	0.0933	9.0574	21.1751

The pattern of the data variation drawn from Table 4.1 is of practical significance and can provide a practical method for detecting abnormal events and identify some of these event types.

4.4.2 Various Contamination Levels at a Fixed Supply Voltage

Following on from examining a polluted insulator for various supply voltages, the experiment was repeated with various levels of contamination at a fixed supply voltage, to examine the effect of the contamination level on the leakage current. The voltage was fixed at 12.7 kV being the line-neutral voltage for a 22 kV distribution system, which is the voltage level used for the majority of Victoria, Australia. The artificial contamination material was introduced and various conductivity levels of the pollution layer were achieved by adjusting the amount of salt content from 5 g up to 20 g. The current waveforms shown in Figure 4.8 are again distorted with harmonics and noise suggesting a nonlinear system. The two waveforms are again both periodic with the same period. Note the phase shift between the voltage and current waveforms in the figure.

Correlation Coefficient and the Nonlinearity Measure

In signal processing theory, data is usually pre-processed which induces loss of information. In this section, data pre-processing is not required to calculate the nonlinearity measure n_d. Therefore, the information is preserved as much as possible. To calculate n_d, the phase shift between these two waveforms needs to be adjusted so that the maximum value of the

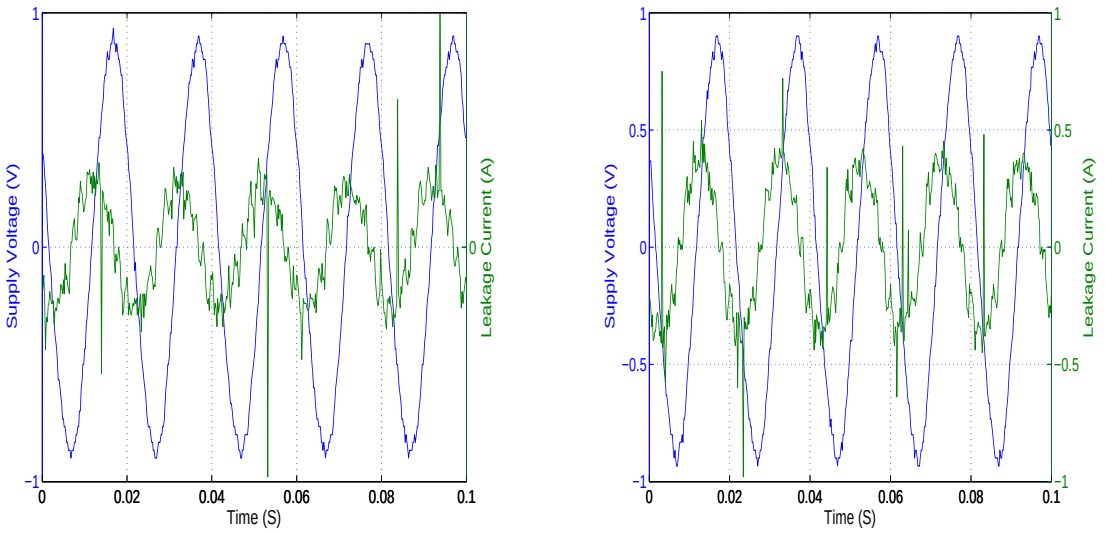

(a) (b)

Fig. 4.8 The scaled supply voltage and leakage current before phase compensation for: (a) a dry non-contaminated insulator; (b) a wet non-contaminated insulator.

correlation coefficient can be obtained. Since the data is discrete, it is easy to determine the phase adjustment value. The waveforms after phase adjustment are shown in Figure 4.9 (the amplitudes of the voltage and current waveforms have no effect on the correlation coefficient, so the magnitude of the voltage and leakage current waveforms in each figure are scaled to fit).

The maximum correlation coefficient derived is 0.7238 and therefore the calculated nonlinearity measure is $n_d = 0.2762$. Before contamination material is applied to the insulator, the insulator is cleaned and dried. The leakage current waveform is recorded and shown in Figure 4.8 (a). The calculated nonlinearity measure is $n_d = 0.1241$. Then, water is sprayed onto the clean insulator to obtain the leakage current waveform for a wet insulator (Figure 4.8 (b)). The obtained nonlinearity measure is $n_d = 0.0697$. Figures 4.8 (a) and (b) suggest that the nonlinearity measures decrease considerably when the surface is wet. The contamination material is then sprayed uniformly onto the surface of the insulator and the leakage current data is collected.

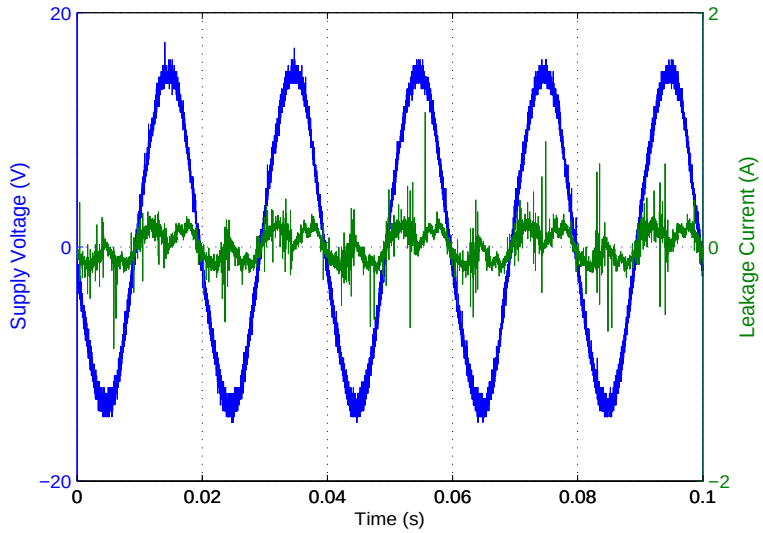

Fig. 4.9 The scaled supply voltage and leakage current after phase compensation for a dry clean insulator.

After the contamination layer is dried naturally, the leakage current is collected again to compare with the other data. The calculated nonlinearity measures are depicted in Figure 4.10 with the horizontal axis indicating the amount of salt mixed in the material. In the figure, the dashed horizontal line indicates the nonlinearity measure ($n_d = 0.1241$) for a clean insulator in a dry condition. Using this dry state as a benchmark, the nonlinearity measures for contaminated insulators in a dry condition drop to values less than 0.1241. The solid horizontal line indicates the nonlinearity measure ($n_d = 0.0697$) for a clean insulator in a wet condition. Compared with the insulator in a dry condition, the degree of nonlinearity falls. When the insulators are contaminated, the nonlinearity measure drops more than half of the value for a dry clean insulator, that is, in a wet condition, the supply voltage and the leakage current are more linearly dependent. In summary, the insulator nonlinearity can be concluded to decrease the nonlinearity measure when the insulator is either wet, contaminated or both wet and contaminated.

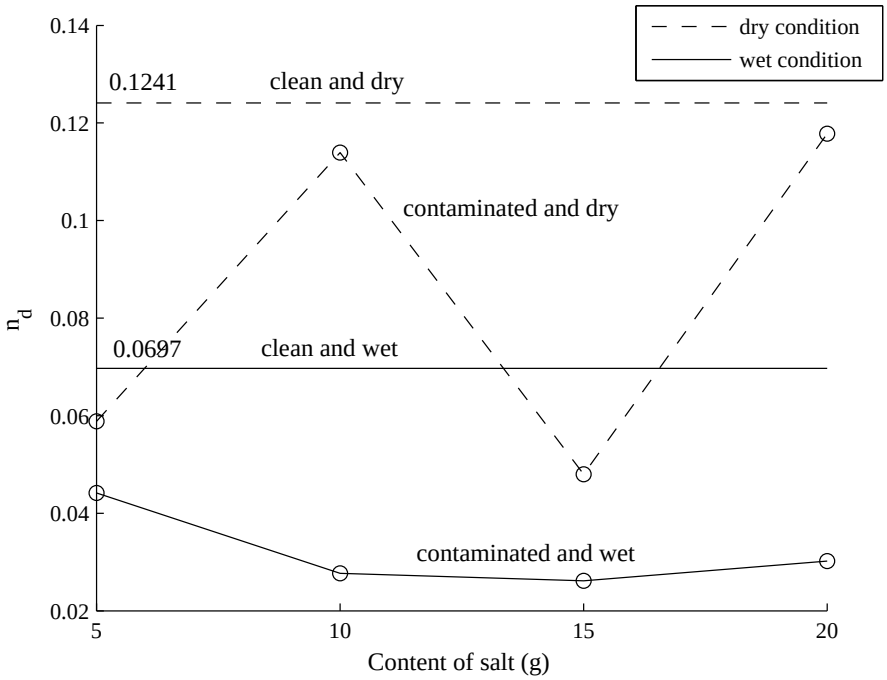

Fig. 4.10 Variation of the nonlinearity measure n_d with respect to the content of salt in the contamination mixture.

Representative Power as a Measure

When assuming the leakage path resistance remains constant, then the power dissipated by the leakage current may be represented by the square of the Euclidean norm of the vector, representing the leakage current waveform, divided by the vector length. Examining this representative power, a considerable increase in its magnitude is observed (Figure 4.11) when the insulator is wet, or contaminated, or both wet and contaminated. It must be noted this is only representative as Section 3.6.2 showed the resistance of a wooden pole (forming part of the leakage path) does not remain constant but in fact decreases under wet weather conditions. In this experiment there was no simultaneous wetting of such a wooden pole. Similarly, insulator contamination also decreases the resistance of the leakage path. Understanding the change in resistance of the leakage path on the insulator may help in identifying the different health states of the insulator.

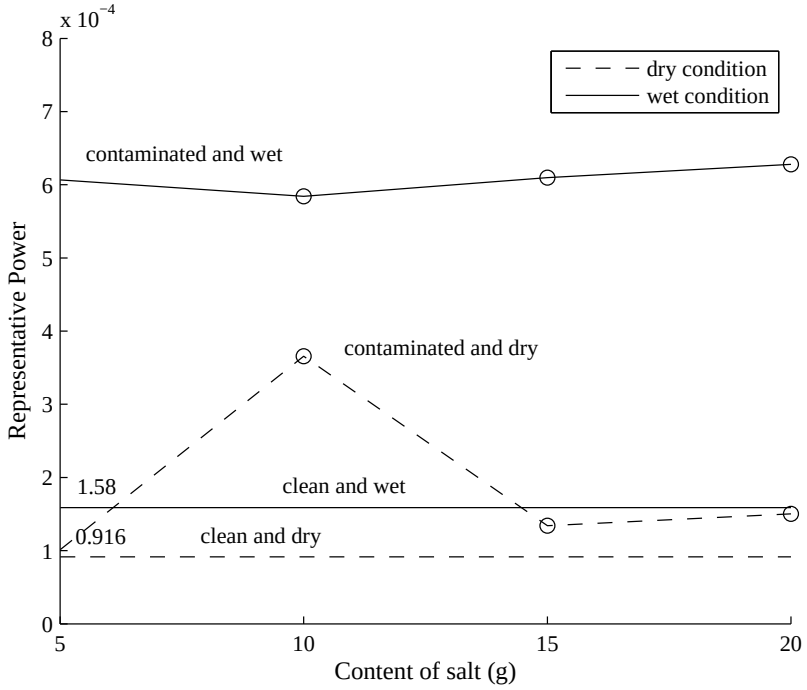

Fig. 4.11 Variation of the representative power of leakage current with respect to the content of salt in the contamination mixture.

For the insulator with a clean surface, the representative power of the leakage current before and after wetting are 0.916×10^{-4} and 1.58×10^{-4} respectively. This is shown in Figure 4.11 by two horizontal baselines. When the insulator is both contaminated and wet, the representative power increase to a magnitude larger than 5.8×10^{-4} which is six times the value for the dry clean insulator, or half an order of magnitude. Thus, representative power of leakage current serves as another quantitative measure of leakage current on a single insulator with various contamination levels and weather conditions.

Fractal Dimension as a Measure

Fractal dimension is useful for describing non-Euclidean geometry as explained in Section 2.5.2. Hence, the fractal dimension can also be used to measure nonlinear systems, in particular the single insulator system. Examining the phase portraits of the insulator system for a qualitative description will provide a useful visual characterisation of the time-evolving

behaviour [147]. Once there is a qualitative understanding of this behaviour, several fractal dimensions can be examined for use as a quantitative measure to follow the evolution of the insulator system.

Figure 4.12 shows the progressive changes in the phase portraits for the insulator system as the level of contamination increases from no pollution to medium pollution levels. Note, there is little noticeable change for phase portrait characteristic under dry weather conditions. This is to be expected, as the leakage current path is still highly resistive. Also, when the insulator is very clean and wet the phase portrait characteristic is again similar to that for dry weather conditions. However, when there is any level of pollution under wet weather conditions the phase portrait is different. Furthermore, as the level of pollution increases, the shape of the phase portrait becomes distorted. Thus, measuring the fractal dimension of these phase portraits should provide a good measure for the increased leakage current activity conducive to heating of smaller metal parts in the leakage path.

Using established routines in MATLAB® [148], the three cases of fractal dimension defined in Section 2.5.2 were calculated and are shown in Table 4.2. These three cases are the box dimension (d_b), the information dimension (d_i) and the correlation dimension (d_c). Studying these cases of fractal dimension, it is clear that the box dimension is superior for this application as its magnitude *drops sharply* for the most distorted of the phase portraits, that is for the most contaminated insulator system under wet weather conditions. Thus, for the levels of contamination examined here the box dimension of the insulator system serves as a fair quantitative measure of leakage current, although susceptible to noise.

4.5 Measuring Leakage Current prior to Flashover

There is a stage prior to flashover where the leakage current appears as isolated peaks that occur with increasing frequency [46, 84, 86, 87]. This is owing to the increasing intensity of arcing activity [46]. The waveform is aperiodic which is a typical phenomenon during

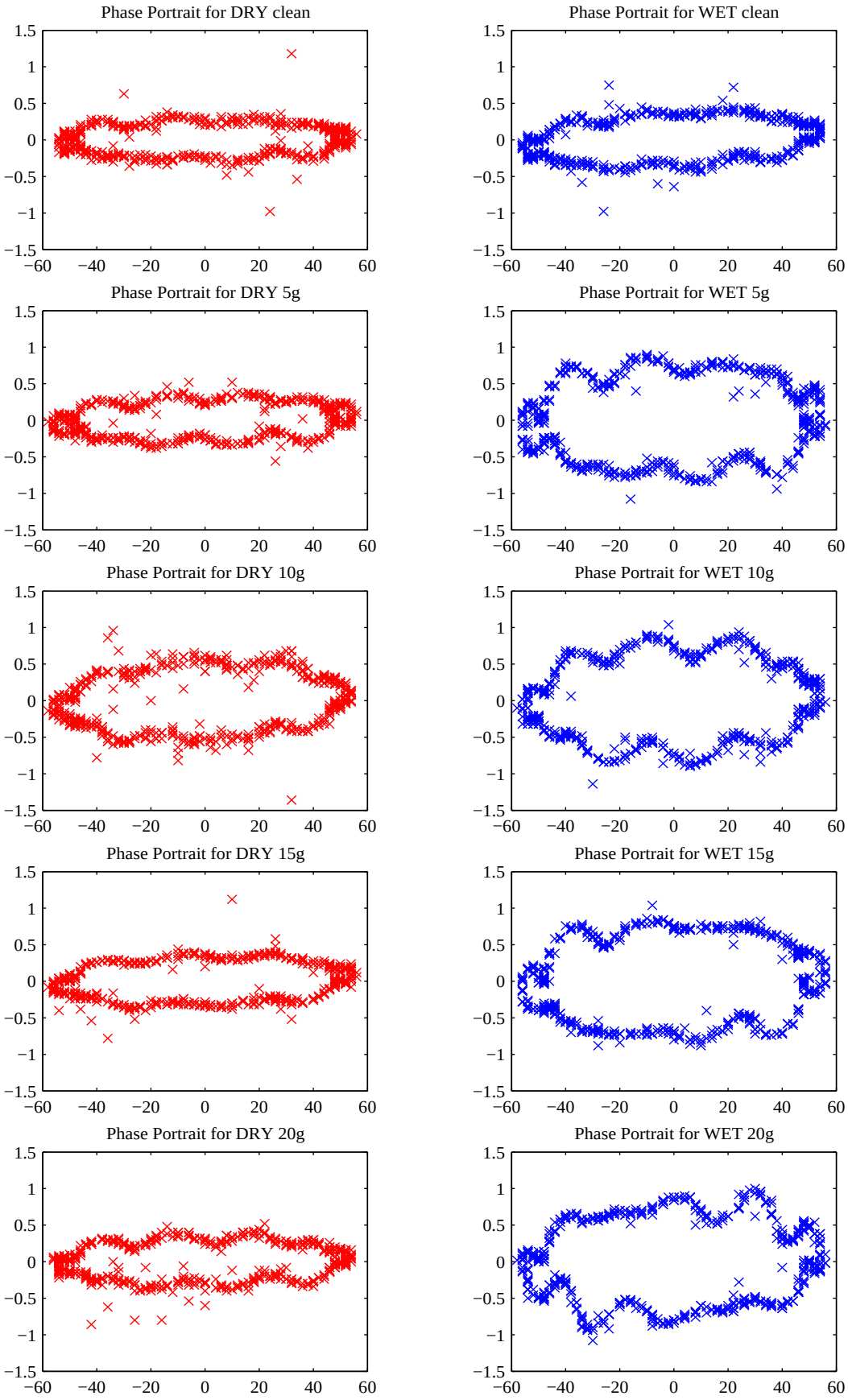

Fig. 4.12 Phase portraits of a high voltage insulator for various levels of contamination under dry and wet weather conditions; x-axis: scaled supply voltage, y-axis: leakage current in milliamps.

Table 4.2 Fractal dimensions with an embedding dimension = 2 of high voltage insulator for various levels of contamination under dry and wet weather conditions.

Pollution Level	Weather Condition	Box Dimension (d_b)	Information Dimension (d_i)	Correlation Dimension (d_c)
clean	dry	1.1745	0.7631	0.2011
5g	dry	1.1488	0.7662	0.2041
10g	dry	1.1442	0.7902	0.2138
15g	dry	1.1703	0.7640	0.1934
20g	dry	1.1308	0.7709	0.2051
clean	wet	1.1661	0.7750	0.2006
5g	wet	1.1618	0.8336	0.3586
10g	wet	1.1531	0.7804	0.2053
15g	wet	1.1661	0.8082	0.3425
20g	wet	1.0927	0.7675	0.2083

the development of flashover. This stage is the transition period to flashover. If this stage can be identified, then the flashover can be predicted and avoided. Therefore, analysing the leakage current waveform in this period is of much significance. A typical leakage current waveform at this stage is depicted in Figure 4.13 (a) [46] (this type of waveform is also reported in [84, 86, 87]). The supply voltage for this case has a frequency of 60 Hz. In the transition stage, the contamination layer on the insulator changes its physical condition which results in the variation of the nonlinearity of the insulator which is reflected in the leakage current.

To calculate the nonlinearity measure n_d, a time window with 5 periods was utilised to obtain a segment of the leakage current waveform and the supply voltage waveform to calculate the nonlinearity measure n_d. Here, the supply voltage was a sinusoid. By sliding the time window along the time axis of the leakage current, the variation of n_d was derived and shown in Figure 4.13 (b). This figure illustrates the nonlinearity measure was considerably large for most points of time, reaching the highest level of 0.7 at $t \approx 0.05$s, indicating strong nonlinearity. The measure reached a low of 0.1390 at $t \approx 0.175$s, larger than most of the n_d data obtained in Section 4.4. Examining the representative power in

Figure 4.13, a bell-shaped curve peaking at $t \approx 0.175$s was observed. This measure does not pick up when nonlinearities begin occurring, but is useful in corroborating the increase in dissipation of power caused by the leakage current after the nonlinearity effects have occurred.

The leakage current waveform is again reproduced in Figure 4.14, this time for comparison with the box dimension d_b, the information dimension d_i and the correlation dimension d_c. Surprisingly the box dimension produces a bell-shaped curve similar to the representative power, which is explained by the shapely leakage current disturbance, although contrary to the observations for much lower levels of contamination in Section 4.4. Both the information dimension d_i and the correlation dimension d_c detect the nonlinearity changes at $t \approx 0.075$s, 25 ms later than the nonlinearity measure n_d. Between $t = 0.15$s and $t = 0.225$s d_i picks up the shapely leakage current activity which was also picked up by d_b, however d_c discounts this activity similar to the nonlinearity measure. At $t = 0.25$s, both d_i and d_c detect more changes in the leakage current activity, that is the nonlinearity which was also picked up by n_d. Thus, the correlation dimension also picks up the nonlinearities detected by the nonlinearity measure, however with a slight time lag of approximately 25 ms.

4.6 Discussion

This chapter has established a new nonlinearity measure useful for providing quantitative information regarding nonlinear systems. This measure adds to the suite of techniques used for leakage current analysis. This technique has the advantage of including interharmonics which have been omitted by other established techniques. The nonlinearity measure was defined in terms of the correlation coefficient. It was determined when examining waveforms, the sample window size and the dataset being contemplated do not have to be too large to capture waveform changes. Furthermore, when assuming noise was uncorrelated, the correlation coefficient was deemed suitable as a measure for comparing waveforms. The

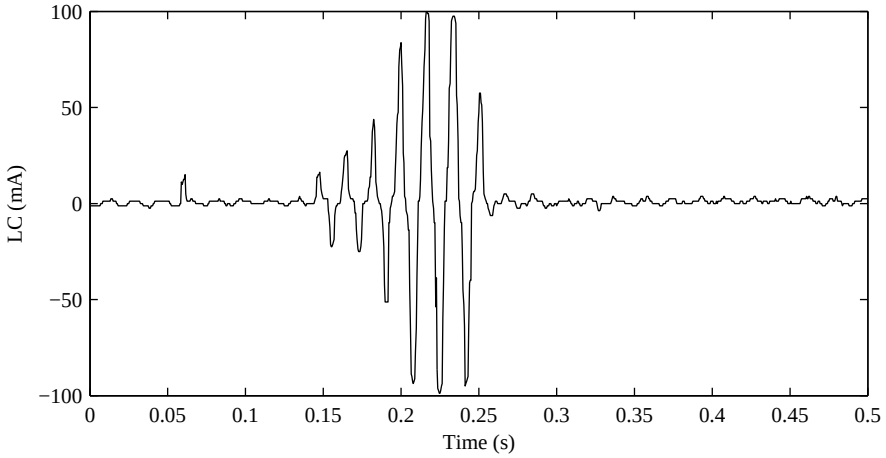

(a) Leakage current waveform

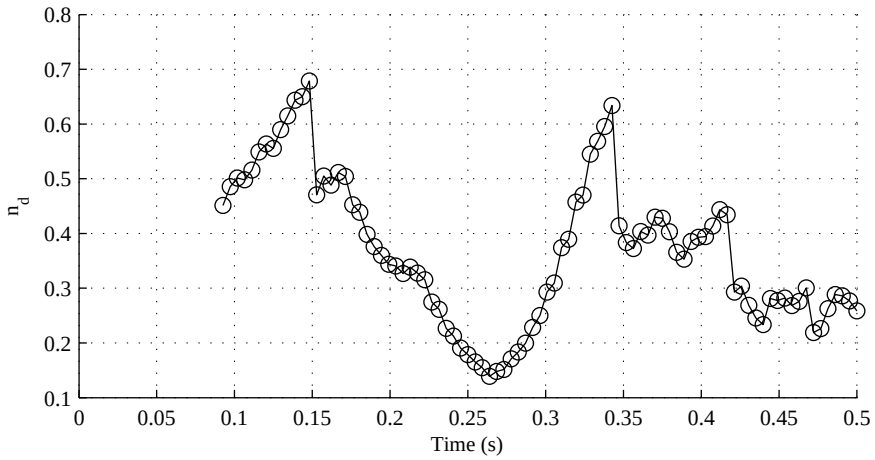

(b) Nonlinearity measure progression

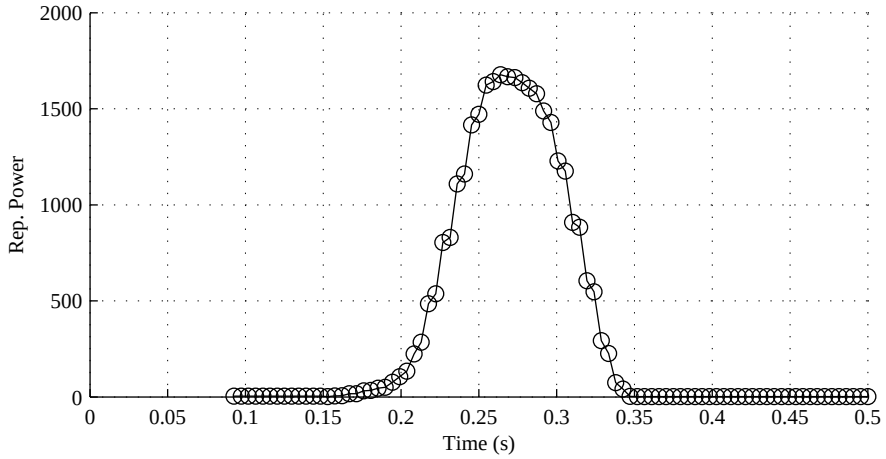

(c) Representative power progression

Fig. 4.13 A typical leakage current waveform in the stage prior to a flashover, and the corresponding progression of the nonlinearity measure n_d and representative power measure.

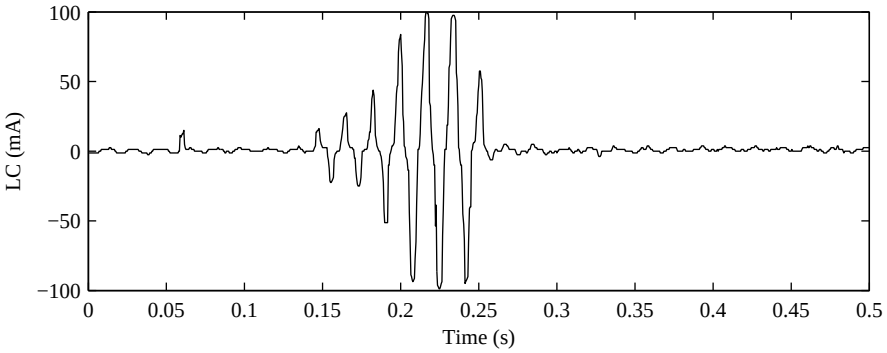

(a) Leakage current waveform

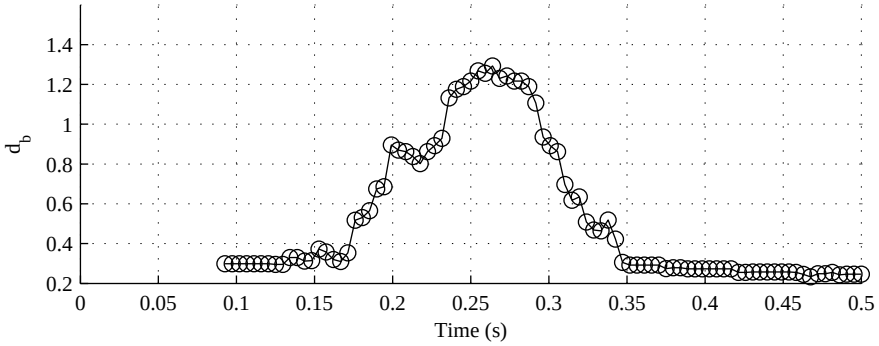

(b) Box dimension progression

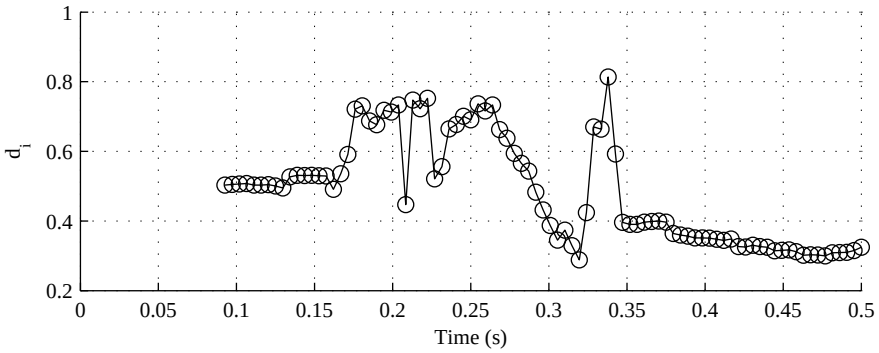

(c) Information dimension progression

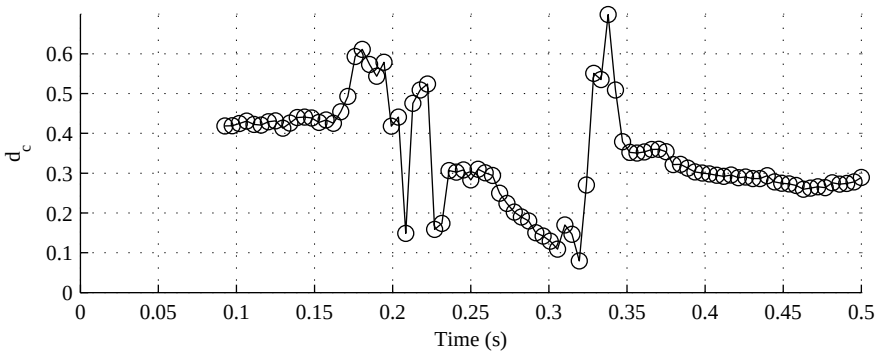

(d) Correlation dimension progression

Fig. 4.14 A typical leakage current waveform in the stage prior to a flashover, and the corresponding progression of three fractal dimensions as measures.

high voltage insulator was then examined and the results observed highlighted the leakage current signature of contaminated insulators represented by a nonlinearity measure.

Further examination via a representative power measure and fractal dimensions also prove useful. Representative power can be used to corroborate the presence of heat dissipation caused by leakage current. Inspecting the phase portraits at different levels of contamination under different weather conditions for qualitative information revealed a changing shapely trajectory, suitable for measurement by fractal dimension. The box fractal dimension identified shapely leakage current activity while the correlation fractal dimension detected nonlinearities. The information fractal dimension only provided just that, information indicating some sort of activity was occurring, however, this fractal dimension was unable to distinguish what that information represented.

Utilising a leakage current waveform accepted in the literature as typical in the stage prior to flashover, the nonlinearity measure, representative power, and three fractal dimensions were examined. The results confirmed that both the nonlinearity measure and the correlation fractal dimension do indeed identify nonlinearities in a waveform, even of small magnitude. Thus, based on the knowledge provided by the nonlinearity measure and the information fractal dimension, the health state of the insulators can be identified and are quite suitable for contributing to a LCHI. This is of great importance for flashover prediction to help reduce the number of fire starts. Moreover, carefully combining the measures established in this chapter with a combination of traditional leakage current analysis techniques and learning algorithms or neural networks are expected to provide a LCHI with speed and accuracy. A further benefit of the nonlinearity measure technique is that it can be implemented on a quasi real-time basis because only a few cycles of the leakage current waveform are required to calculate the nonlinearity measure. This means the condition of the insulators can be monitored almost in real-time.

There are a number of points to be clarified here about the completeness of this work

and the practical implementation. The insulator used in the experiment had various levels of pollution applied. The data was drawn under dry and wet conditions. More experiments are needed to consider much higher levels of pollution as well as different types of insulators and a large range of humidity levels [88, 91]. Insulators under different temperatures should also be studied [149]. Furthermore, different contamination mixtures should be tested with the proposed techniques [150]. Arcing and flashover waveforms should also be collected to further verify the profile in Section 4.5.

This chapter has only considered a single high voltage insulator. To build a more complete profile of contaminated insulators forming a distribution feeder, further systematic analysis will be considered in Chapter 5.

4.7 Summary

A nonlinearity measure has been used to present a new leakage current analysis technique, which can be applied to a vast variety of insulation systems in power grids. Further measures which include the representative power, the box dimension, the information dimension and the correlation dimension are also considered. A profile for a contaminated insulator has been built under different weather scenarios. It can be concluded that light contamination and wetting reduce the degree of nonlinearity of the insulators. For the leakage current waveform in the stage prior to flashover, the profile captured is unique and contains a high degree of fluctuating nonlinearity with a significant increase of the representative power of leakage current. The results suggest that the insulator exhibits various degrees of nonlinearity under different weather conditions and at different stages of the development of flashover. The new nonlinearity measure and the correlation fractal dimension provide valuable quantitative tools for the study of insulator flashover prediction.

Chapter 5

Systematic Power Line Modelling and Leakage Current Analysis

5.1 Overview

Following on from the concepts, techniques and measures established for a single polluted high voltage ceramic insulator, this chapter aims to extend these to application to an overhead power line and a group of power lines. Utilising measures, the health state and health profile of a power line shall be developed, paving the way for a future 'health index' to smartly monitor leakage currents. Section 5.2 applies the results from Chapter 4 to a set of insulators forming a high voltage power line under three different scenarios. For each scenario, a model of the power line configuration is systematically created, followed by performing measure analysis on the leakage current results. Section 5.3 tests the measures established in Chapter 4 utilising data collected in the field for a pole fire event. Section 5.4 discusses how each measure performs and contemplates on how these measures may be used to establish a LCHI.

5.2 Systematic Power Line Modelling and Analysis

In practice, it is impractical to monitor every insulator. Instead, it is more reasonable to monitor the leakage current on a set of insulators on a power line (feeder) or at the very least a segment of the power line. In this section, a systematic approach to analysing power lines is considered. The feeder will be constructed as a set of polluted insulators. The feeder will be considered under partly dry and partly wet weather conditions. Some assumptions and basic analysis will be made. Then, based on the experimental results in Chapter 4, correlation coefficients, the nonlinearity measure, the representative power and the fractal dimensions will be computed for various feeder configurations. By increasing the number of insulators, the weather conditions that affect the leakage current will be examined. Comparing various levels of contamination on a set of insulators under wet weather conditions with that of a clean set of insulators shall shed light on identifying the contamination level of the insulators.

5.2.1 Case Study I: A Simple Set of Insulators System

For this first case study of leakage current for a set of insulators, a simple single-phase system is established where the resistance, inductance and capacitance of the power line is assumed negligible such that all of the insulators receive the same voltage supply. The source impedance is also assumed negligible, and the line is assumed unloaded. The insulators on the feeder are assumed to have the same level of contamination (with the same amount of salt) but under different weather conditions. Various contamination levels will be considered. The supply voltage is assumed to be an ideal sinusoidal waveform. The data acquired in Chapter 4 for a single insulator system can be utilised through summation of individual insulator leakage currents to generate the overall leakage current for a feeder subject to controlled conditions for the entirety of the feeder. This takes into account the phase difference between the leakage current and the supply voltage.

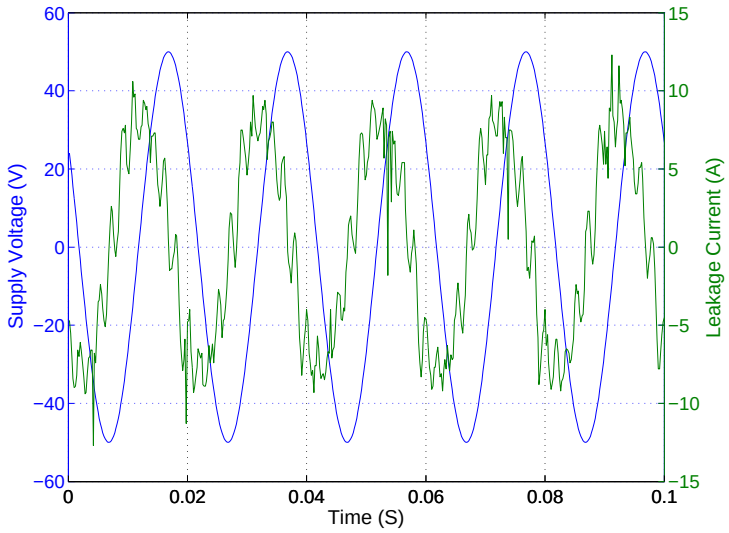

Fig. 5.1 The scaled waveforms of the supply voltage and the leakage current for the case study of a simple system set of insulators.

Feeder Circuit Configuration

The feeder considered in this scenario consists of 25 insulators. The conditions are controlled as explained in the following example: if the supply voltage is 12.7 kV and there are 20 insulators in a dry weather condition together with another 5 insulators in a wet weather condition, then the leakage current generated in the overall 25 insulators will be the sum of the leakage current of the 20 dry insulators and the leakage current of the 5 wet insulators. The waveform generated in this scenario is shown in Figure 5.1. The procedure for calculating the leakage current for this simple system set of insulators is straightforward. It imitates a set of insulators in the same area which have similar contamination levels. Nevertheless, it has some short comings. For instance, it neglects the interaction among the insulators and the impedance of the feeder. However, these shortcomings do not affect the introduction of the idea before further analysing lossless and lossy lines in Sections 5.2.2 and 5.2.3.

Measure Results and Analysis

The nonlinearity measure, the representative power, and the three fractal dimensions box dimension, information dimension and correlation dimension all as measures of the leakage current were calculated accordingly. The fractal dimensions were all calculated with an embedding dimension equal to 2. By increasing the number of wet insulators from 0 to 25, curves were derived reflecting the variation of the nonlinearity measure, the representative power and the fractal dimension as shown in Figures 5.2, 5.3 and 5.4 respectively. For the convenience of comparison, the corresponding values for a clean insulator are marked in Figures 5.2 and 5.3 by solid horizontal lines.

Figure 5.2 indicates that the relationship between n_d and the number of wet insulators in the set is nonlinear. When more than 6 insulators are wet, n_d drops to less than half of the value for a single clean dry insulator. Figure 5.3 shows there is a monotonic increase in representative power when there were more wet insulators, no matter the insulators' contamination level. Furthermore, the representative power increases significantly in comparison with a clean set of insulators. Examining the three graphs of fractal dimension in Figure 5.4, there was no discerning difference between the three dimensions, nor was there any noticeable difference between contamination levels as the number of wet insulators increase. Thus, the fractal dimension provides no further information for this simple set of insulators system.

5.2.2 Case Study II: A Lossless Set of Insulators System

In this case study of leakage current for a set of insulators, a lossless line will be considered. A typical single-phase equivalent circuit diagram for an overhead distribution feeder mounted on insulators via a crossarm fixed to a wooden pole is shown in Figure 5.5. This system is in a quasi-steady state condition without any transients, that is, the feeder is a leaky line, where the leakage current data acquired in Chapter 4 is again used to generate

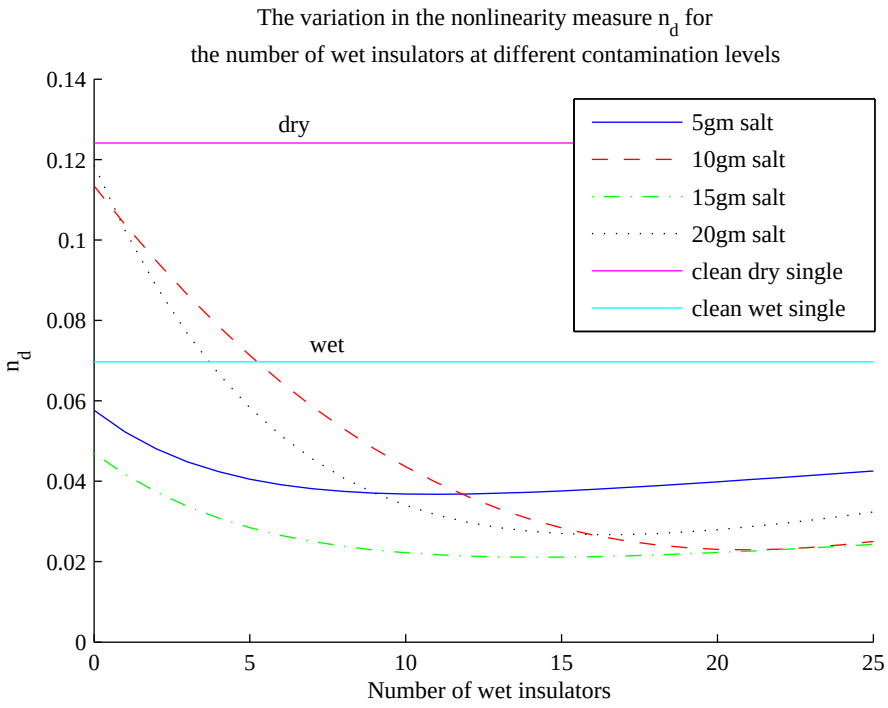

Fig. 5.2 Variation in the nonlinearity measure n_d for the number of wet insulators on a simple insulator set system at different levels of salt contamination.

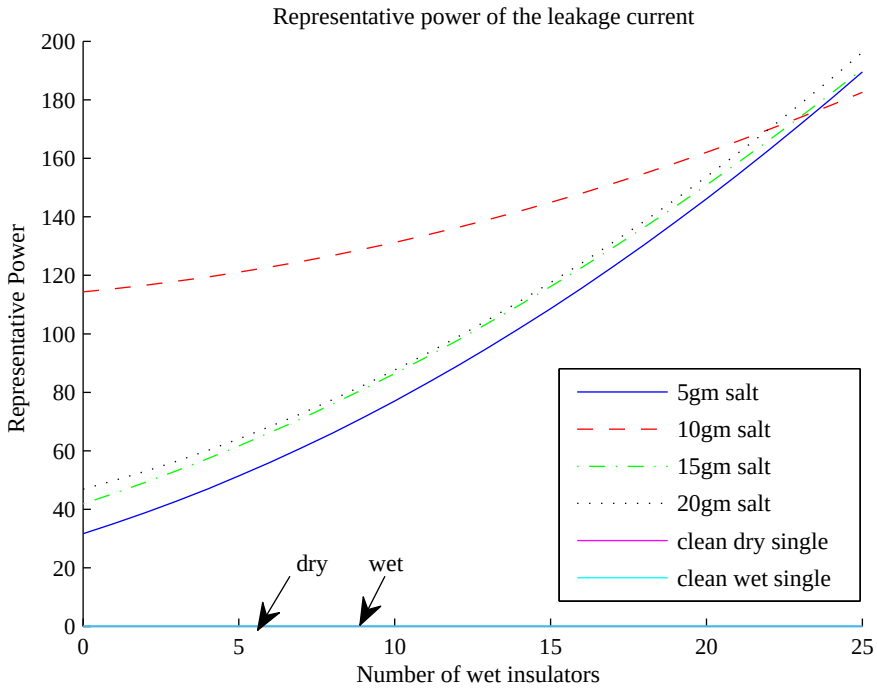

Fig. 5.3 Variation in the representative power of leakage current for the number of wet insulators on a simple insulator set system at different levels of salt contamination.

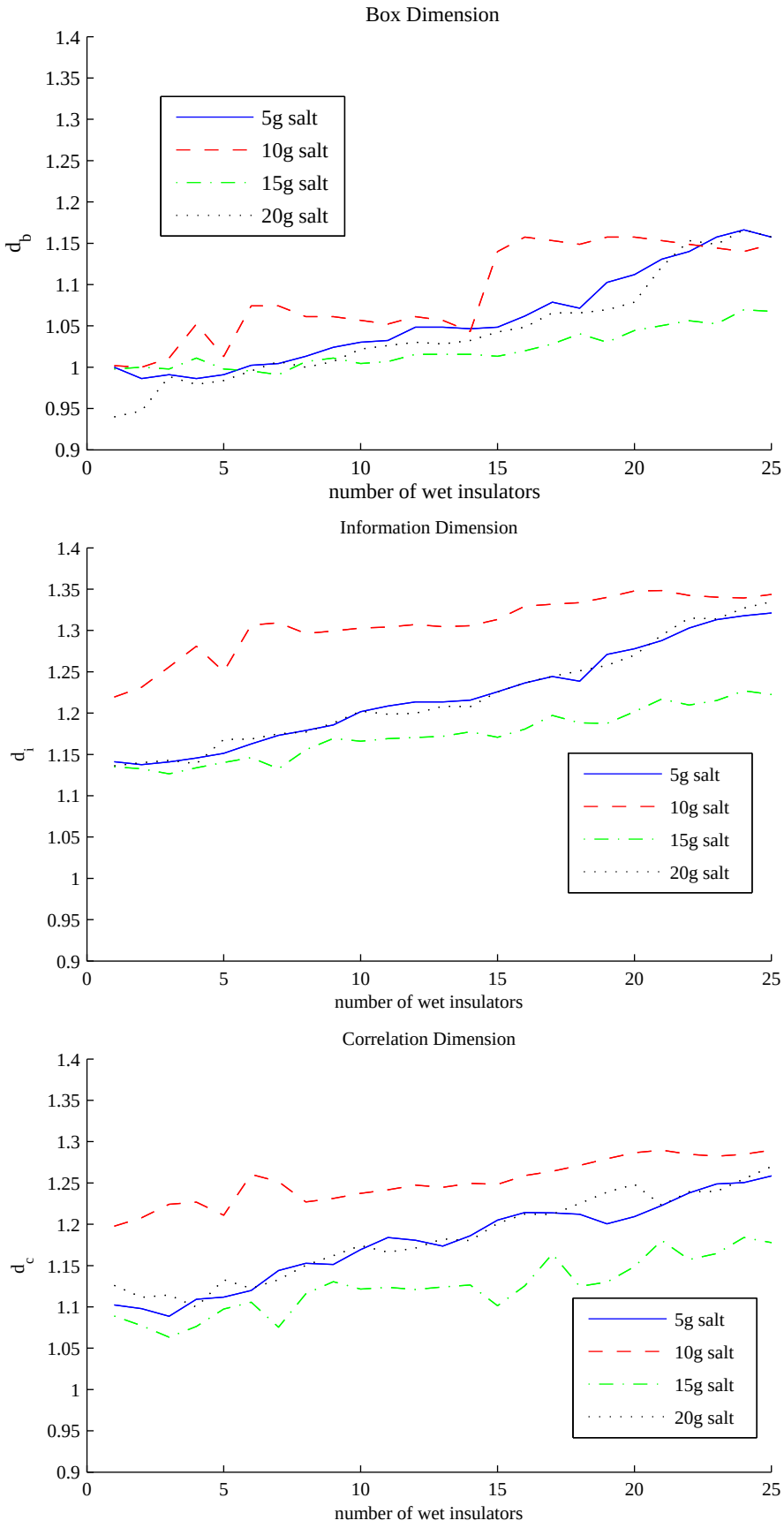

Fig. 5.4 Fractal dimensions for a simple system of a set of high voltage insulators on a feeder at different levels of contamination as the number of wet insulators is varied.

each leakage current on the line. These line leakage currents are small in magnitude without any line load in the proposed scenarios, so the following modelling needs to be treated with caution as the models may deviate from practical expectations for full line currents.

Feeder Circuit Configuration

The circuit parameters for the overhead power line feeder configuration assumes the line resistances R_{L-1}, $R_{L-2}, \ldots, R_{L-n}$ are all zero. The distance between each pole is assumed to be equal, and the conductor is assumed to be of the same type for the entire length of the line, hence the inductive impedance of each line segment being equal. Thus, the inductive impedances are $X_{L-1} = X_{L-2} = \cdots = X_{L-n} = X_L$. The crossarm resistances R_{arm-1}, R_{arm-2}, $\ldots, R_{arm-n}$, the wooden pole resistances $R_{pole-1}, R_{pole-2}, \ldots, R_{pole-n}$ and the capacitive impedance of each wooden pole $X_{C-1}, X_{C-2}, \ldots, X_{C-n}$ are assumed to be each of zero magnitude, hence being a zero impedance. The high voltage insulator resistances R_{ins-1}, R_{ins-2}, $\ldots, R_{ins-n}$ are known to be nonlinear resulting in leakage currents $I_{LC-1}, I_{LC-2}, \ldots, I_{LC-n}$ derived as indicated above. The voltage source resistance R_s is assumed negligible. The supply voltage source is assumed similar to the data acquired in Chapter 4.

The leakage currents I_{LC-i} where $i = 1, 2, \ldots n$ are assumed to be in phase with the voltage source, that is synchronised. Now, using Kirchhoff's current law for each segment $n, n-1, \ldots, 2, 1$ the currents out of each node sum to be the current into the node. At each node i except for node $i = n$, the line current goes through a 90° phase shift by way of the inductance X_{L-i}. The line current I_{L-i} in each segment $i = 1, 2, \ldots, n-1$ is resolved by summing the leakage current I_{LC-i} with the next segment's line current I_{L-i+1}. Thus, the source current $I_s = I_{L-1}$ can be calculated using a procedure where each leakage current $I_{LC-n-1}, \ldots, I_{LC-2}, I_{LC-1}$ is shifted in turn by the phase angle 90° and summed to produce I_{L-1}. For the purposes of this scenario, the line is unloaded, and the feeder is 7.5 km long with power poles spaced 50 m apart. Hence, the line consists of 150 insulators. The condi-

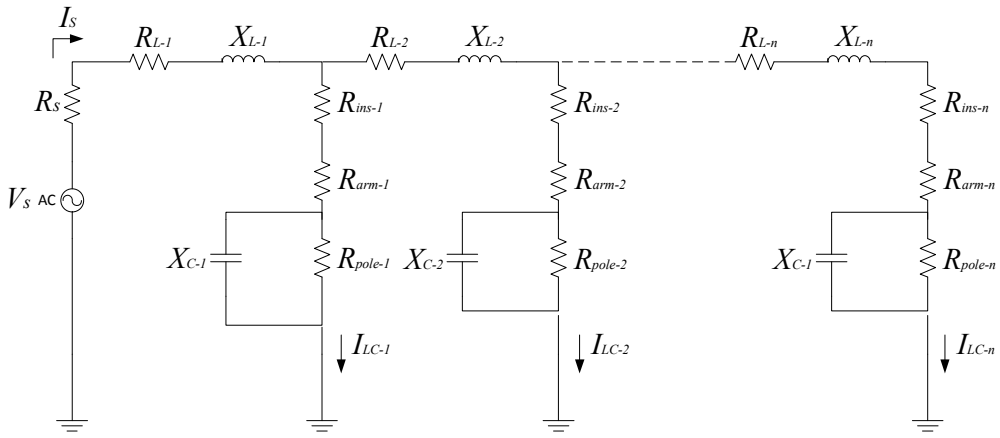

Fig. 5.5 Circuit diagram of overhead distribution feeder with line suspended on insulators mounted on a crossarm attached to wooden poles.

tions are again controlled as explained in Section 5.2.1, however 150 insulators are used in place of the 25 insulators considered in the simple system case.

Measure Results and Analysis

Once the system voltage V_s and system current I_s of the lossless line were established, the nonlinearity measure, the representative power, and the three fractal dimensions being examined were calculated. Again, the fractal dimensions were calculated with an embedding dimension of 2. By increasing the number of wet contaminated insulators from 0 to 150, curves were derived which reflect the nonlinearity measure, the representative power and the fractal dimension as illustrated in Figures 5.6, 5.7 and 5.8 respectively. The measure values for a single clean insulator and single wet insulator are also shown in Figures 5.6 and 5.7 for comparison.

The relationship between n_d and the number of wet insulators in the set was clearly cyclic and nonlinear. The cyclic nature was most likely caused by the construction of the lossless line, that is with equal pole spacings and zero resistance lines. In this case, the nonlinearity measure provides little useful information for the change in contamination of an increased number of wet insulators. The representative power also displays an unusual char-

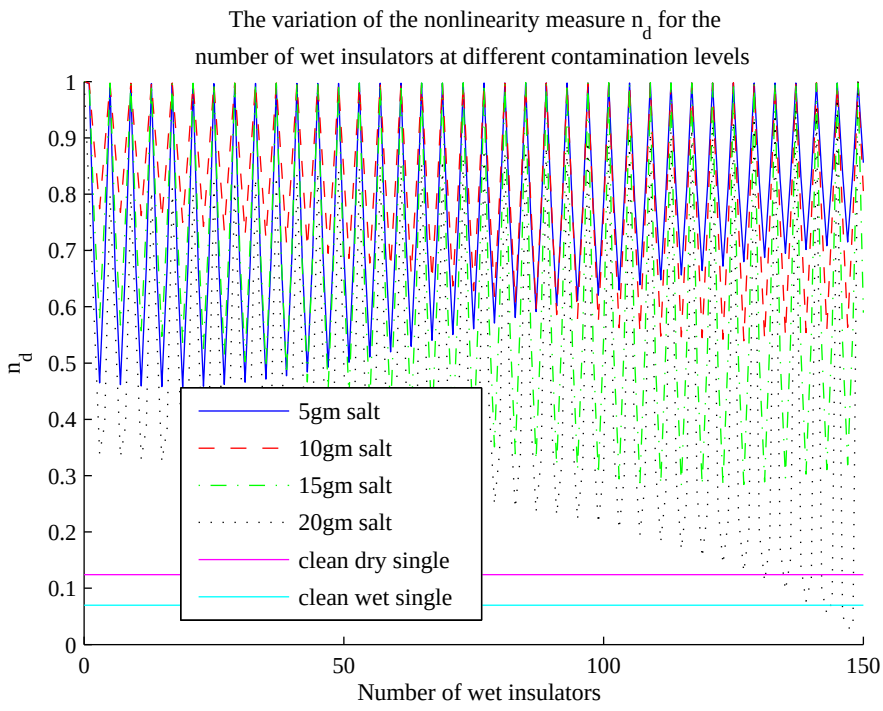

Fig. 5.6 Variation in the nonlinearity measure n_d for the number of wet insulators on a lossless feeder at different levels of salt contamination.

acteristic, that is cyclically increasing for low contamination levels, and cyclically decreasing as the contamination levels increase. Again, this is likely attributed to the interference pattern being created by the lossless line. Examining the fractal dimension graphs, the box dimension shows little difference between contamination levels, but both the information dimension and the correlation dimension show a fall in the dimension magnitude (although with a cyclic behaviour). The correlation dimension magnitude drops away from the lower levels of contamination for only 80 insulators, as does the information dimension. However the drop by the correlation dimension is much more dramatic. Thus, the information and correlation dimensions were able to distinguish the higher level of contamination for the lossless line case study.

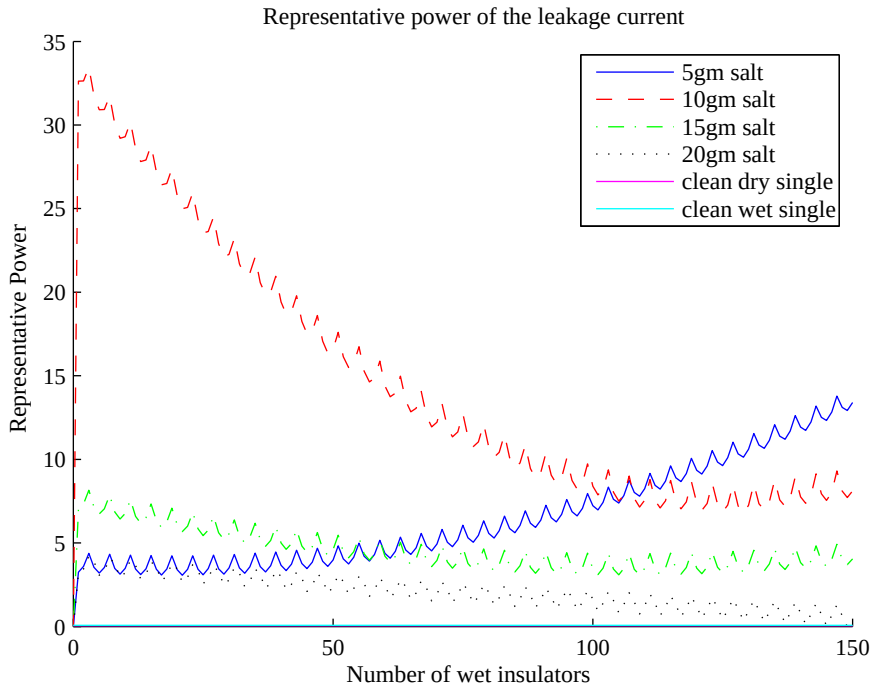

Fig. 5.7 Variation in the representative power of leakage current for the number of wet insulators on a lossless feeder at different levels of salt contamination.

5.2.3 Case Study III: A Lossy Set of Insulators System

The third case study will investigate the leakage current for a set of insulators forming a lossy line. The single-phase equivalent circuit diagram for an overhead distribution feeder shown in Figure 5.5 will once again be used. In this scenario, the system is again a quasi-steady state condition without any transients and the feeder is a leaky line. The distance between each pole is assumed to be equal. The power line will be based on the feeder 'MC3' featured in the single line diagram of a zone substation pictured in Figure 5.9 [151]. This feeder is approximately 7.5 km long and the conductors making up the overhead part of the feeder consist of sections of aluminium conductor with steel reinforcement (ACSR) and all aluminium conductor (AAC) [152], while the underground cable sections are made of copper and aluminium cables [153]. For the purposes of this analysis, the feeder will be assumed to be ACSR conductor for the entire length of the feeder.

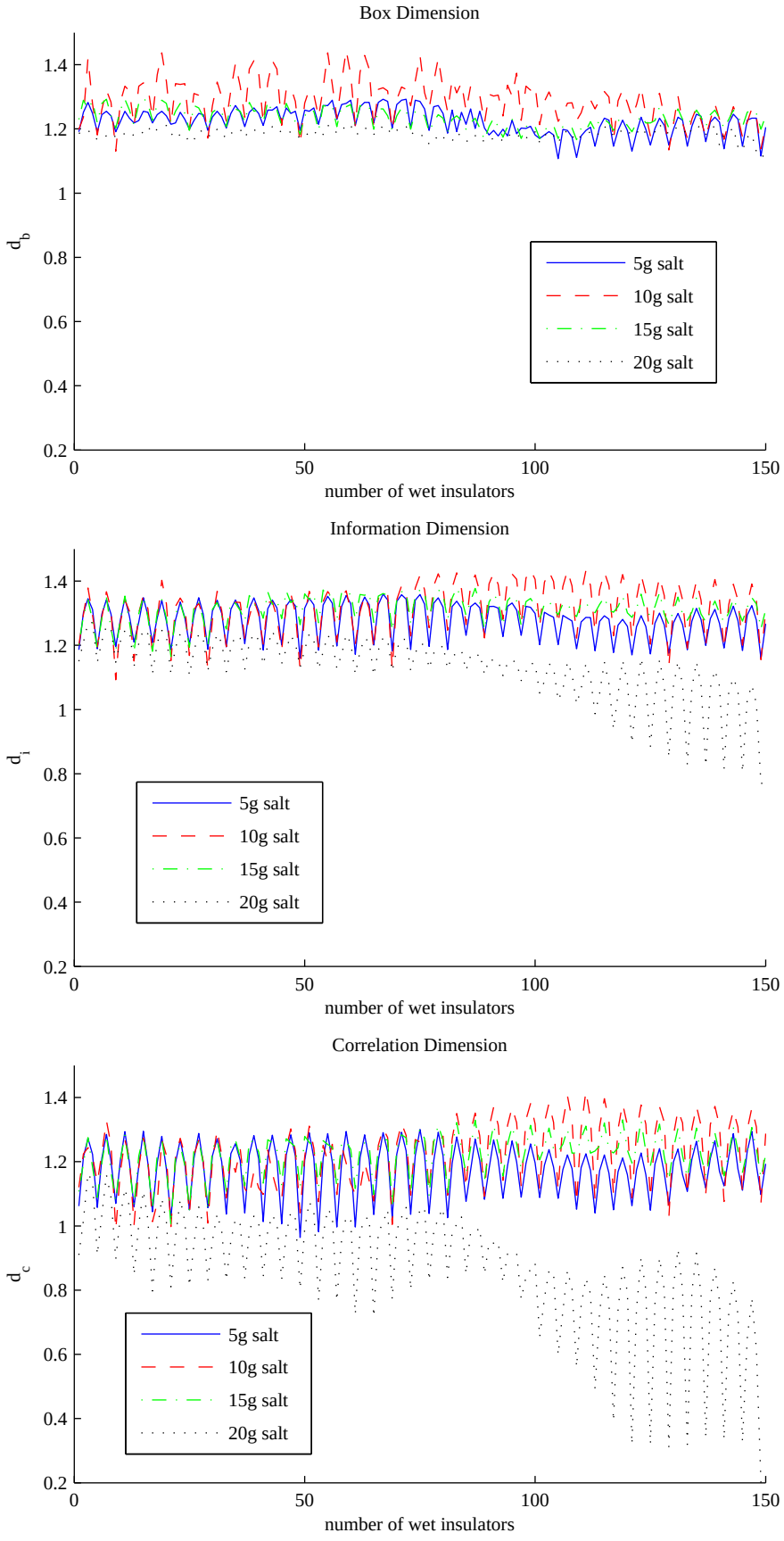

Fig. 5.8 Fractal dimensions for a lossless system of a set of high voltage insulators on a feeder at different levels of contamination as the number of wet insulators is varied.

Feeder Circuit Configuration

The parameters for the overhead power line circuit assumes positive equal line resistance segments such that $R_{L-1} = R_{L-2} = \cdots = R_{L-n} = R_L$ and positive equal line reactance segments such that $X_{L-1} = X_{L-2} = \cdots = X_{L-n} = X_L$, that is a lossy line. The crossarm resistances $R_{arm-1}, R_{arm-2}, \ldots, R_{arm-n}$, the wooden pole resistances $R_{pole-1}, R_{pole-2}, \ldots, R_{pole-n}$ and the capacitive impedance of each wooden pole $X_{C-1}, X_{C-2}, \ldots, X_{C-n}$ are assumed to be each of zero magnitude, hence being a zero impedance. The high voltage insulator resistances R_{ins-i} where $i = 1, 2, \ldots n$ are known to be nonlinear, resulting in corresponding leakage currents I_{LC-i} which shall be derived in a similar fashion to Case Study II. The voltage source resistance R_s is assumed negligible. The supply voltage source is assumed similar to the data acquired in Chapter 4.

Examining the fault level database [153] for the zone substation, which details the resistance and reactance of the feeder conductors, section by section, the ACSR conductor components corresponding to the feeder 'MC03' were derived to be $r_l = 0.001\,\Omega\,\mathrm{m}^{-1}$ and $x_l = j0.0023\,\Omega\,\mathrm{m}^{-1}$. Hence $R_L = 0.051\,163\,\Omega$ and $X_L = j0.115\,116\,\Omega$ for each 50 m span. Utilising the following electrical impedance relationships [154]:

$$\|Z\| = \sqrt{ZZ^*} = \sqrt{R^2 + X^2} \tag{5.1}$$

and

$$X = \|Z\| sin\theta \tag{5.2}$$

where Z is apparent impedance, R is resistance, X is reactance, and θ is the phase shift between the voltage across it and the current through it, the phase shift between each leakage current I_{LC-i} can be shown to equal 66°. The leakage currents I_{LC-i} where $i = 1, 2, \ldots n$ are assumed to be in phase with the voltage source, similar to the case study in Section 5.2.2.

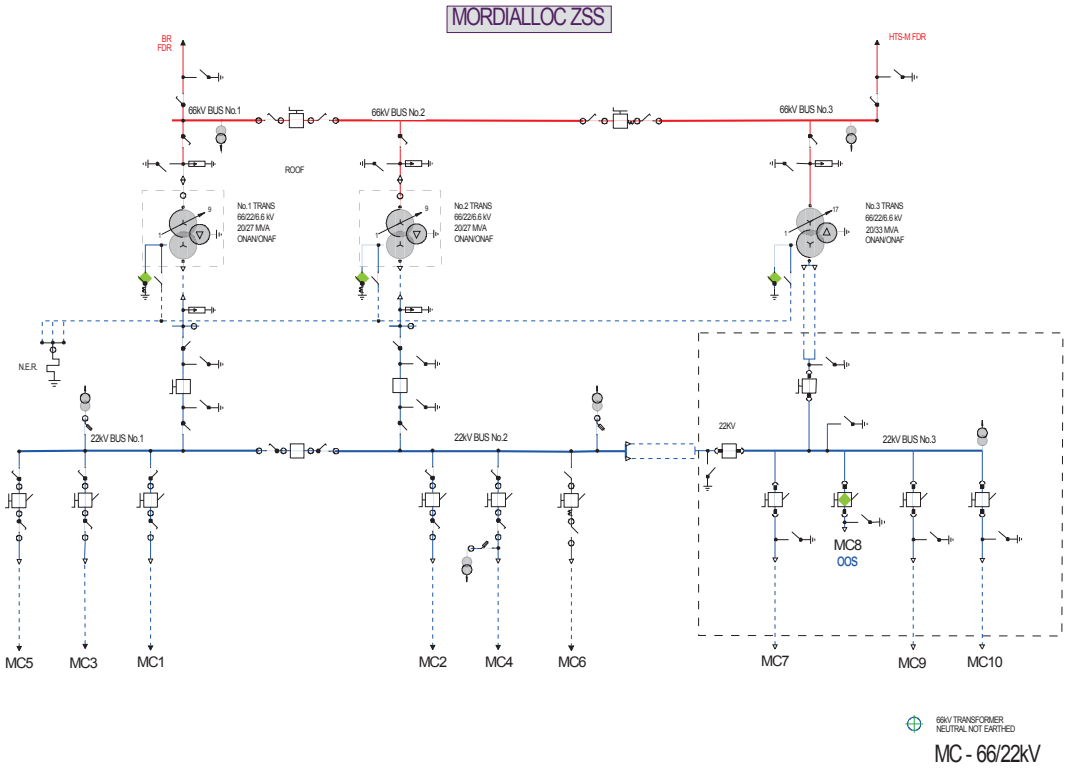

Fig. 5.9 Single Line Diagram (SLD) of a typical Zone Substation with ten 22 kV radial feeders for distribution in Melbourne, Victoria.

Using the same procedure illustrated in Section 5.2.2, the source current I_s can be calculated but in this case using a phase shift angle of 66°. For the purposes of this scenario, the line is unloaded, and the feeder's power poles spaced 50 m apart. Hence, the line consists of 150 insulators. The contamination and weathering conditions are controlled in a similar fashion to that in Section 5.2.2.

Measure Results and Analysis

After establishing the system voltage V_s and system current I_s of the lossy line, the nonlinearity measure, the representative power, and the three fractal dimensions under consideration were again calculated. The fractal dimensions had an embedding dimension of 2. The number of wet contaminated insulators were increased from 0 to 150, similar to Section 5.2.2 and the nonlinearity measure, the representative power and the fractal dimension

were plotted in Figures 5.10, 5.11 and 5.12 respectively. For reference, the measure values for both a single clean insulator and single wet insulator are shown in Figures 5.10 and 5.11.

The relationship between n_d and the number of wet insulators in the set clearly differs from that of the lossless line in Figure 5.6. There is again a cyclic nonlinear nature to the graph, however the cycles now do not hit the ceiling of 1 as the number of wet insulators increase. Again, there seems to be resonances occurring owing to interference patterns created by the structure of the line which are causing these oscillations. The representative power has a different structure completely to that of the simple system and lossless lines in Figures 5.3 and 5.7 respectively. The representative power has very different progression for each contamination level as the number of wet insulators increase. This could possibly be used as a measure with a training algorithm.

Studying the fractal dimension graphs in Figure 5.12, the box dimension provides no discernible difference between each contamination level. The information dimension and the correlation dimension do show a drop in magnitude past 120 wetted insulators. Moreover, the correlation dimension drops dramatically, achieving $d_i \approx 0.2$ for 150 wetted insulators. Thus, the correlation dimension is able to distinguish the higher level of contamination for this lossy line case study.

5.2.4 Adding Finite Pole Impedance to the Case Studies

The diagram in Figure 5.5 details the components making up a power line feeder. The case studies proposed scenarios where the pole impedance and crossarm impedances were both neglected. Data collected in the laboratory measured leakage current through a high voltage insulator where its pin was directly connected to ground. Thus, that data was valid for use in the proposed scenarios. For the situations of adding crossarm impedance, or wooden pole impedance or both, the leakage currents through each pole $i = 1, 2, \ldots n$ would be altered from that in the case studies. This will reduce the current magnitude and alter the current

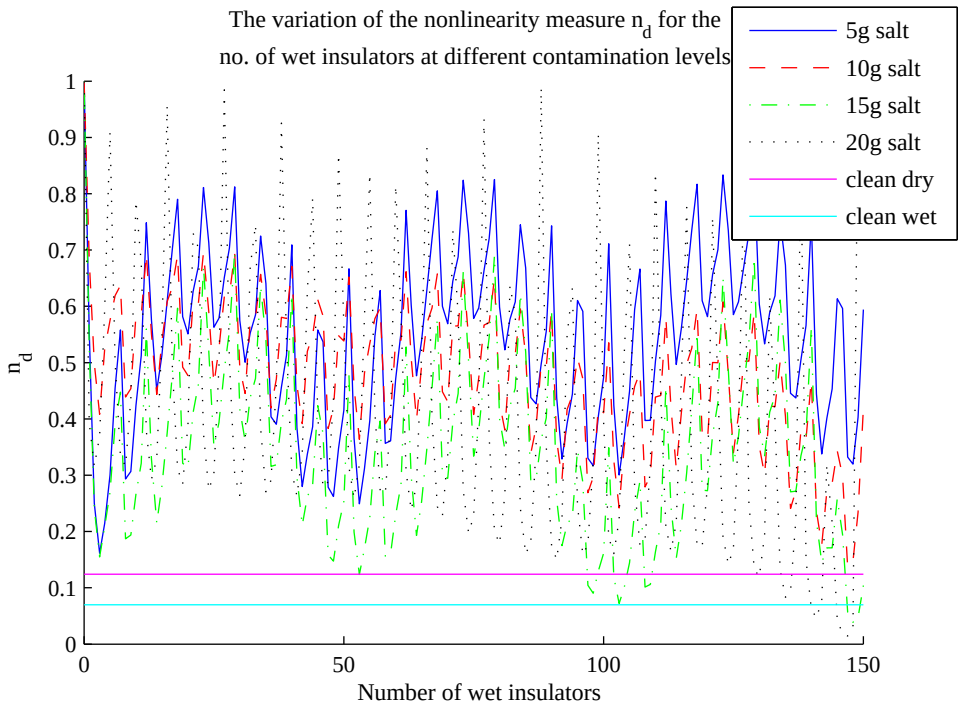

Fig. 5.10 Variation in the nonlinearity measure n_d for the number of wet insulators on a lossy feeder at different levels of salt contamination.

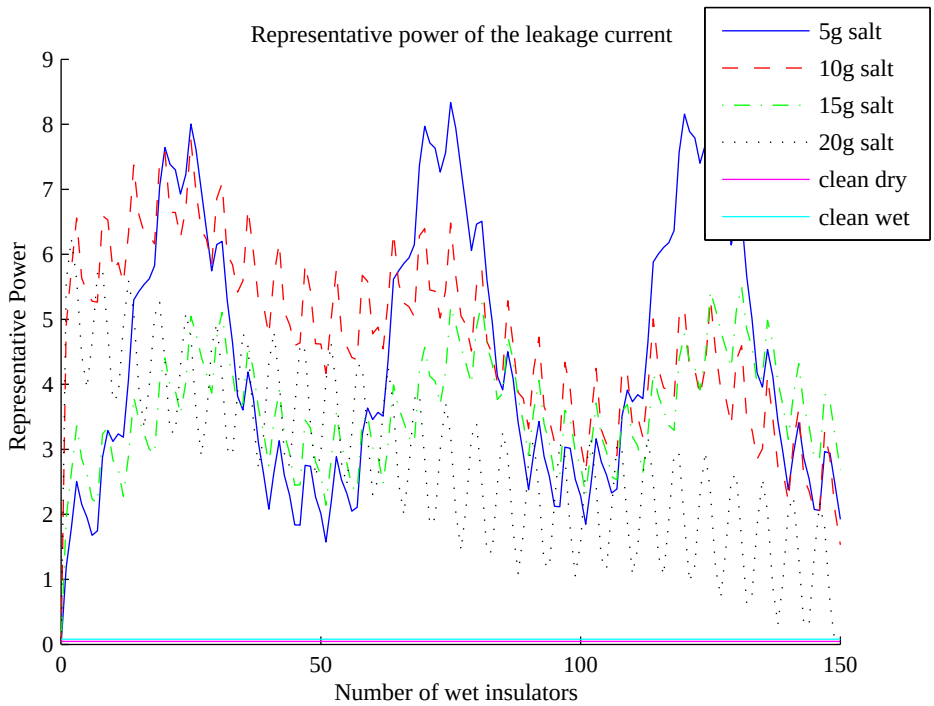

Fig. 5.11 Variation in the representative power of leakage current for the number of wet insulators on a lossy feeder at different levels of salt contamination.

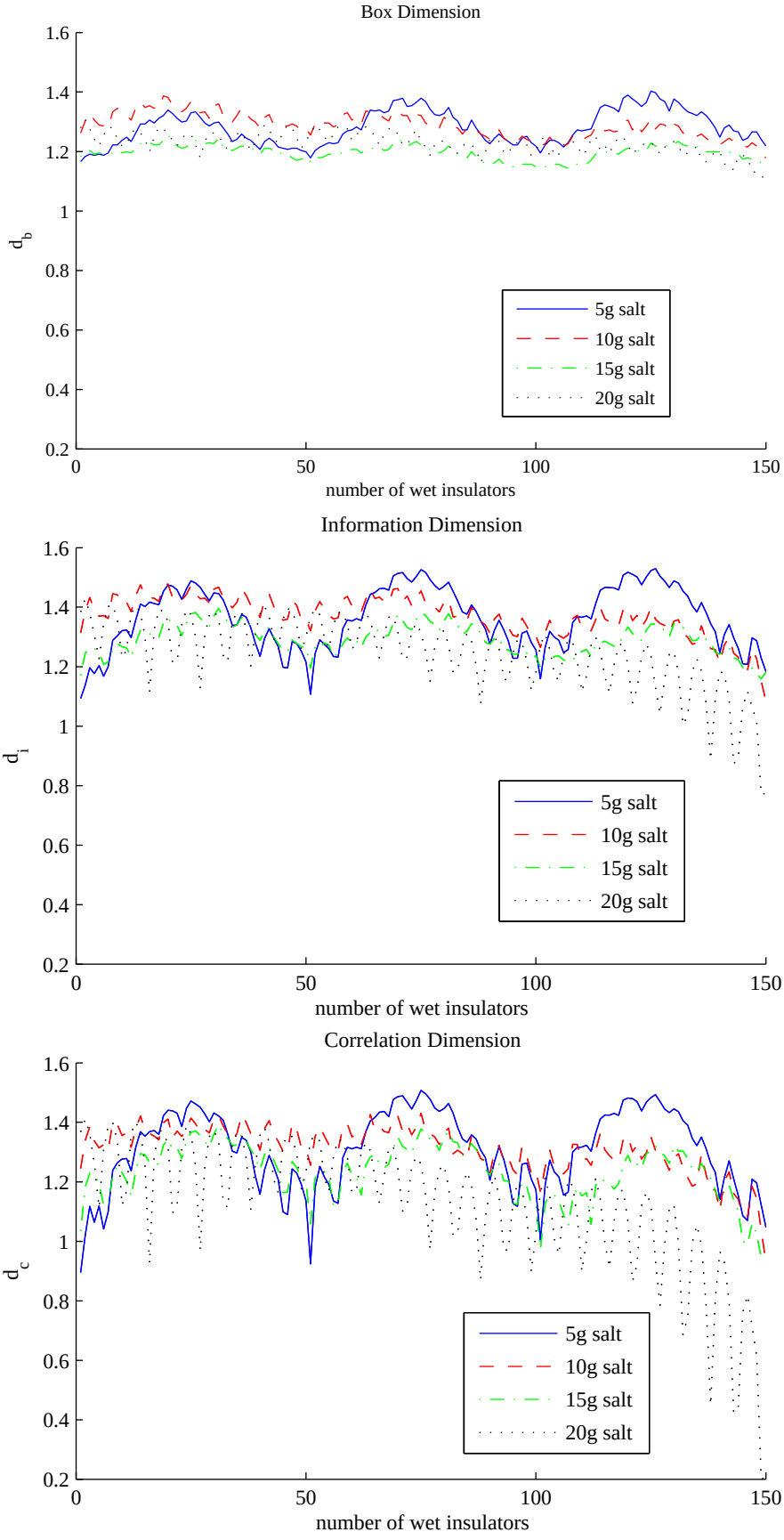

Fig. 5.12 Fractal dimensions for a lossy system of a set of high voltage insulators on a feeder at different levels of contamination as the number of wet insulators is varied.

phase.

Chapter 3 established 2700 kΩ and 143 kΩ as the resistances R_{arm-i} of a typical weathered wooden pole operating at 22 kV in a dry and wet weather condition respectively and 0.49 nF and 2.82 nF as the capacitances $C_i = 1/j\omega X_{C-i}$ of a typical weathered wooden pole operating at 22 kV in a dry and wet weather condition respectively. However, Kirchhoff's current law does not alter the fact the current through any current path i must be equal along the path length. So unfortunately no further modelling which includes pole impedance can be justified as a valid recreation of typical observations from an overhead distribution feeder. Further laboratory experiments including either a wooden pole or a simulated wooden pole with the above attributes are needed for analysis and was beyond the laboratory capabilities at the time of study.

5.2.5 Further Extensions of Power Line Modelling

Radial feeders make up the majority of a distribution system in Victoria, Australia. A natural extension to the lossy line modelling would be to a radial feeder. The expected outcome of such a model would be an emphasised effect on each measure caused by the 'paralleling effect' of each feeder branch. Hence, the measures would be likely to further decrease the nonlinearity measure during normal operation (including light to medium levels of contaminated insulators). The more interesting effect would be a polluted insulator somewhere along the feeder in the pre-flashover stage examined in Section 4.5. The pre-flashover stage data from that section was based on accepted leakage current waveforms with a supply frequency at 60 Hz. To incorporate pre-flashover stage data at 50 Hz further laboratory data collection and model building would be required to replicate the pre-flashover stage on a Victorian power line. The high voltage protection facilities of the laboratory at the time of study were inadequate for protecting expensive high resolution data collection equipment needed to allow data collection, so the next section turns to examining field data as an alter-

native, while also being useful to validate the measuring techniques established.

5.3 The Needle in the Haystack: Power Utility Zone Substation Data Analysis for a Pole Top Fire

Up until now, this thesis has considered a bottom-up approach, that is "looking at the needle itself" (the leakage current indicative of an incipient pole top fire) rather than "the haystack" (the distribution network). This section comes full circle to a top-down approach, that is "looking at the haystack" to determine if there is a needle in the haystack. "Where is the needle in the haystack" is not considered as this concept is another research problem in itself and studied in several research papers [155–162]. To date, leakage current in distribution systems have not been very well understood. Changes in harmonic content before and after pole fire events have been observed in the past, but with no qualitative or quantitative understanding. The analysis in this section will utilise and validate the techniques established in the previous chapter while bringing both a qualitative and quantitative understanding to pole top fire events within distribution systems.

An area prone to pole top fires in the suburb Mordialloc of Melbourne, Victoria was investigated by interrogating data collected by the local distributor (United Energy). The distributor's Distribution Management System (DMS), Geographic Information System (GIS), Supervisory Control And Data Acquisition (SCADA) system and offline field devices (Power Quality Meters) were all examined. The most ideal pole top fire scenario for study was chosen by the availability of concurrent data across these systems. Some data recorded by field hardware devices [163, 164] were manually retrieved as these devices were yet to be integrated into the SCADA system.

The most suitable month for examination was January 2008. An extract of the events that occurred on 20 January are recorded in Table 5.1. The field device hardware was a

Table 5.1 Extract from Distribution Management System (DMS) database for events that occurred on 20 January 2008 relating to the Mordialloc 'MC' Zone Substation.

Time	Asset	Outage Note	Protection Note	Outage Type
01:36:59	FDR MC2 CB	HV cross arm burnt in Mount View St	EF Prot	Distribution - Intermediate Structure
01:57:13	FDR MC2 CB	HV cross arm burnt in Mount View St	O/C & EF. IL1=0.08kA, IL2=0.09kA, IL3=1.35kA	Distribution - Intermediate Structure
01:58:06	FDR MC6 CB	HV bridge burnt off at Warren St	O/C & EF. IL1=5.46kA, IL2=5.89kA, IL3=4.52kA	Distribution - Line Hardware/Tie
09:10:57	FS 0618	X-arm in Mount View nth Mill St. Eio confirmed HVI MBN0803 @ DVA-Mount View and a cct from Pine-Mill s/s	Nil	Distribution - Intermediate Structure

PowerLogic® ION® 7700 Power Quality Meter [163] which captured waveform data when triggered by an abnormal event such as voltage sags and swells, overcurrents and earth faults. Field device waveform data corresponding to the tabled events were available for $t = 01:35:37.607$ and $t = 01:57:32.779$. The waveform data was captured at a sampling rate of 3200 Hz for a period of 28 cycles. Australia's supply voltage frequency is 50 Hz. The single line diagram for the zone substation in Mordialloc is illustrated in Figure 5.9 and the geographic layout of the 22 kV distribution network emanating from the zone substation is shown in Figure 5.13. The location of the pole top fire in Mount View Street is circled on the geographic layout, that is, several kilometres down the green radial feeder 'MC2' just past Fuse Switch FS618.

The events detailed in Table 5.1 show the first Pole Top Event when an Earth Fault protection operation occurs at 01:36:59. The corresponding c-phase current waveform is shown in Figure 5.14 (a). The second Pole Top Event occurs when a single phase fault and

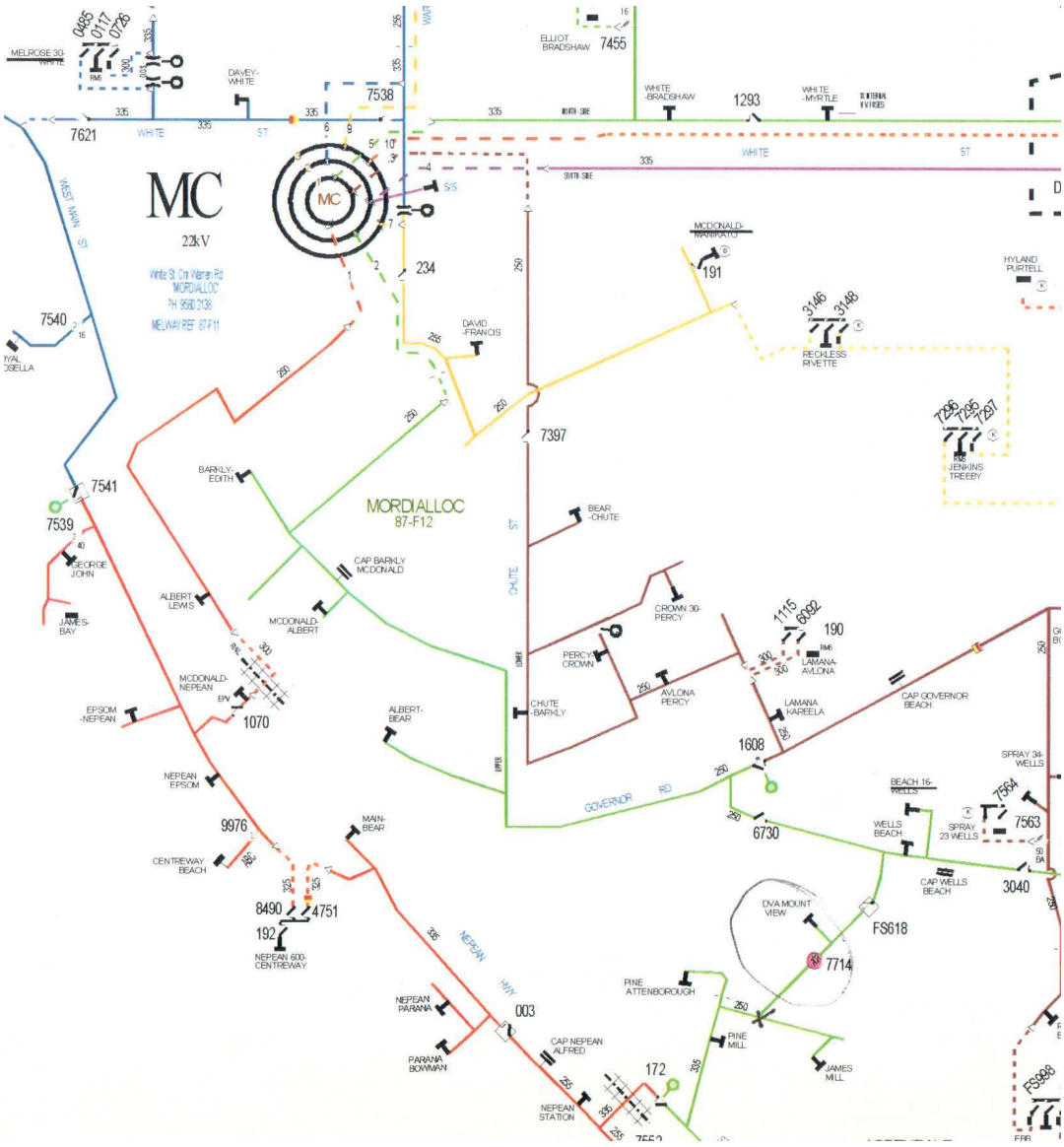

Fig. 5.13 Geographic layout and normal operating feeder configuration for part of the Mordialloc 'MC' 22 kV distribution network [2].

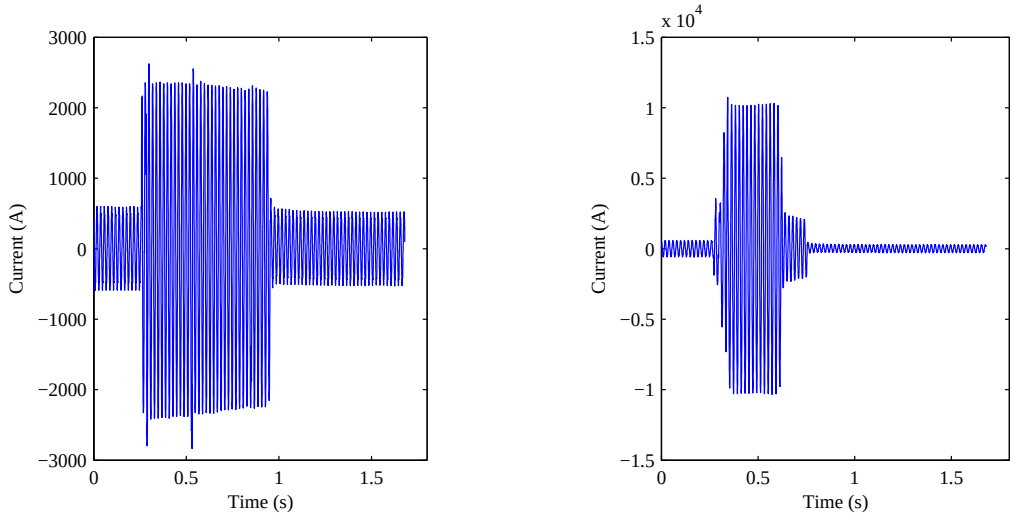

(a) (b)

Fig. 5.14 Mordialloc 'MC' Zone Substation c-phase load current recordings on 20 January 2008 for (a) Pole Top Event I at $t = 01:35:37.607$; and, (b) Pole Top Event II at $t = 01:57:32.779$.

a three phase fault occur within 1 second of each other at 01:57:13 and 01:58:06 respectively. Owing to clock synchronisation discrepancies, for the purposes of this study the field device hardware clock times shall be used owing to the devices being fitted with Geosynchronous Position System (GPS) clocks. The corresponding c-phase current waveform is shown in Figure 5.14 (b). These two pole top events shall be examined in detailed in the Sections 5.3.1 and 5.3.2.

5.3.1 Pole Top Event I

Several measures established in Chapter 4 shall be utilised to analyse the load currents collected at the 'MC' Zone Substation. In this context, the load current is considered to be the sum of the load current and the leakage currents. The representative power measure shall not be used, as this is only appropriate for examining leakage currents rather than load currents. Hence, the nonlinearity measure and the three fractal dimensions being the box dimension, the information dimension and the correlation dimension shall be examined.

When considering the measurement of the waveforms, a sliding window size must be chosen. Section 4.3.1 determined the larger the window size the less effect that the size of the dataset has on changing the nonlinearity measure, that is, a smaller sliding window side may produce steeper gradients, while longer windows may be less likely to 'miss data', although recording smoother gradients, and so producing less dramatic changes in magnitude. Hence, 3 window sizes were chosen, the smallest fitting 7 windows into the 28 cycles, the largest fitting 2 windows into the 28 cycles, and an intermediate size fitting 4 windows into the 28 cycles. Utilising these 3 window sizes, the sensitivity of the measurements can be examined.

The event captured three (3) waveform segments commencing at $t = 01 : 35 : 37.607$. Each segment consists of 28 cycles. The chosen measures were calculated for the current in each phase, with the above window sizes (as a fraction of the waveform segment) and the range of results detailed in Table 5.2. The measures which deviated in range by more than 0.20 are highlighted orange to indicate significant change. Measures of lesser significance in change were highlighted in yellow. Those with no significance were not highlighted. Any measures of particular interest were highlighted green.

In this case, the pole top event was a c-phase fault. Examining the nonlinearity measures in the table there is clearly interaction between b-phase and c-phase during this fault. To help visualise the progressing measures of n_d and d_c for the load currents, the a-, b- and c-phase load currents and corresponding measures have been reproduced in Figure 5.15 for waveform segments 1 and 2. The window sizes chosen for n_d and d_c were $\frac{1}{2}$ and $\frac{1}{4}$ respectively, owing to their range diversity. When looking at segment 1 of the waveform, n_d for c-phase was already at the level of 0.25 compared with 0.01 in a-phase. This was a level of significant nonlinear activity. Unfortunately, with the field device only configured to capture waveforms when abnormal events occur, there was no historical data preceding segment 1, thus restricting any knowledge of identifying the initial development of nonlinear activity. Observing the magnitude range for n_d in b-phase, there is also considerable nonlin-

ear activity, although to a lesser extent than c-phase. The box dimensions and information dimensions do not show any significant changes between the ranges for a- and b-phase or a- and c-phase, hence not providing any additional quantitative information. The correlation dimension d_c ranges for c-phase are significantly different to those of a- and b-phase. Hence, combining the d_c and n_d 'picks out' c-phase as exhibiting significant nonlinear activity.

Moving to the next waveform segment, that is segment 2, n_d and d_c act in a similar manner to segment 1, 'picking out' c-phase with the most significant nonlinear activity. A further interesting feature of d_c with a window size of $\frac{1}{2}$ is the sustained elevation of this measure at 0.49 (coloured green) for c-phase. This highlights the findings of Section 4.3.1 showing that the larger window size does indeed slow down and smooth changes of each measure. Again, the box dimensions and information dimensions do not show any significant changes between each phase. Finally, examining segment 3, all measures were of similar range owing to the absence of any nonlinearity after protection operating the circuit breaker supplying the feeder which experienced the pole top event. Unfortunately there was no recorded waveform data for after the reclose of the circuit breaker, again restricting any knowledge of identifying nonlinearities present caused by failing assets on the pole top under question.

5.3.2 Pole Top Event II

The measures established in Chapter 4 were again considered for the second Pole Top Event. The sliding window sizes used were the same as in Section 5.3.1. This event captured three (3) waveform segments commencing at $t = 01:57:32.779$. Each segment again consists of 28 cycles. The chosen measures were calculated and tabulated following the same process as Section 5.3.1 and detailed in Table 5.3. In addition to the previous highlighting scheme, the measures were highlighted in red when the range deviated extremely (that is by more than 0.85).

Table 5.2 Measures of waveforms for a fault occurring on 20 January 2008 at $t = 01:35:37.607$, with measures of interest highlighted.

		Waveform segment								
		1			2			3		
	size	*a-ph*	*b-ph*	*c-ph*	*a-ph*	*b-ph*	*c-ph*	*a-ph*	*b-ph*	*c-ph*
n_d	$\frac{1}{2}$	0.01	0.03-0.16	0.01-0.25	0.01-0.02	0.00-0.08	0.01-0.18	0.01	0.01	0.01
	$\frac{1}{4}$	0.01-0.02	0.00-0.22	0.00-0.26	0.01-0.02	0.00-0.11	0.00-0.22	0.01	0.01	0.01
	$\frac{1}{7}$	0.00-0.02	0.00-0.25	0.00-0.23	0.01	0.00-0.13	0.00-0.21	0.01	0.01	0.01
d_b	$\frac{1}{2}$	1.09-1.15	1.12-1.19	1.13-1.19	0.99-1.14	1.08-1.15	1.12-1.17	1.13-1.15	1.10-1.15	1.09-1.14
	$\frac{1}{4}$	0.91-1.14	0.89-1.16	0.92-1.19	0.91-1.01	0.90-1.03	0.92-1.15	0.95-1.00	0.91-1.00	0.92-1.00
	$\frac{1}{7}$	0.79-1.06	0.77-1.12	0.79-1.19	0.78-1.06	0.75-1.09	0.77-1.09	0.82-1.04	0.77-1.02	0.79-1.06
d_i	$\frac{1}{2}$	0.73-0.85	0.75-0.88	0.79-1.02	0.72-0.89	0.73-0.85	0.90-1.01	0.73	0.72-0.73	0.73
	$\frac{1}{4}$	0.64-0.93	0.63-0.83	0.64-1.00	0.63-0.85	0.63-0.81	0.63-0.96	0.65-0.67	0.64-0.66	0.65-0.68
	$\frac{1}{7}$	0.59-0.92	0.58-0.85	0.58-0.98	0.58-0.81	0.58-0.76	0.59-0.95	0.60-0.74	0.59-0.73	0.59-0.76
d_c	$\frac{1}{2}$	0.27-0.42	0.24-0.42	0.27-0.73	0.25-0.49	0.23-0.41	0.49-0.77	0.25	0.21	0.25
	$\frac{1}{4}$	0.24-0.55	0.21-0.43	0.25-0.72	0.24-0.48	0.18-0.42	0.24-0.72	0.25	0.20-0.21	0.24-0.25
	$\frac{1}{7}$	0.24-0.55	0.22-0.36	0.24-0.70	0.24-0.32	0.17-0.40	0.23-0.66	0.24-0.33	0.20-0.28	0.24-0.33

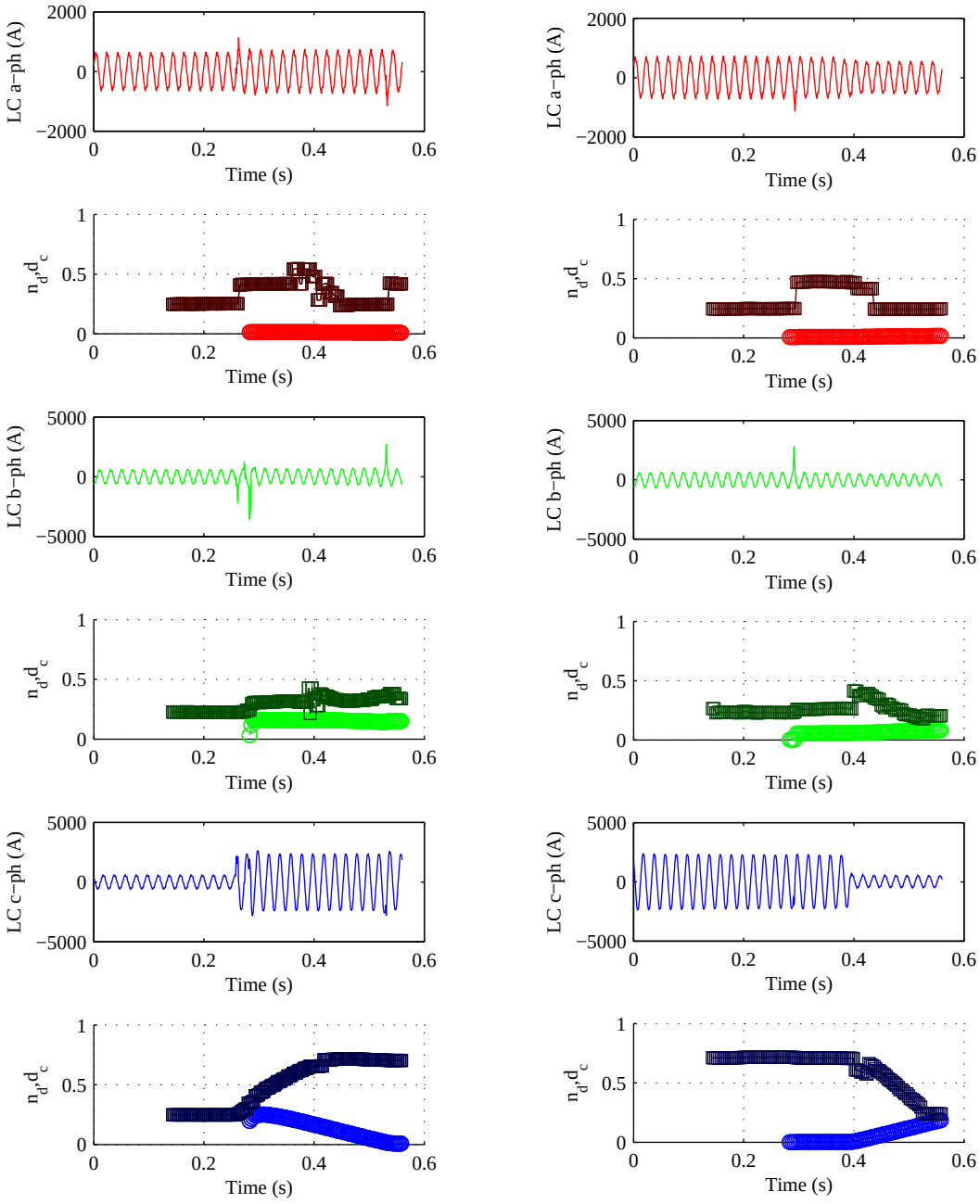

(a) (b)

Fig. 5.15 Mordialloc 'MC' Zone Substation a-, b- and c- phase load current comparisons with n_d (light colour circles) and d_c (dark colour squares) measures at $t = 01 : 35 : 37.607$ for: (a) segment 1 of 3; and, (b) segment 2 of 3.

In this case, the pole top event was a 3-phase fault. Examining the nonlinearity measures in the table there is clearly interaction between all three phases during this fault. To aid visualising the progression of n_d and d_c for the load currents, the a-, b- and c-phase load currents and corresponding measures have been reproduced in Figure 5.16 for waveform segments 1 and 2. The window sizes chosen for n_d and d_c were both $\frac{1}{2}$, owing to their range diversity.

When looking at segment 1 of the waveform, n_d for c-phase (highlighted green) starts at the level of 0.08 compared with 0.01 and 0.02 for a- and b-phase. This shows there was some level of nonlinear activity prior to the 3-phase fault and the ensuing pole top fire. Unfortunately, the field device again misses the preceding historical data. The magnitude range for n_d for all phases were more than 50%, indicating a high level of nonlinear activity. The box dimension with a sliding window size of $\frac{1}{7}$ highlighted in yellow identified the significant shape of each phase's waveform. The correlation dimension d_c ranges for all 3 phases were very large in magnitude, indicating the high nonlinear nature of the event. The information dimension blurred the results observed for the box dimension and correlation together. Thus, n_d hints that c-phase initiated the following 3-phase fault and fire, and both d_c and n_d indicate a highly nonlinear event, while d_b profiles very shapely waveforms.

Examining waveform segment 2 was indeed fascinating. The nonlinearity measure n_d for a- and b-phase was now above 60%, however c-phase has dropped to 42%, and 32% when using the smaller window size of $\frac{1}{7}$. The measure brings attention to the c-phase insulator and/or conductor breaking away from the 3-phase fault, most likely being caused by the crossarm or insulator breaking away from the pole. The correlation dimension d_c for each phase were much lower than the previous segment but in this case c-phase had a higher magnitude than the other two phases. These results were contrary to the results for n_d warranting further study of the measure changes. Examining the load current and measure progression in Figure 5.16 show d_c monotonically decreasing for all three phases, while n_d

first continues to peak for a- and b-phases while c-phase's n_d sustained for 0.15 s longer than a- and b-phases. Hence, c-phase actually continued conducting to ground while the other two phases stopped contributing to the fault. Thus, the original hypothesis of the conductor breaking away from the fault based on the range of the measure n_d was incorrect, and the opposite in fact occurred. This highlights the importance of following the progression of the measures as well as the magnitude ranges of the measures. Examining the box dimension d_b also revealed less involvement by a-phase during the second segment, a phenomenon not detected by n_d nor d_c. The information dimension did not reveal any discerning differences between the phase waveforms in this segment. In summary, a profile for this segment may be built using the n_d, d_c and d_b measures, and the progression of those measures, where each measure provides different information about the pole top fire event.

For the third waveform segment, a finding similar to Pole Top Event I was observed, that is, all measures were of a similar range owing to the absence of any nonlinearity after protection operating the circuit breaker supplying the feeder which experienced the pole top event. Again, unfortunately there was no recorded waveform data for after the reclose of the circuit breaker.

5.4 Discussion

A systematic method to model an increasing number of leaking high voltage insulators is attempted for the first time in Section 5.2. There is little or no research to date where leakage current is investigated for an entire feeder length. For a single insulator, the nonlinearity measure decreased when a clean insulator became wet. For a simple insulator set system with more than 6 wet insulators, this was also the case for contaminated insulators. The fractal dimensions for a simple insulator set system generally had an increase in magnitude as the number of wet insulators increased. As this was the most trivial case, this was useful for information when extending the analysis to lossless and lossy lines.

Table 5.3 Measures of waveforms for a fault occurring on 20 January 2008 at $t = 01:57:32.779$, with measures of interest highlighted.

		Waveform segment								
		1			2			3		
	size	*a-ph*	*b-ph*	*c-ph*	*a-ph*	*b-ph*	*c-ph*	*a-ph*	*b-ph*	*c-ph*
n_d	$\frac{1}{2}$	0.02-0.56	0.01-0.51	0.08-0.54	0.02-0.65	0.01-0.64	0.01-0.42	0.01-0.02	0.01	0.01
	$\frac{1}{4}$	0.00-0.50	0.00-0.42	0.00-0.44	0.02-0.57	0.01-0.57	0.01-0.36	0.01-0.02	0.01	0.01
	$\frac{1}{7}$	0.00-0.45	0.00-0.37	0.00-0.33	0.01-0.53	0.01-0.52	0.00-0.34	0.01-0.02	0.01	0.01
d_b	$\frac{1}{2}$	0.85-1.27	0.91-1.28	0.93-1.23	1.07-1.16	1.10-1.30	1.09-1.20	1.12-1.14	1.09-1.15	1.09-1.14
	$\frac{1}{4}$	0.70-1.29	0.71-1.28	0.72-1.23	1.03-1.17	1.00-1.30	1.08-1.21	0.93-1.18	0.90-1.18	0.88-1.17
	$\frac{1}{7}$	0.60-1.22	0.63-1.29	0.63-1.20	0.98-1.19	0.97-1.36	0.95-1.27	0.81-1.10	0.76-1.10	0.80-1.09
d_i	$\frac{1}{2}$	0.73-1.28	0.72-1.38	0.73-1.36	0.73-1.08	0.73-1.08	0.72-1.17	0.72-0.73	0.67-0.69	0.71-0.73
	$\frac{1}{4}$	0.63-1.34	0.65-1.37	0.63-1.36	0.69-1.21	0.69-1.21	0.77-1.30	0.64-0.80	0.60-0.74	0.63-0.79
	$\frac{1}{7}$	0.54-1.35	0.61-1.40	0.56-1.38	0.72-1.25	0.72-1.24	0.73-1.27	0.60-0.78	0.55-0.71	0.59-0.77
d_c	$\frac{1}{2}$	0.29-1.18	0.35-1.29	0.38-1.32	0.25-0.56	0.22-0.54	0.25-0.76	0.25	0.14-0.15	0.23-0.24
	$\frac{1}{4}$	0.25-1.30	0.29-1.30	0.27-1.35	0.24-0.84	0.18-0.84	0.30-1.11	0.25-0.33	0.15-0.19	0.23-0.30
	$\frac{1}{7}$	0.24-1.31	0.26-1.32	0.24-1.36	0.20-1.12	0.19-1.15	0.27-1.18	0.25-0.33	0.15-0.19	0.23-0.31

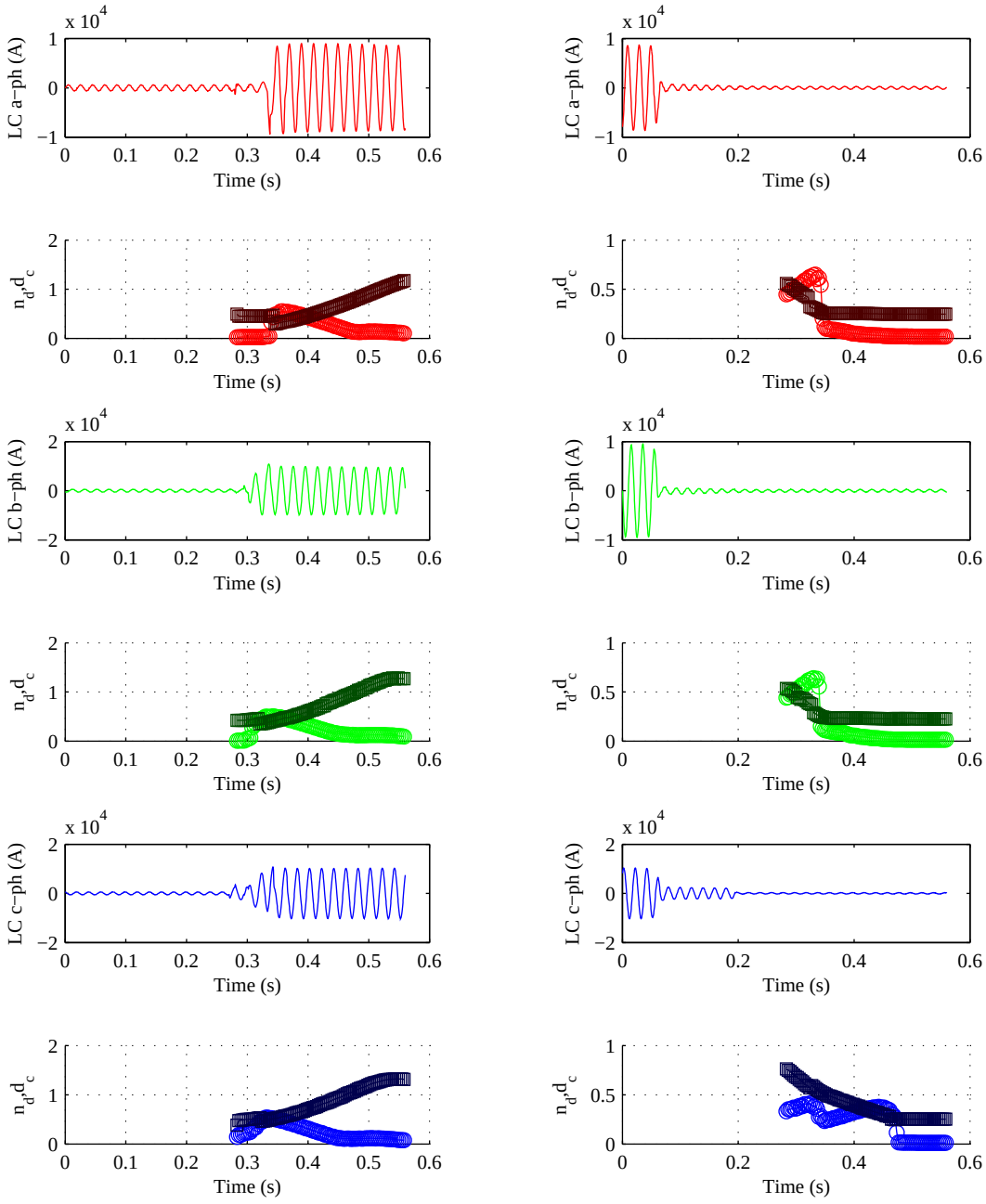

Fig. 5.16 Mordialloc 'MC' Zone Substation a-, b- and c- phase load current comparisons with n_d (light colour circles) and d_c (dark colour squares) measures at $t = 01:57:32.779$ for: (a) segment 1 of 3; and, (b) segment 2 of 3.

Some interesting results were observed for both a lossless and a lossy line. The correlation dimension dropped significantly for a high number of wet insulators contaminated with 20 g of pollutant, while pollution levels between 5 g and 15 g returned very similar dimension. This warrants further investigation of insulators with higher levels of pollutant, to enhance the pollution profiles found. The nonlinearity measure n_d was difficult to interpret for the lossless line, as the results were highly cyclically, most likely to the symmetric construction causing a resonant line. The only interesting phenomenon for the nonlinearity measure in this case was the decreasing minimum of n_d as the pollution levels increased. For the lossy line, n_d minimums also decreased as the pollution levels increased. In this case, the magnitude of n_d was expected to more closely resemble that of a practical line, however further resonances were observed. Examining the corresponding representative power measure, these resonances are very pronounced for the 5 g case. By discounting the resonances observed by the representative power measure, a better feel for n_d may be deduced in the range $0.00 - 0.40$, depending on how contaminated and how wet the insulators may be.

The analysis of the pole top fire in Section 5.3 has shown the techniques established in Chapter 4 can follow and verify the progressing pole top events. Furthermore, comparing these results with that of the power line modelling in Section 5.2 shows that when load is applied to a feeder, and when several feeders are all paralleled together at a zone substation, the n_d measure drops significantly from that observed in the modelling of a lossy line. The analysis also verified the smoothing effect of larger sliding window sizes and confirmed that data events are not missed with larger sliding windows, however the change in measure is not as dramatic as for smaller sliding window sizes. Hence, when monitoring changes in measures a smaller sliding window size is more appropriate.

Utilising examination of a combination of the n_d, d_c and d_b measures applied to field data revealed the c-phase fault for Pole Event I and the 3-phase fault for Pole Event II.

The 3-phase fault measures also revealed pre-existing nonlinearity in c-phase, as well as the slower fault clearance time of c-phase not identified through any other means. Hence, combining these measures to form a pole top fault profile would be a very powerful tool not available today. Moreover, a suite of profiles for high impedance faults (such as fallen tree branches, possums/vermin, etc.) could be built using the same techniques. Other simpler fault profiles such as 3-phase and single phase faults could also be built to enable the use of learning algorithms to distinguish each fault profile.

Employing the measuring techniques established in Chapter 4 identified "there is a needle in the haystack", that is, validated the nonlinearity measure and fractal dimensions for measuring incipient pole top fire leakage current events. The limited quantity of data prior to a pole top fire (owing to data only being recorded when pre-determined parameters trigger capture) has made it difficult to determine the precise profile for an incipient pole top fire. Pole Event II did show an elevation of 4-8% of n_d for c-phase prior to the 3-phase fault, however better pre-fault data capture would certainly assist in building a robust incipient pole top fire profile. This profile, utilising these measures can thus provide an overall 'health index' to smartly monitor leakage currents. Furthermore, the health index may provide leakage current status to the distribution network operators via SCADA, and if robust, also provide high impedance protection.

5.5 Summary

This chapter has for the first time introduced extension of leakage current measuring techniques to systematically modelled power distribution lines. It has discussed reasoning of the observed measures under the three scenarios examined. Finally, data collected from a power utility zone substation for a pole top fire was analysed using the established leakage current measure techniques, verifying the validity of these techniques while providing a quantitative measure that may contribute to a 'health index', enabling smart monitoring of leakage

currents from insulators on wooden poles.

Chapter 6

Conclusions and Future Research

6.1 Overview

This chapter draws an overarching commentary of the dissertation including the research undertaken and the subsequent findings. Section 6.2 provides an overall conclusion and outlines the main findings of this thesis. Section 6.3 closes the thesis with recommendations for future research directions.

6.2 Conclusions

The aim of this thesis was to determine which measure or combination of measures are best suited for creating a LCHI. The thesis has demonstrated that observing a combination of the nonlinearity measure, the fractal correlation dimension measure and the box dimension measure for power line feeder voltages and currents can reveal pre-existing nonlinearity caused by leakage currents leading to a pole top fire. This has been achieved by firstly investigating the role of wood on leakage current, then measuring the nonlinearity of the leakage current signature for a high voltage insulator under several contamination levels and different weather conditions. The leakage current signature for the stage prior to flashover was

examined using measuring techniques to provide quantitative information. These measures were also applied to power lines rather than a single isolated insulator, and further validated by application to data collected from a zone substation for a pole top fire.

The main results and research contributions of this thesis can be summarised as follows:

1. Gaining an understanding of the mechanisms causing leakage current signature:

   (a) The effective impedance of CCA impregnated wooden pole samples were examined under different weather conditions and various voltage levels, showing the capacitive components increase during wet weather, while also reducing the resistive components of impedance, consequently promoting an increase to the leakage current and heat dissipation owing to I^2R losses;

   (b) The leakage current concentration at wood-metal contact points contribute significantly to heating causing smouldering of the wood with temperatures no littler than 50 °C;

   (c) The impedance studies showed that wet weather reduces effective resistance to approximately 60% of the resistance in a dry weather state at line voltages of 22 kV, thereby more than doubling the leakage current, which can cause smouldering and ignition of those parts of wood in a rainshadow; and,

   (d) The impedance studies also uncovered dangerous conductance magnitudes for 66 kV poles with insulators mounted at heights similar to 22 kV poles. This observation provides an explanation for 66 kV poles catching fire at triple the rate of 22 kV poles, which was not previously understood.

2. Finding appropriate methodologies that measure and quantify leakage current signature, in particular, from HV insulators, for identifying insulator condition and detecting incipient pole fires:

(a) The proposed nonlinearity measure based on the Pearson correlation coefficient was able to distinguish high voltage insulator conditions, thus serving well as a condition identifier. The nonlinearity measure accounted for both the nonlinearity exhibited by the insulator leakage current signature, as well as the interharmonics which previous research ignored;

(b) The nonlinearity measure and the fractal measures were able to track and distinguish the changing conditions of an insulator in the stage prior to a flashover, identifying both heating and arcing signatures, which are necessary in forecasting incipient wooden pole top fires; and,

(c) The nonlinearity and fractal measures may be applied to any type of insulator, whether it be of different form factor (shape) or made of different materials. This makes it ideal for measuring incipient pole top fires on a distribution network where any combination of insulators may be used, rather than measures which are only suited to one particular insulator owing to their derivation from specific modelling.

3. Testing the methodologies found for identifying insulator condition and detecting incipient pole fires on data, both constructed from laboratory data, and real world data:

(a) The application of measuring leakage current signature nonlinearity to overhead power line models based on experimental laboratory data showed that nonlinearity decreases as the number of wet insulators increase, as well as also decreasing when the number of power line feeders in parallel are increased. This finding assists in picking out incipient pole top fires as the nonlinearity of a rogue insulator would be noticeable over the low measure of nonlinearity for the power line; and,

(b) When the measures of leakage current were tested on pole top fire load current

and supply voltage data collected from a zone substation, their magnitudes quantified the increased activity in the moment prior to flashover and the pole top fire. Therefore, these measures were deemed suitable for identifying incipient pole top fires.

6.3 Future Research Scope

Following the studying into leakage current on high voltage insulators mounted on wooden poles, there are many aspects to the problem of incipient wooden pole top fires that could be investigated further. Therefore, a few possible future research directions are listed below before concluding this thesis:

Data Capture

When studying the data from zone substations, the most interesting data occurred during the 20 minute period between Event I and Event II where arcing would have continued up until the pole top fire. This data has not been captured owing to the settings of trigger parameters. These parameters are usually set to capture data when there are excursions beyond voltage tolerance levels. An approach to capturing this 'missing data' utilising the measures established in this thesis as additional parameters which trigger data capture for further analysis would add much value to this area of research. Furthermore, once that data is captured, refinement of these measures would be possible with further analysis.

Data Quality

The influence of power quality effects of the network on measurements and network performance has always been of interest to engineers. The experiments conducted on high voltage insulators and wooden poles in this thesis has been without any harmonic filtering of the applied voltages. A comparison study between filtered and unfiltered

voltages would be interesting to observe for refinement of modelling.

Fault Detection and Prevention

Leakage current causing incipient pole top fires is one of many types of high impedance faults. A suite of high impedance fault profiles could be built to forecast impending or incipient faults, prior to any catastrophic event or power outages. Profiles for short circuit faults could also be built. Moreover, the building of learning algorithms based on a suite of profiles for high impedance faults could provide a LCHI for a smart monitoring system in SCADA and possibly protection in high risk bushfire regions.

Fault Location

By using the measures derived in this thesis to identify that there is an incipient pole top fire on a feeder from a zone substation, further research may be able to determine the distance this fault is from the zone substation to quickly located where the fault will occur. Knowing this information would make it possible to efficiently allocate resources to geographically locate the fault for rectification prior to any power outage.

6.4 Concluding Remarks

In brief, incipient wooden pole top fires have been impossible to predict. By studying the nonlinearity of leakage current signatures from high voltage insulators mounted on wooden poles, a combination of measures have proven useful for identifying signature changes which may be used to forecast incipient pole top fires. Using these measures as part of a smart monitoring system would make it possible to reduce any consequential losses from pole top fires by preventing the fault developing before any fire starts.

Bibliography

[1] “Distribution management system asset event database,” Internal database warehouse, Jemena Asset Management, Mt Waverley, Victoria, Australia, 2008.

[2] Jemena Asset Management, “MC - Mordialloc 22kV Distribution Geographic Layout,” 2009, Geographic Information System (GIS) Extract.

[3] W. Ward, “Risk modelling for pole top fire mitigation,” in *Proceedings of the ICOMS Asset Management Conference*, 2007.

[4] (2014, April). [Online]. Available: http://science.howstuffworks.com/environmental/energy/power.htm

[5] *Secondary System Requirements for Major Substations*, Ausgrid Std. NS178, April 2008.

[6] “IEEE Guide for Electric Power Distribution Reliability Indices,” *IEEE Std 1366-2012 (Revision of IEEE Std 1366-2003)*, pp. 1–43, May 2012.

[7] Australian Energy Regulator. (2014) Network performance. [Online]. Available: http://www.aer.gov.au/node/483

[8] P. Fearon, “Safety performance on victorian electricity distribution and transmission businesses 2012,” Energy Safe Victoria, Tech. Rep., 2013.

[9] Parliament of Victoria, “2009 Victorian Bushfires Royal Commission,” July 2010.

[10] J. Forrest, P. Lambeth, and D. Oakeshott, “Research on the performance of high-voltage insulators in polluted atmospheres,” *Proceedings of the IEE - Part A: Power Engineering*, vol. 107, no. 32, pp. 172–187, April 1960.

[11] A. McElroy, W. Lyon, J. D. M. Phelps, and H. Woodson, “Insulators with contaminated surfaces, Part I: Field conditions and their laboratory simulation,” *IEEE Transactions on Power Apparatus and Systems*, vol. PAS-89, no. 8, pp. 1848–1858, November 1970.

[12] A. de la O, R. Gorur, and J. Chang, “AC clean fog tests on nonceramic insulating materials and a comparison with porcelain,” *IEEE Transactions on Power Delivery*, vol. 9, no. 4, pp. 2000–2008, October 1994.

[13] T. Sorqvist and A. Vlastos, “Hydrophobicity and leakage current statistics of polymeric insulators long-term exposed, to coastal contamination,” in *Proceedings of the 1996 IEEE International Symposium on Electrical Insulation*, vol. 1, June 1996, pp. 335–340.

[14] S. A. Sokolovsky and V. G. Santotsky, “Environmental impact on the insulation of 10 kV distribution power lines,” in *Proceedings of the 1998 Conference on Electrical Insulation and Dielectric Phenomena*, vol. 1, October 1998, pp. 56–59.

[15] W. Vosloo and J. Holtzhausen, "The effect of thermal characteristics of power line insulators on pollution performance," in *Proceedings of the IEEE 6th Africon Conference in Africa*, vol. 2, October 2002, pp. 609–612.

[16] ——, "The prediction of insulator leakage currents from environmental data," in *Proceedings of the IEEE 6th Africon Conference in Africa*, vol. 2, October 2002, pp. 603–608.

[17] K. Chrzan and F. Moro, "Concentrated discharges and dry bands on polluted outdoor insulators," *IEEE Transactions on Power Delivery*, vol. 22, no. 1, pp. 466–471, January 2007.

[18] "IEEE Recommended Practice for Monitoring Electric Power Quality," *IEEE Std 1159-1995*, pp. i–70, 1995.

[19] J. Beesley, "A survey of the causes of service failing of crossarms throughout australia. summary of results, conclusions and recommendations," Australia CSIRO division Forest Products, Tech. Rep. Report 7, Sub-Project P2-2, September 1954.

[20] "Distribution management system asset event database," Internal database warehouse, Jemena Asset Management, Mt Waverley, Victoria, Australia, 2003.

[21] "Distribution management system asset event database," Internal database warehouse, Jemena Asset Management, Mt Waverley, Victoria, Australia, 2007.

[22] P. J. Sokolowski, A. Dwivedi, S. Pathak, F. Buratto, and X. Yu, "Investigating the impedance of a wooden power pole after a pole fire," in *Proceedings of the Australasian*

Universities Power Engineering Conference (AUPEC 2008), December 2008, pp. 1–6.

[23] L. Francis and J. Norton, "Australian timber pole resources for energy networks," Department of Primary Industries and Fisheries, The State of Queensland, Australia, Tech. Rep., 2006.

[24] P. M. Ross, "Burning of wood structures by leakage currents," *Transactions of the American Institute of Electrical Engineers*, vol. 66, no. 1, pp. 279–287, January 1947.

[25] ——, "Wood structure burning by leakage currents," *Electrical Engineering*, vol. 66, no. 5, pp. 472–474, May 1947.

[26] W. H. Wickham, H. Adler, and M. S. Oldacre, "Pole fires due to insulator contamination," *Transactions of the American Institute of Electrical Engineers*, vol. 67, no. 2, pp. 1741–1744, January 1948.

[27] J. Clayton and D. Shankle, "Insulation characteristics of wood and suspension insulators in series [includes discussion]," *Transactions of the American Institute of Electrical Engineers Power Apparatus and Systems, Part III.*, vol. 74, no. 3, pp. 1305–1312, January 1955.

[28] M. Darveniza, G. Limbourn, and S. Prentice, "Line design and electrical properties of wood," *IEEE Transactions on Power Apparatus and Systems*, vol. Pas-86, no. 11, November 1967.

[29] M. Darveniza, *The Electrical Properties of Wood and Line Design*, Various, Ed. University of Queensland Press, 1980.

[30] E. Robertson, "Conductivity of hardwood power line poles," *Electrical Engineer, Australia*, pp. 14–18, November 1968.

[31] ——, "Electrical conductivity of three treated pole timbers," *Electrical Engineer, Australia*, p. 22, June 1969.

[32] L. N. Clarke and R. Donaldson, "Electrical conductivity of three treated pole timbers," *Electrical Engineer, Australia*, p. 26, May 1969.

[33] R. Filter, "The influence of wood pole preservatives on wood fire and electrical safety," *IEEE Transactions on Power Apparatus and Systems*, vol. PAS-103, no. 10, pp. 3089–3095, October 1984.

[34] G. E. Lusk and S. Mak, "EHV wood pole fires: Their cause and potential cures," *IEEE Transactions on Power Apparatus and Systems*, vol. 95, no. 2, pp. 621–629, March 1976.

[35] R. Filter and J. D. Mintz, "An improved 60 Hz wood pole model," *IEEE Transactions on Power Delivery*, vol. 5, no. 1, pp. 442–448, January 1990.

[36] M. Al-Dabbagh and S. Pathak, "Leakage current estimation of H.V insulators on power distribution lines," in *Proceedings of TENCON 2005 - 2005 IEEE Region 10 Conference*, November 2005, pp. 1–4.

[37] H. L. Rasara, M. F. Rahmat, and K. Wong, "Study of leakage current distribution in a wooden pole using a three dimensional resistance model," in *Proceedings of the 20th Australasian Universities Power Engineering Conference (AUPEC 2010)*, December 2010, pp. 1–6.

[38] K. Wong and M. F. Rahmat, "Study of leakage current distribution in wooden pole using ladder network model," *IEEE Transactions on Power Delivery*, vol. 25, no. 2, pp. 995–1000, April 2010.

[39] J. G. Schroder and R. S. Richmond, "Wood preservation process engineered to extend the economic and commercial service life of hardwood transmission poles," in *Proceedings of the 1st International Conference on Technology for Development*, Canberra, Australia, November 1980, pp. 183–187.

[40] M. L. Parry, *Climate Change 2007: Impacts, Adaptation and Vulnerability: Contribution of Working Group II to the Fourth Assessment Report of the Intergovernmental Panel on Climate Change*. Cambridge University Press, 2007, vol. 4.

[41] Z. Zhang, X. Jiang, H. Huang, C. Sun, J. Hu, and D. Gao, "Study on the wetting process and its influencing factors of pollution deposited on different insulators based on leakage current," *IEEE Transactions on Power Delivery*, vol. 28, no. 2, pp. 678–685, April 2013.

[42] R. Sarathi, S. Chandrasekar, and N. Yoshimura, "Investigations into the surface condition of silicone rubber insulation material using multiresolution signal decompo-

sition," *IEEE Transactions on Power Delivery*, vol. 21, no. 1, pp. 243–252, January 2006.

[43] United States Environmental Protection Agency. (2014) Pentachlorophenol. [Online]. Available: http://www.epa.gov/ttn/atw/hlthef/pentachl.html

[44] G. G. Karady and F. Amarh, "Signature analysis for leakage current wave forms of polluted insulators," in *Proceedings of the 1999 IEEE Transmission and Distribution Conference*, vol. 2, New Orleans, LA, USA, April 1999, pp. 806–811.

[45] K. Wong, S. Pathak, and X. Yu, "Aging effect on leakage current flow in wooden poles," *IEEE Transactions on Dielectrics and Electrical Insulation*, vol. 16, no. 1, pp. 133–138, February 2009.

[46] F. Amarh, G. G. Karady, and R. Sundararajan, "Linear stochastic analysis of polluted insulator leakage current," *IEEE Transactions on Power Delivery*, vol. 17, no. 4, pp. 1063–1069, October 2002.

[47] H. Kordkheili, H. Abravesh, M. Tabasi, M. Dakhem, and M. Abravesh, "Determining the probability of flashover occurrence in composite insulators by using leakage current harmonic components," *IEEE Transactions on Dielectrics and Electrical Insulation*, vol. 17, no. 2, pp. 502–512, April 2010.

[48] Obenaus, "Fremdschichtüeberschlag und kriechweglänge," *Deutsche Elektrotechnik*, vol. 4, pp. 135–136, 1958.

[49] B. F. Hampton, "Flashover mechanism of polluted insulation," *Proceedings of the Institution of Electrical Engineers*, vol. 111, no. 5, pp. 985–990, May 1964.

[50] R. Wilkins, "Flashover voltage of high-voltage insulators with uniform surface-pollution films," *Proceedings of the Institution of Electrical Engineers*, vol. 116, no. 3, pp. 457–465, March 1969.

[51] H. Woodson and A. McElroy, "Insulators with contaminated surfaces, Part II: Modeling of discharge mechanisms," *IEEE Transactions on Power Apparatus and Systems*, vol. PAS-89, no. 8, pp. 1858–1867, November 1970.

[52] M. Kawai, "Research at project UHV on the performance of contaminated insulators Part II - Application to practical design," *IEEE Transactions on Power Apparatus and Systems*, vol. PAS-92, no. 3, pp. 1111–1120, May 1973.

[53] F. A. M. Rizk, "Mathematical models of pollution flashover," *Electra*, vol. 78, pp. 71–103, 1981.

[54] F. A. M. Rizk and D. H. Nguyen, "AC source-insulator interaction in HV pollution tests," *IEEE Transactions on Power Apparatus and Systems*, vol. PAS-103, pp. 723–732, April 1984.

[55] F. A. M. Rizk and M. Bourdages, "Influence of AC source parameters on flashover characteristics of polluted insulators," *IEEE Transactions on Power Apparatus and Systems*, vol. PAS-104, pp. 948–958, April 1985.

[56] J. Holtzhausen and D. A. Swift, "The pollution flashover of AC and DC energised cap

and pin insulators: the role of shortening of the arc," in *Proceedings of the Eleventh International Symposium on (Conference Publication no. 467) High Voltage Engineering, 1999.*, vol. 4, 1999, pp. 333–336.

[57] J. Holtzhausen and W. Vosloo, "The pollution flashover of AC energized post type insulators," *IEEE Transactions on Dielectrics and Electrical Insulation*, vol. 8, no. 2, pp. 191–194, April 2001.

[58] ——, "An analysis of leakage current waveforms, measured on-site, with reference to insulator pollution flashover models," in *Proceedings of the Thirteenth International Symposium on High Voltage Engineering, Delft, Netherlands*, 2003.

[59] N. Dhahbi-Megriche, A. Beroual, and L. Krähenbühl, "A new proposal model for flashover of polluted insulators," *Journal of Physics D: Applied Physics*, vol. 30, no. 5, p. 889, 1997.

[60] N. Dhahbi-Megriche and A. Beroual, "Model for calculation of flashover characteristics on polluted insulating surfaces under DC stress," in *Proceedings of the 1998 Conference on Electrical Insulation and Dielectric Phenomena*, vol. 1, October 1998, pp. 80–83.

[61] ——, "Flashover dynamic model of polluted insulators under AC voltage," *IEEE Transactions on Dielectrics and Electrical Insulation*, vol. 7, no. 2, pp. 283–289, April 2000.

[62] ——, "Predictive dynamic model of the leakage current and flashover voltage of dis-

continuously polluted insulators under AC voltage: experimental validation," *Journal of Physics D: Applied Physics*, vol. 40, no. 24, p. 7782, 2007.

[63] M. A. Douar, A. Mekhaldi, and M. C. Bouzidi, "Flashover process and frequency analysis of the leakage current on insulator model under non-uniform pollution conditions," *IEEE Transactions on Dielectrics and Electrical Insulation*, vol. 17, no. 4, pp. 1284–1297, August 2010.

[64] M. A. M. Piah and A. Darus, "Modeling leakage current and electric field behavior of wet contaminated insulators," *IEEE Transactions on Power Delivery*, vol. 19, no. 1, pp. 432–433, January 2004.

[65] J. S. T. Looms, *Insulators for High Voltages*. London, UK: The Institution of Engineering and Technology, 2006.

[66] L. L. Alston and S. Zoledziowski, "Growth of discharges on polluted insulation," *Proceedings of the Institution of Electrical Engineers*, vol. 110, no. 7, pp. 1260–1266, July 1963.

[67] H. Woodson and A. McElroy, "Insulators with contaminated surfaces, Part III: Modeling of dry zone formation," *IEEE Transactions on Power Apparatus and Systems*, vol. PAS-89, no. 8, pp. 1868–1876, November 1970.

[68] F. A. M. Rizk and D. H. Nguyen, "Digital simulation of source-insulator interaction in HVDC pollution tests," *IEEE Transactions on Power Delivery*, vol. 3, no. 1, pp. 405–410, January 1988.

[69] P. S. Ghosh and N. Chatterjee, "Polluted insulator flashover model for AC voltage," *IEEE Transactions on Dielectrics and Electrical Insulation*, vol. 2, no. 1, pp. 128–136, February 1995.

[70] I. Gonos, S. Suflis, F. Topalis, and I. Stathopulos, "Computer methods for the determination of the critical parameters of polluted insulators," in *Proceedings of the 1st Mediterranean Conference on Power Generation, Transmission and Distribution*, vol. 7, 1998.

[71] I. F. Gonos, F. V. Topalis, and S. I. A., "A model for the determination of the dielectric strength of non-uniformly polluted insulators," in *Proceedings of the 3rd IASTED International Conference on Power and Energy Systems*, Las Vegas, USA, November 1999, pp. 472–476.

[72] F. Topalis, I. Gonos, and I. Stathopulos, "Dielectric behaviour of polluted porcelain insulators," *IEE Proceedings - Generation, Transmission and Distribution*, vol. 148, no. 4, pp. 269–274, July 2001.

[73] I. Gonos, F. Topalis, and I. Stathopolos, "Genetic algorithm approach to the modelling of polluted insulators," *IEE Proceedings - Generation, Transmission and Distribution*, vol. 149, no. 3, pp. 373–376, May 2002.

[74] S. Venkataraman and R. Gorur, "Prediction of flashover voltage of non-ceramic insulators under contaminated conditions," *IEEE Transactions on Dielectrics and Electrical Insulation*, vol. 13, no. 4, pp. 862–869, August 2006.

[75] M. T. Gençoğlu and M. Cebeci, "The pollution flashover on high voltage insulators," *Electric Power Systems Research*, vol. 78, no. 11, pp. 1914–1921, 2008.

[76] M. Gençoğlu and M. Cebeci, "Computation of AC flashover voltage of polluted HV insulators using a dynamic arc model," *European Transactions on Electrical Power*, vol. 19, no. 5, pp. 689–701, 2009.

[77] M. Verma, W. Heise, H. Liphen, G. Luxa, and H. Schreiber, "The criterion for pollution flashover and its application to insulation dimensioning and control," *CIGRE report*, pp. 33–09, 1978.

[78] C. H. A. Ely, P. Lambeth, and J. S. T. Looms, "The booster shed: Prevention of flashover of polluted substation insulators in heavy wetting," *IEEE Transactions on Power Apparatus and Systems*, vol. PAS-97, no. 6, pp. 2187–2197, November 1978.

[79] D. Jolly, "A quantitative method for determining the resistance of polymers to surface discharges," *IEEE Transactions on Electrical Insulation*, vol. EI-17, no. 4, pp. 293–299, August 1982.

[80] R. Gorur, E. A. Cherney, and R. Hackam, "A comparative study of polymer insulating materials undern salt-fog conditions," *IEEE Transactions on Electrical Insulation*, vol. EI-21, no. 2, pp. 175–182, April 1986.

[81] W. Starr, "Polymeric outdoor insulation," *IEEE Transactions on Electrical Insulation*, vol. 25, no. 1, pp. 125–136, February 1990.

[82] A. E. Vlastos, "Basic leak currents of generic silicone and EPDM transmission line

polymeric insulators," in *Proceedings of the 3rd International Conference on Properties and Applications of Dielectric Materials*, vol. 2, July 1991, pp. 977–980.

[83] A. Vlastos and T. Sorqvist, "Leakage current and performance of silicone rubber insulators during salt-storms," in *Proceedings of the 1994 IEEE International Symposium on Electrical Insulation*, June 1994, pp. 530–533.

[84] J. Li, W. Sima, C. Sun, and S. Sebo, "Use of leakage currents of insulators to determine the stage characteristics of the flashover process and contamination level prediction," *IEEE Transactions on Dielectrics and Electrical Insulation*, vol. 17, no. 2, pp. 490–501, April 2010.

[85] T. Suda, "Study on the frequency characteristics of leakage current waveforms of artificially polluted 12t suspension insulators by the clean fog method," in *Proceedings of the Eleventh International Symposium on (Conference Publication no. 467) High Voltage Engineering*, vol. 4, 1999, pp. 115–118.

[86] ——, "Frequency characteristics of leakage current waveforms of an artificially polluted suspension insulator," *IEEE Transactions on Dielectrics and Electrical Insulation*, vol. 8, no. 4, pp. 705–709, August 2001.

[87] ——, "Frequency characteristics of leakage current waveforms of a string of suspension insulators," *IEEE Transactions on Power Delivery*, vol. 20, no. 1, pp. 481–487, January 2005.

[88] C. Richards, C. Benner, K. Butler-Purry, and B. Russell, "Electrical behavior of con-

taminated distribution insulators exposed to natural wetting," *IEEE Transactions on Power Delivery*, vol. 18, no. 2, pp. 551–558, April 2003.

[89] M. Fernando and S. Gubanski, "Leakage current patterns on contaminated polymeric surfaces," *IEEE Transactions on Dielectrics and Electrical Insulation*, vol. 6, no. 5, pp. 688–694, October 1999.

[90] J. Fierro-Chavez, I. Ramirez-Vazquez, and G. Montoya-Tena, "On-line leakage current monitoring of 400 kV insulator strings in polluted areas," *IEE Proceedings - Generation, Transmission and Distribution*, vol. 143, no. 6, pp. 560–564, November 1996.

[91] C. Richards, C. L. Benner, K. Butler, and B. D. Russell, "Leakage current characteristics caused by contaminated distribution insulators," in *Proceedings of the 31st Annual North American Power Symposium*, 1999, pp. 484–489.

[92] X. Li, Y. Feng, K. L. Wong, P. Sokolowski, and X. Yu, "Analysis of the leakage current on polluted insulators using correlation coefficient," in *Proceedings of the 37th Annual Conference on IEEE Industrial Electronics Society (IECON 2011)*, November 2011, pp. 3338–3342.

[93] D. Pylarinos, K. Siderakis, E. Pyrgioti, E. Thalassinakis, and I. Vitellas, "Impact of noise related waveforms on long term field leakage current measurements," *IEEE Transactions on Dielectrics and Electrical Insulation*, vol. 18, no. 1, pp. 122–129, February 2011.

[94] M. Shah, "Signature analysis of flashover voltage phenomena on contaminated insulator surfaces," in *Proceedings of the 1996 IEEE Conference on Electrical Insulation and Dielectric Phenomena*, vol. 2, October 1996, pp. 459–462.

[95] G. G. Karady, F. Amarh, and R. Sundararajan, "Dynamic modeling of AC insulator flashover characteristics," in *Proceedings of the Eleventh International Symposium on (Conference Publication no. 467) High Voltage Engineering*, vol. 4, 1999, pp. 107–110.

[96] A. H. El-Hag, "Leakage current characterization for estimating the conditions of non-ceramic insulators' surfaces," *Electric Power Systems Research*, vol. 77, pp. 379–384, March 2007.

[97] Suwarno, "Study on the wave form of leakage current on the 20 kV post-pin ceramic insulators under various conditions," in *Proceedings of the 2001 International Symposium on Electrical Insulating Materials (ISEIM 2001)*, 2001, pp. 387–390.

[98] H. Ahmad, M. A. Salam, L. Y. Ying, and N. Bashir, "Harmonic components of leakage current as a diagnostic tool to study the aging of insulators," *Journal of Electrostatics*, vol. 66, no. 3, pp. 156–164, 2008.

[99] N. Bashir and H. Ahmad, "Odd harmonics and third to fifth harmonic ratios of leakage currents as diagnostic tools to study the ageing of glass insulators," *IEEE Transactions on Dielectrics and Electrical Insulation*, vol. 17, no. 3, pp. 819–832, June 2010.

[100] G. G. Karady and F. Amarh, "Extreme value analysis of leakage current envelope of polluted insulators," in *Proceedings of the IEEE Power Engineering Society Summer Meeting, 2000*, vol. 4, 2000, pp. 2531–2535.

[101] F. Amarh, "Electric transmission line flashover prediction system," Ph.D. dissertation, Arizona State University, 2001.

[102] F. Amarh and G. G. Karady, "PSERC electric transmission line flashover prediction system," 2001.

[103] S. Chandrasekar, C. Kalaivanan, A. Cavallini, and G. Montanari, "Investigations on leakage current and phase angle characteristics of porcelain and polymeric insulator under contaminated conditions," *IEEE Transactions on Dielectrics and Electrical Insulation*, vol. 16, no. 2, pp. 574–583, April 2009.

[104] S. Mallat, "A theory for multiresolution signal decomposition: the wavelet representation," *IEEE Transactions on Pattern Analysis and Machine Intelligence*, vol. 11, no. 7, pp. 674–693, July 1989.

[105] ——, *A Wavelet Tour of Signal Processing*. San Diego: Academic Press, 1999.

[106] M.-T. Yang, J.-C. Gu, C.-Y. Jeng, and W.-S. Kao, "Detection of high impedance fault in distribution feeder using wavelet transform and artificial neural networks," in *Proceedings of the 2004 International Conference on Power System Technology (PowerCon 2004)*, vol. 1, November 2004, pp. 652–657.

[107] H. Mokhtari and R. Aghatehrani, "A new wavelet-based method for detection of high

impedance faults," in *Proceedings of the 2005 International Conference on Future Power Systems*, November 2005, pp. 1–6.

[108] I. Baqui, A. Mazon, I. Zamora, and R. Vicente, "High impedance faults detection in power distribution system by combination of artificial neural network and wavelet transform," in *Proceedings of the 18th International Conference and Exhibition on Electricity Distribution (CIRED 2005)*, June 2005, pp. 1–4.

[109] M. Michalik, W. Rebizant, M. Lukowicz, S.-J. Lee, and S. hee Kang, "High-impedance fault detection in distribution networks with use of wavelet-based algorithm," *IEEE Transactions on Power Delivery*, vol. 21, no. 4, pp. 1793–1802, October 2006.

[110] G. Vijayachandran and B. Mathew, "High impedance arcing fault detection in MV networks using discrete wavelet transform and artificial neural networks," in *Proceedings of the 2012 International Conference on Green Technologies (ICGT)*, December 2012, pp. 89–98.

[111] J.-H. Ko, J.-C. Shim, C.-W. Ryu, C.-G. Park, and W.-Y. Yim, "Detection of high impedance faults using neural nets and chaotic degree," in *Proceedings of the 1998 International Conference on Energy Management and Power Delivery (EMPD '98)*, vol. 2, March 1998, pp. 399–404.

[112] A. Mamishev, B. Russell, and C. Benner, "Analysis of high impedance faults using fractal techniques," *IEEE Transactions on Power Systems*, vol. 11, no. 1, pp. 435–440, February 1996.

[113] C. Zhao and Y. Guo, "Mesh fractal dimension detection on single-phrase-to-earth fault in the non-solidly earthed network," in *Proceedings of the 2005 IEEE Power Engineering Society General Meeting*, vol. 1, June 2005, pp. 752–754.

[114] B. Mandelbrot, *The Fractal Geometry of Nature*. New York: W.H. Freeman and Co., 1982.

[115] J. C. Sprott, *Chaos and Time-Series Analysis*, J. Hall and C. Hall, Eds. Oxford University Press, 2003.

[116] A. Kanashiro and G. Burani, "Leakage current monitoring of insulators exposed to marine and industrial pollution," in *Proceedings of the 1996 IEEE International Symposium on Electrical Insulation*, vol. 1, June 1996, pp. 271–274.

[117] P. R. Silva, J. Santos, A., W. C. Boaventura, G. C. Miranda, and J. A. Scott, "Impulse response analysis of a real feeder for high impedance fault detection," in *Proceedings of the 1994 IEEE Power Engineering Society Transmission and Distribution Conference*, April 1994, pp. 276–283.

[118] A. Bansal and G. Pillai, "High impedance fault detection using LVQ neural networks." *International Journal of Computer, Information & Systems Science & Engineering*, vol. 1, no. 3, 2007.

[119] A. Sharaf, R. M. El-Sharkawy, R. Al-Fatih, and M. Al-Ketbi, "High impedance fault detection on radial distribution and utilization systems," in *Proceedings of the Cana-*

dian Conference on Electrical and Computer Engineering, vol. 2, May 1996, pp. 1012–1015.

[120] M. Khalifa, A. El-Morshedy, O. E. Gouda, and S.-D. Habib, "A new monitor for pollution on power line insulators. II. Simulated field tests," *IEE Proceedings - Generation, Transmission and Distribution*, vol. 135, no. 1, pp. 24–30, January 1988.

[121] K. Isaka, Y. Yokoi, K. Naito, R. Matsuoka, S. Ito, K. Sakanishi, and O. Fujii, "Development of real-time system for simultaneous observation of visual discharges and leakage current on contaminated DC insulators," *IEEE Transactions on Electrical Insulation*, vol. 25, no. 6, pp. 1153–1160, December 1990.

[122] A. E. Vlastos and T. Orbeck, "Outdoor leakage current monitoring of silicone composite insulators in coastal service conditions," *IEEE Transactions on Power Delivery*, vol. 11, no. 2, pp. 1066–1070, April 1996.

[123] I. Kamwa, R. Grondin, and D. McNabb, "On-line tracking of changing harmonics in stressed power systems: application to Hydro-Quebec network," *IEEE Transactions on Power Delivery*, vol. 11, no. 4, pp. 2020–2027, October 1996.

[124] V. Saiz and J. Guadalupe, "Application of Kalman filtering for continuous real-time tracking of power system harmonics," *IEE Proceedings - Generation, Transmission and Distribution*, vol. 144, no. 1, pp. 13–20, January 1997.

[125] B.-H. Lee and S.-M. Kang, "A new on-line leakage current monitoring system of ZnO

surge arresters," *Materials Science and Engineering: B*, vol. 119, no. 1, pp. 13–18, 2005.

[126] L. Hengzhen, L. Gang, L. Xiaodong, H. Ziang, and H. Song, "Discussion on the application of leakage current and optical sensor online monitoring equipments," in *Proceedings of the 2008 IEEE International Symposium on Electrical Insulation (ISEI 2008)*, June 2008, pp. 85–88.

[127] H. Ng, "Distribution fault anticipator phase 2: Third interim report," EPRI, Tech. Rep., 2003.

[128] (2009) Distribution fault anticipator phase 3 - system integration. EPRI. [Online]. Available: http://www.epri.com/abstracts/Pages/ProductAbstract.aspx?ProductId=000000000001016036

[129] C. Steineke, "Multi-channel synchronous PD-measurements on power transtormers," in *Proceedings of TechCon® Asia-Pacific*, 2007.

[130] P. Lambeth, J. S. T. Looms, A. Stalewski, and W. Todd, "Surface coatings for H.V. insulators in polluted areas," *Proceedings of the Institution of Electrical Engineers*, vol. 113, no. 5, pp. 861–869, May 1966.

[131] *Distribution Construction Standard*, Citipower and Powercor Australia Std., 2005.

[132] *Guidelines for Design and Maintenance of Overhead Distribution and Transmission Lines*, Standards Australia, Energy Networks Association Std. ENA2006, 2006.

[133] *Overhead line design - Detailed procedures*, SAI Global Limited, Standards Australia Std. AS/NZS 7000:2010, 2010.

[134] *Guide for the selection of insulators in respect of polluted conditions*, SAI Global Limited, Standards Australia Std. AS4436, 1996.

[135] S. A. Prentice, "Report on pole and cross arm fire," State Electricity Commission of Victoria, Australia, Internal Report, August 1952.

[136] *Specifications for preservative treatment - Sawn and round timber*, SAI Global Limited, Standards Australia Std. AS1904.1, 2005.

[137] *Timber - Poles for overhead lines*, SAI Global Limited, Standards Australia Std. AS2209, 1994.

[138] S. Pathak, "Leakage current in wooden structures used for power distribution," Ph.D. dissertation, RMIT University, 2011.

[139] (2008, June) ThermoVision A320 Datasheet - MoviMED. [Online]. Available: http://www.movimed.com/PDF/A320%20Data%20Sheet.pdf

[140] Electricity Authority of NSW, "Electrical hazards associated with conductivity of australian hardwood power line poles," *Australian Power Engineering*, vol. 7, no. 2, pp. 6–8, 10, September 1967.

[141] F. Buratto, "Investigation into predictive and preventative pole fire detection technology," Internal Report, Powercor Australia, June 2003.

[142] T. Schweickhardt and F. Allgower, "On system gains, nonlinearity measures, and linear models for nonlinear systems," *IEEE Transactions on Automatic Control*, vol. 54, no. 1, pp. 62–78, January 2009.

[143] B. Widrow and S. D. Stearns, *Adaptive Signal Processing*, A. V. Oppenheim, Ed. Prentice-Hall, 1985.

[144] B. Ninness, "Lecture notes in signal processing," 1998, Univeristy of Newcastle.

[145] Mathworks, "Fast Fourier Transform (FFT)," 2014. [Online]. Available: http://www.mathworks.com.au/help/matlab/math/fast-fourier-transform-fft.html

[146] CEI/IEC, *Artificial Pollution Tests on High-Voltage Insulators to be used on A.C. Systems*, International Standard, Std. 507, 1991.

[147] A. Namajunas and A. Tamasevicius, "A technique for measuring fractal dimensions from time series on a real-time scale," *Physica D: Nonlinear Phenomena*, vol. 58, no. 1-4, pp. 482 – 488, 1992. [Online]. Available: http://www.sciencedirect.com/science/article/pii/0167278992901338

[148] S. Mohammadi, "Fractaldim: Matlab function to compute fractal dimension," 2009. [Online]. Available: http://EconPapers.repec.org/RePEc:boc:bocode:t741507

[149] C. Phan and M. Hara, "Leakage current and flashover performance of iced insulators," *IEEE Transactions on Power Apparatus and Systems*, vol. PAS-98, no. 3, pp. 849–859, May 1979.

[150] G. Montoya, I. Ramirez, and J. I. Montoya, "Correlation among ESDD, NSDD and leakage current in distribution insulators," *IEE Proceedings - Generation, Transmission and Distribution*, vol. 151, no. 3, pp. 334–340, May 2004.

[151] "T14/31/115 Single Line Diagram, Zone Substation, MC - Mordialloc," Jemena Asset Management, Mt Waverley, Victoria, Australia, 2007.

[152] (2009) High Voltage Catalogue - Olex. Olex. [Online]. Available: http://www.olex.com.au/eservice/Australia-en_AU/fileLibrary/Download_540225176/Australasia/files/OLC12641_HighVoltageCat_1.pdf

[153] "United Energy Mordialloc Fault Level Database," Internal database warehouse, Jemena Asset Management, Mt Waverley, Victoria, Australia, 2008.

[154] T. L. Floyd, *Principles of Electric Circuits*, L. Ludewig, Ed. Prentice-Hall International, 1997.

[155] A. Girgis, C. Fallon, and D. Lubkeman, "A fault location technique for rural distribution feeders," *IEEE Transactions on Industry Applications*, vol. 29, no. 6, pp. 1170–1175, November 1993.

[156] M. M. Saha, R. Das, P. Verho, and D. Novosel, "Review of fault location techniques for distribution systems," *Power Systems and Communications Infrastructures for the future, Beijing*, 2002.

[157] F. Han, X. Yu, M. Al-Dabbagh, and Y. Wang, "Locating phase-to-ground short-

circuit faults on radial distribution lines," *IEEE Transactions on Industrial Electronics*, vol. 54, no. 3, pp. 1581–1590, June 2007.

[158] J. Mora-Florez, J. Melendez, and G. Carrillo-Caicedo, "Comparison of impedance based fault location methods for power distribution systems," *Electric Power Systems Research*, vol. 78, no. 4, pp. 657–666, 2008.

[159] J. J. Mora Flórez, G. Morales España, and S. Pérez Londoño, "Classification methodology and feature selection to assist fault location in power distribution systems," *Revista Facultad de Ingeniería Universidad de Antioquia*, no. 44, pp. 83–96, 2008.

[160] L. Peretto, R. Sasdelli, E. Scala, and R. Tinarelli, "Performance characterization of a measurement system for locating transient voltage sources in power distribution networks," *IEEE Transactions on Instrumentation and Measurement*, vol. 58, no. 2, pp. 450–456, February 2009.

[161] A. Dwivedi, X. Yu, P. Sokolowski, P. Wong, and F. Buratto, "Fault location in power networks using graph theory," in *Proceedings of the 36th Annual Conference on IEEE Industrial Electronics Society (IECON 2010)*, 2010, pp. 2436–2441.

[162] A. Dwivedi and X. Yu, "Fault location in radial distribution lines using travelling waves and network theory," in *Proceedings of the 2011 IEEE International Symposium on Industrial Electronics (ISIE 2011)*, 2011, pp. 1051–1056.

[163] *PowerLogic 7700 ION User's Guide*, Power Measurement Ltd.

[164] *PowerLogic ION7550/ION7650 Energy & Power Quality Meter User's Guide*, Schneider Electric.